Separation of Chiral Active Pharmaceutical Ingredients

A First Step towards Continuous Preferential Crystallization in the Pharmaceutical Industry

Chaaban, Joussef Hussein; Dam-Johansen, Kim; Skovby, Tommy; Kiil, Søren

Publication date:
2013

Document Version
Publisher's PDF, also known as Version of record

Technical University of Denmark

Department of Chemical and Biochemical Engineering

Separation of Chiral Active Pharmaceutical Ingredients:

A First Step towards Continuous Preferential Crystallization in the Pharmaceutical Industry

PhD Thesis

Author:

Joussef Hussein Chaaban,
Ph.D. student

Supervisors:

Kim Dam Johansen,
Professor, Ph.D.

Søren Kiil,
Associate Professor, Ph.D.

Tommy Skovby,
Head of Department for
Chemical Technology and
Implementation

March 26, 2013

Danmarks Tekniske Universitet

Institut for Kemiteknik

Separation af chirale farmaceutiske ingredienser:

Første trin mod kontinuert selektiv krystallisation i den farmaceutiske industri

Phd-afhandling

Forfatter:

Joussef Hussein Chaaban,
Phd-studerende

Vejledere:

Kim Dam Johansen,
Professor, Phd.

Søren Kiil,
Lektor, Phd.

Tommy Skovby,
Afdelingsleder for kemisk teknologi og implementering

26 marts 2013

With love,
to the love of my life,
to my lovely family and parents

Preface

This dissertation is the result of my three years of research towards the Ph.D. degree at the Technical University of Denmark, DTU. The work presented was conducted at the Center for Harmful Emission Control (CHEC) at the Department of Chemical and Biochemical Engineering from January 2010 to March 2013. The Ph.D. project was carried out in collaboration with H. Lundbeck A/S. Professor Kim Dam-Johansen, Associate professor Søren Kiil, and Head of Department for Chemical Technology and Implementation at H. Lundbeck A/S Tommy Skovby have been supervisors on the project.

First of all, I wish to thank my three supervisors for very valuable contributions to the project through many interesting and helpful discussions. I am deeply grateful to Søren Kiil, who has constantly supported me with valuable ideas and suggestions since the beginning of the Ph.D. project and the three months before working as research assistant.

I am also deeply grateful to Kim Dam-Johansen and Tommy Skovby for valuable and stimulating discussions, for the continued trust in my work, and for the maintenance of a stable and inspiring research environment.

During the Ph.D. project I had the greatest pleasure to work with very talented and hard working students: Diana Hudecz, Annalicia Poehler, and Hulovan Kamal Ibrahim. They were highly motivated with many interesting ideas and suggestions and a motivation for going to work. To all of them, I am also very grateful for the nice moments together and for the experience I got working with you, with successes and failures.

I am very grateful to the highly motivated and experienced technician Mette Larsen, for her constant help in the laboratory and for her many constructive discussion and ideas for solving laboratory challenges and the analyses made at CHEC. I am also very grateful for the helpful and motivated technician Emine Yüksel Coskun for her help and assistance in the STA measurements and help in the laboratory. To the other lab technicians at KT: Thank you for your help. I would also like to thank Finn Eliasen

from Termometri Lab at Risøe-DTU for his help in thermocouple calibration.

I wish also to thank the highly motivated and experienced Jens Henry Poulsen, Michael Lindaa, Ivan Pedersen, and their colleagues at the KT workshop. They were of great help and inspiration in building the experimental setup.

Great thanks to H. Lundbeck A/S for financial and technical support, and especially to Troels Christensen, Claus Mortensen, Michael Mealy, Robert Dancer, and Thomas Holm for very interesting and inspiring discussions on the setup and the fundamentals and process engineering aspects of continuous crystallization. I wish also to thank Heidi Lopez for her experience and help in crystallization and crystallography. I am also very grateful to the highly motivated and experienced technician Fatma Celik for her help in HPLC analyses and laboratory work performed at H. Lundbeck A/S.

I would like to thank all my friends and colleagues for three wonderful and interesting years spent together. I am grateful for the valuable discussions and interesting ideas provided by Brian Bruun Hansen, Vikas Narayan, and my office mates Mohammad Bashir, Ngoc Trung, and Shizhong.

Finally, I am deeply grateful to my family, especially my wife, for their love and patience and for being my source of inspiration and constant support every day, in success as well as in failure. Thanks to my lovely parents and siblings, for reminding me every day of the beauty of life, for their education, love, and infinite support.

Joussef Hussein Chaaban
Lyngby, March 2013

Summary

The objective of this PhD project is to experimentally and theoretically investigate the separation performance and to improve the process understanding of a newly developed continuous preferential crystallization (PC) process for the separation of enantiomers forming conglomerates. This PC process is regarded as a first step towards a fully continuous PC process. The current knowledge of the importance of crystallization processes in the pharmaceutical industry and the complex thermodynamic and kinetic phenomena accompanied with the separation of chiral compounds are addressed. The experimental work covers laboratory studies and the theoretical work is based on the experimental data and observations.

A large fraction of active pharmaceutical ingredients (APIs) are enantiomers and the desired biological activity is provided only by one of the enantiomers. Strict regulatory requirements, increasing public demand, and fierce competition have forced the pharmaceutical industry to redevelop existing methods or develop completely new methods to produce pharmaceuticals consisting of APIs of the desired enantiomer. PC is one of several methods used industrially to obtain pure enantiomers by separation of a racemic mixture. The potential application of PC is strongly dependent on requirements to the thermodynamics and crystallization kinetics of the considered solute-solvent(s) system, and the desired operating conditions. Meeting these requirements are essential to achieve predefined physical attributes of the final product and process economical targets. In this respect, an increasing interest in converting from the conventional batch to continuous PC has initiated the search for new process development opportunities of PC processes. The reason is the many advantages of continuous operation, especially in the case of separation of enantiomers.

A newly developed lab-scale continuous PC process, so-called continuous coupled preferential crystallization (CC-PC) process, consisting of two mixed flow crystallizers coupled via crystal-free mother liquor exchange streams and with only the liquid phases operated continuously, was built as the main part of this PhD project. Experiments in triplicate were conducted for the experimental investigation to assess the robustness of the CC-PC process and to investigate the achievement of simultaneous separation of the enantiomers of the conglomerate forming system of the amino

acid asparagine monohydrate by crystal growth of seed crystals. The achievement of a racemic liquid phase composition consisting of nearly equal distribution of enantiomers in solution was also investigated. Finally, the performance of the CC-PC process and its potential for further development to a fully continuous PC process was discussed. A nearly racemic composition of the liquid phase in the crystallizers was obtained. Successfull enantioseparation by crystal growth was verified, with the repeatability being within $\pm 10\%$ deviation. Productivities, yields, and purities of solid products were influenced by the morphological differences in the seed crystals. Due to irregularly shaped seed crystals of L-asparagine mnohydrate (L-AsnH_2O), increase in the productivities and yields were achieved in the L-Tank, i.e. the crystallizer in which L-AsnH_2O crystals grow. Lower purities of solid products from the L-Tank compared to solid products from the D-Tank, in which seeds of D-asparagine monohydrate (D-AsnH_2O) were used, were obtained. This could be due to surface nucleation of D-AsnH_2O, ascribed to the surface structure of the seeds of L-AsnH_2O supplied. An additional experiment was also carried out using seed crystals of a smaller average particle size having a smoother surface structure than used in the reference experiments. Productivity, yield, and purity were slightly improved in the L-Tank, for the same process duration. It should be emphasized, however, that it was found that the growth rate of the desired enantiomer was very low at the given experimental conditions and therefore practically no consumption of the enantiomer in the feed occurred in the crystallizer. This was ascribed to the nature of the controlling mechanism for crystal growth comprising slow surface integration of the asparagine monohydrate molecules onto the surfaces of the supplied seed crystals. The main advantages of the CC-PC process compared to other separation processes are low capital cost, high crystal purity and yield, ease of upscaling, increased safety, and reduced environmental impact due to reduction in amount of solvent used. Currently, the application is, however, limited to conglomerate forming systems. Nevertheless, the separation concept may open new possibilities for process improvements for enantioseparation of racemic compound forming systems as well.

The theoretical investigation of the CC-PC process consisted of the establishment of a dynamic one-dimensional model describing the continuous separation of enantiomers by simultaneous preferential crystallization. The evolution in the moments of the crystal population balances in combination with the liquid phase mass balances for the enantiomers were presented. The model was validated against experimental data for the conglomerate forming system of asparagine monohydrate in aqueous solution. The kinetic parameters required were taken from available literature sources and simulations compared to experimental data. The simulations were found to be in good agreement with the experimental data. The sensitivity analysis conducted suggests

that the separation process can be improved by increasing the mean residence time of the liquid phase in the crystallizers, the crystallization temperature, and the mass of seeds supplied. Reducing the size of seed crystals will also lead to an improved separation. The model can be used to simulate the performance of the continuous crystallization process for a racemic compound forming system. The racemic compound and the pure enantiomer can be separated simultaneously in each crystallizer having sufficient enrichment of the pure enantiomer in the feed solution. The model can also be extended to represent a fully continuous separation process taking into account the continuous supply of enantiopure seed crystals and liquid feed solution and the continuous removal of solid product and mother liquor.

Resumé

Formålet med dette phd-projekt er, at eksperimentelt og teoretiskt undersøge separationens ydeevne, og at forbedre procesforståelsen af et nyudviklet kontinuert proces for selektiv krystallisation (SK) til separation af enantiomere, som danner et konglomerat system. Denne SK proces betragtes som det første trin mod et fuldt kontinuert SK proces. Et litteraturstudie over vigtigheden af krystallisationsprocesser i den farmaceutiske industri og de kompleske termodynamiske og kinetiske fænomener tilknyttet separationen af chirale komponenter er udarbejdet. Det eksperimentelle arbejde dækker laboratoriestudier, og det teoretiske arbejde er baseret på eksperimentelle data og observationer.

En stor del af aktive farmaceutiske ingredienser (AFI'er) er enantiomere, og den ønsket biologiske aktivitet tildeles kun én af enantiomererne. Strenge myndighedskrav, forøget efterspørgsel, og hård konkurrence har tvunget den farmaceutiske industri at genudvikle eksisterende metoder eller udvikle helt nye metoder til produktionen af lægemidler bestående af AFI'er af den ønsket enantiomer. SK er en af et antal industrielt anvendte metoder at opnå rene enantiomere på ved separation af en racemisk blanding. Anvendelsespotentialet af SK er stærkt afhængigt af krav til termodynamikken og krystallisationskinetikken af det betragtet solut-solvent system, og de ønskede driftsbetingelser. At opfylde disse krav er afgørende for at opnå foruddefinerede fysiske egenskaber af det endelige produkt og procesekonomiske mål. I denne sammenhæng, en forøget interesse i omdannelsen fra konventionel batch til kontinuert SK har indledt søgningen efter nye procesudviklingsmuligheder af SK processer. Årsagen er de mange fordele ved kontinuert drift, særligt når det gælder separation af enantiomere.

En nyudviklet lab-skala kontinuert SK proces, såkaldt kontinuert koblet selektiv krystallisation (KK-SK), bestående af to strømningsreaktorer (krystallisationstanke) koblede via vekslingsstrømme af krystalfri moderlud, og kun med væskefasen i kontinuert drift, blev bygget som hovedparten af dette phd-projekt. Eksperimenter i triplikater blev udført for den eksperimentelle undersøgelse for at vurdere robustheden af KK-SK processen, og at undersøge opnåelsen af samtidig separation of enantiomererne af det konglomeratdannende system af aminosyren asparagin monohydrat

via krystalvækst af podekrystaller. Opnåelsen af en næsten racemisk væskefasesammensætning bestående af næsten ligelig fordeling af enantiomere i opløsning blev også undersøgt. Endeligt blev ydeevnen af KK-SK processen og dets potentiale for videre udvikling til en fuld kontinert SK proces diskuteret. En næsten racemisk sammensætning af væskefasen blev opnået. Succéfuld separation af enantiomere via krystalvækst blev verificeret med en repetérbarhed indenfor $\pm 10\%$ afvigelse. Produktiviteter, udbytter, og renhedsgrader af krystallint produkt var påvirkede af de morfologiske forskelle i de tilførte podekrystallerne. Forøgelse i produktiviteter og udbytter var opnåelige i L-Tanken på grund af den irregulær form af podekrystaller af L-asparagin monohydrat (L-AsnH_2O). Lavere renhedsgrader af krystallint produkt fra L-Tanken blev opnået sammenlignet med produkt fra D-Tanken, hvori podekrystaller af D-asparagin monohydrat (D-AsnH_2O) blev tilført. Dette kan skyldes overfladenuklering af D-AsnH_2O tilskrevet overfladestrukturen af tilførte podekrystaller af L-AsnH_2O. Et yderligere eksperiment, hvori podekrystaller af L-AsnH_2O af mindre gennemsnitlig partikelstørrelse med en mere fin overfladestruktur blev anvendt, resulterede i en anelse forbedring af produktivitet, udbytte, og renhedsgrad i L-Tanken for samme procesvarighed. Det skal dog understreges at væksthastigheden af den ønsket enantiomer var meget lav under de givne driftsbetingelser. Derfor opstod der praktisk set inget forbrug af enantiomere fra fødeblandingen i krystallisationstankene. Dette var tildelt den kontrollerende mekanisme for krystalvækst som udgjorde langsom overfladeintegration af asparagin monohydrat molekylerne på overfladen af de tilførte rene podekrystaller. Hovedfordelene ved KK-SK processen sammenlignet med andre separationsprocesser er lave kapitalomkostninger, høj krystalrenhed og udbytte, let at opskalere, forbedret sikkerhed, og reduceret miljøpåvirkning på grund af reduktion i mængde af opløsningsmiddel anvendt. Anvendelsen af KK-SK processen er på nuværende tidspunkt dog begrænset til konglomeratdannende systemer. Ikke desto mindre kan separationskonceptet åbne nye muligheder for procesforbedringer indenfor selektiv separation af enantiomere i systemer som danner racemisk stof såvel som i konglomeratdannende systemer.

Den teoretiske undersøgelse af KK-SK processen bestod af etableringen af en dynamisk én-dimensionel model, som beskriver den kontinuerte separation af enantiomere via samtidig SK. Udviklingen i krystalpopulationsbalancens momenter i kombination med massebalancerne for enantimererne i væskefasen blev præsenteret. Modellen blev valideret imod eksperimentelle data for det konglomeratdannende system af asparagin monohydrat i vandig opløsning. De påkrævede kinetiske parametre blev taget fra tilgængelig litteratur, og simuleringer sammenlignet med eksperimentelle data. Simuleringerne var i overensstemmelse med de eksperimentelle data. Den udførte sensitivitetsanalyse foreslår, at separationsprocessen kan forbedres ved at forøge

den gennemsnitlig opholdstid af væskefasen i krystallisationstankene, krystallisationstemperaturen, og massen af tilført podemateriale. Formindskning i størrelsen af podekrystaller vil også medføre en forbedret separation. Modellen kan anvendes til at simulere ydeevnen af den kontinuerte krystallisationsproces for et system som danner et racemisk stof. Det racemiske stof og den rene enantiomer kan separeres samtidigt i hver sin krystallisationstank, når en tilstrækkelig berigelse af den rene enantiomer i fødeblandingen er mulig. Modellen kan også udvides til at beskrive en fuld kontinuert separationsproces, hvori kontinuert tilførsel af podemateriale af den rene enantiomer og fødeblanding, og kontinuert udtag af fast produkt og moderlud er taget i betragtning.

Contents

		Page
PREFACE		**i**
SUMMARY		**iii**
RESUMÉ		**vi**
CONTENTS		**ix**
LIST OF FIGURES		**xiv**
LIST OF TABLES		**xxi**
Chapter 1	**INTRODUCTION**	**1**
	1.1 Background and motivation	1
	1.2 Batch vs. Continuous	5
	1.3 Project objectives	7
	1.4 Outline of thesis	7
	1.5 Conclusions	8
Chapter 2	**LITERATURE SURVEY**	**9**
	2.1 Methods for the production of pure enantiomers	9
	2.2 Crystallization in the pharmaceutical industry: Objectives and constraints	11
	2.2.1 Separation and purification	11
	2.2.2 Product attributes and performance	11
	2.2.2.1 Solid forms of an API	12
	2.2.2.2 Particle size and PSD	15
	2.2.2.3 Morphology and flow properties	16
	2.3 Solid-liquid phase equilibria of chiral systems	17
	2.3.1 Conglomerate forming systems	17
	2.3.2 Racemic compound forming systems	19
	2.3.3 Pseudoracemate forming systems	22
	2.4 Crystallization theory	22

2.4.1 Crystallization driving force: Supersaturation 22
2.4.1.1 Crystallization modes 23
2.4.2 Metastable region 23
2.4.3 Nucleation 26
2.4.3.1 Primary homogeneous nucleation 26
2.4.3.2 Primary heterogeneous nucleation 28
2.4.3.3 Secondary nucleation 28
2.4.4 Crystal growth 29
2.4.4.1 Size-dependent growth and growth rate dispersion 32
2.5 Conclusions 33

Chapter 3 SEPARATION OF ENANTIOMERS BY CONTINUOUS PREFERENTIAL CRYSTALLIZATION: EXPERIMENTAL REALIZATION USING A COUPLED CRYSTALLIZER CONFIGURATION 35
3.1 Introduction 36
3.1.1 Coupled-Batch Preferential Crystallization 37
3.1.2 Coupled Continuous Preferential Crystallization 38
3.1.3 Chemical model system 39
3.2 Experimental section 40
3.2.1 Materials 40
3.2.2 Experimental setup and procedures 40
3.2.2.1 Continuous Preferential Crystallization (CC-PC) process 40
3.2.2.2 Preparation of undersaturated racemic feed solution 41
3.2.2.3 Continuous Preferential Crystallization (CC-PC) experiments 42
3.3 Process Metrics 44
3.3.1 Analysis 44
3.3.1.1 Concentration of enantiomer in the liquid phase 44
3.3.1.2 Supersaturation ratio 44
3.3.1.3 Productivity and yield 44
3.3.1.4 Optical purity 45
3.4 Results and Discussion 45
3.4.1 Crystallization temperature and observed optical rotation 45
3.4.2 Liquid phase concentration profiles of enantiomers 46

3.4.3 Supersaturation and crystal growth 47
3.4.4 Analysis of the solid product 48
3.4.5 Productivity and yield 50
3.4.6 Optical purity 53
3.4.7 Unutilized enantiomer in purge 54
3.5 Conclusions 55

Chapter 4 SEPARATION OF ENANTIOMERS BY CONTINUOUS PREFERENTIAL CRYSTALLIZATION: MATHEMATICAL MODELING OF A COUPLED CRYSTALLIZER CONFIGURATION 56
4.1 Introduction 57
4.1.1 Continuous Coupled Preferential Crystallization 58
4.2 Description of the continuous setup 59
4.3 Mathematical modeling 60
4.3.1 Model development 61
4.3.1.1 Crystal population balance 61
4.3.1.2 Crystal growth kinetics 61
4.3.1.3 Supersaturation ratio 62
4.3.1.4 Concentration of enantiomers 62
4.3.1.5 Liquid phase mass balance for the preferred enantiomer 62
4.3.1.6 Liquid phase mass balance for the counter enantiomer 63
4.3.1.7 Feed flow rates 63
4.3.1.8 Crystal-free liquid exchange flow rate 64
4.3.1.9 Effluent flow rate 64
4.3.2 Process metrics 64
4.3.2.1 Separation efficiency: U-value 64
4.3.2.2 Yield based on feed solution 64
4.3.2.3 Productivity and yield based on seeds 65
4.3.2.4 Crystal size yield 65
4.4 Numerical solution procedure 65
4.5 Estimation of physical and chemical parameters 67
4.5.1 Physical constants 67
4.5.2 Solubility concentration of enantiomer 67
4.5.3 Density of the liquid phase 67
4.5.4 Parameters for growth kinetics 67
4.6 Results and discussion 68

4.6.1 Model validation using the data of Chaaban et al.[11] 68
4.6.1.1 Productivity and yield 68
4.6.1.2 Concentration of enantiomers 71
4.6.1.3 Supersaturation and crystal growth 72
4.6.2 Sensitivity analysis 73
4.6.2.1 Mean residence time of the liquid phase 74
4.6.2.2 Excess of enantiomer in feed solution 75
4.6.2.3 Crystallization temperature and subcooling 77
4.6.2.4 Fraction of the feed solution inlet 79
4.6.2.5 Mass of seeds and average size of seeds 82
4.6.2.6 Pre-exponential factor for growth rate 85
4.7 Validation of model assumptions 87
4.8 Conclusions 88

Chapter 5 CONCLUSIONS AND SUGGESTIONS FOR FUTURE WORK 89
5.1 Conclusions 89
5.2 Suggestions for future work 91

ABBREVIATIONS 93

NOMENCLATURE 95

BIBLIOGRAPHY 98

Appendix A PROCESS DEVELOPMENT: STAGES AND DECISIONS A-1
A.1 Process system selection A-1
A.1.1 Fluidized bed vs. Stirred vessel A-3
A.2 Chemical system selection A-4
A.3 Equipment and auxiliary selection A-4
A.3.1 Pump selection A-4
A.3.2 Tubings and fittings A-5
A.3.3 Impeller selection for mixing A-6

Appendix B MANUAL FOR THE CC-PC PROCESS B-1
B.1 Introduction B-2
B.2 Objective(s) B-2
B.3 Equipment and setup B-2
B.3.1 Crystallization units B-3

B.3.2 Cooling system B-5
B.3.3 Feed system B-7
B.3.4 Purge system B-8
B.3.5 Analysis equipment B-9
B.3.5.1 Liquid phase analysis: Polarimetry B-9
B.3.5.2 Liquid phase analysis: Densitometry B-10
B.3.5.3 Solid phase imaging: Scanning Electron Microscopy (SEM) B-11
B.4 Experimental procedure B-12
B.4.1 Precautions B-12
B.4.2 Materials B-13
B.4.3 Seed preparation: Sieve analysis and Particle size distribution (PSD) B-13
B.4.3.1 Sieve analysis B-13
B.4.3.2 PSD measurement B-14
B.4.4 Preparation of undersaturated racemic feed solution B-14
B.4.5 Preferential crystallization experiments B-15
B.5 Process metrics B-17
B.5.1 Liquid phase concentration of enantiomers B-17
B.5.2 Separation efficiency: U-value B-17
B.5.2.1 Productivity and yield based on seeds B-18
B.5.2.2 Optical purity of solid product B-18
B.5.3 Final remarks B-19

Appendix C CALIBRATION CURVES C-1
C.1 Calibration procedure for estimation of concentration difference by polarimetry C-1
C.2 Calibration procedure for estimation of total concentration by densitometry C-3
C.3 Calibration procedure for optical purity estimation by polarimetry C-4

Appendix D STA MEASUREMENTS D-1
D.1 Purity assessment by STA measurements D-1

Appendix E PBE TRANSFORMATION BY MOM E-1
E.1 Transformation of the Population Balance Equation (PBE) by the Method Of Moments (MOM) E-1

Appendix F MATLAB CODES F-1

List of Figures

Page

Figure 1.1 Amino acid molecules representing chirality, i.e. they are non-superimposable with their mirror images[64]. Only the backbone of the chemical structure of amino acids is shown. The C-atom in the backbone structure is regarded here as chirality center or stereocenter. R refers to the side groups of the amino acids and can also include chiral moieties. 1

Figure 1.2 Distribution in percentage of 2011 sales of chiral and nonchiral small-molecule APIs and protein APIs of the top 20 global pharmaceutical products[59]. Racemic APIs are included in chiral small-molecule APIs segment. Note that protein APIs are often chiral in nature and consist of amino acids of the naturally occurring L-form. Total sales of top 20 pharmaceuticals in 2011 was 132.1 billion US$. 4

Figure 1.3 Distribution of the average costs as percentage of sales in 2008 for 17 major pharmaceutical companies[3]. 6

Figure 2.1 Current methods for obtaining pure enantiomers[78,79].Racemates refer to racemic mixtures consisting of equal quantity of enantiomers. 9

Figure 2.2 A schematic diagram showing the crystallization process in conjunction with the subsequent downstream processing steps and their effects on solid product attributes[3]. 12

Figure 2.3 A schematic diagram showing the different solid forms an API can exhibit. Note that for multicomponent forms different polymorphs and pseudopolymorphs can also exist[1,3,87]. 13

Figure 2.4 The different multicomponent solid forms of an API and the overlap between them[1]. 14

Figure 2.5 Crystal morphologies frequently observed in the pharmaceutical industry[3]. 16

Figure 2.6 Ternary phase diagram of a simple nonsolvated conglomerate forming system[62,93]. E_1 and E_2 represent enantiomer 1 and enantiomer 2, respectively. The dashed and solid lines correspond to the composition dependent solubility curves at one temperature and at a lower temperature, respectively. 18

Figure 2.7 Ternary phase diagram for a simple nonsolvated racemic compound forming system[62,93]. E_1 and E_2 represent enantiomer 1 and enantiomer 2, respectively. The dashed and solid lines correspond to the composition dependent solubility curves at one temperature and at a lower temperature, respectively. 20

Figure 2.8 A hypothetical map between supersaturation and possible crystallization phenomena[87]. Note that the metastable boundary is only kinetically determined and is dependent on process conditions, such as amount and size of seed crystals or stirring rate. The region between the metastable boundary and equilibrium solubility is the metastable region. 25

Figure 2.9 Homogeneous and heterogeneous nucleation rate versus supersaturation ratio[72]. 28

Figure 2.10 Driving forces for crystal growth[72]. c denotes the concentration of solute in the bulk solution, c_i is the concentration of solute at the crystal surface-solution interface, and c^* is the saturation concentration. 30

Figure 2.11 Proposed crystal growth mechanisms. (a) illustrates the attachment of a growth unit into a kink site, (b) illustrates crystal growth arising from surface nucleation, and (c) the development of growth spiral starting from a screw dislocation[15,62,87]. 30

Figure 3.1 Schematic diagram of the CC-PC process for the preferential crystallization experiments. TF symbolizes the temperature in the feed tank, TF1 is the temperature of feed entering the D-Tank, T1 is the temperature in the D-Tank, T2 is the temperature in the L-Tank, TE1 is the temperature of mother liquor effluent from the D-Tank, T1-2 is the temperature of exchange stream from the D-Tank to the L-Tank and T2-1 is the temperature of exchange stream from the L-Tank to the D-Tank. Blue and red filled circles symbolize growing enantiopure seeds of D-AsnH_2O and L-AsnH_2O in the D- and L-Tank, respectively. The grey boxes in the D- and L-Tank represent filters for mother liquor exchange. 40

Figure 3.2 Photograph of experimental setup for the preferential crystallization experiments. The small insert (lower left corner) shows the instrumentation in the crystallization vessels. Six individual pumps are necessary to run the setup in a continuous mode. 41

Figure 3.3 Temperatures and observed optical rotations of the mother liquors in the D- and L-Tank during preferential crystallization experiments. Error bars represent the standard deviation. Where error bars cannot be seen, a standard deviation of zero was found. The racemate has an optical rotation of zero. At time equal zero, enantiopure seeds are introduced. The experimental conditions are provided in Table 3.1. 46

Figure 3.4 Liquid phase concentrations of enantiomers in each tank as a function of time. Error bars represent the standard deviation. At time equal zero, enantiopure seeds are introduced. 47

Figure 3.5 Transient development in the supersaturation ratio for the preferred enantiomer in each tank. At time equal zero, enantiopure seeds are introduced. 48

Figure 3.6 SEM photomicrographs of the seeds of D-AsnH_2O ((a)) and L-AsnH_2O ((b)) and the final solid products showing the growth of the seed crystals of D-AsnH_2O in the D-Tank for experiments Exp 1 and 3 ((c) and (e)) and the growth of the seed crystals of L-AsnH_2O in the L-Tank for experiments Exp 1 and 3 ((d) and (f)). Note the scale of the images. 51

Figure 3.7 Normalized frequency functions of the PSDs for the enantiopure seeds of D- and L-$AsnH_2O$ supplied in experiments Exp 1-3 (sieve fraction 250-355 μm) and Exp 4 (sieve fraction 150-250 μm). Note the logarithmic scale on the abscissa. 52

Figure 4.1 Schematic illustration of the CC-PC process for the separation of enantiomers using the conglomerate forming system of asparagine monohydrate. TF symbolizes the temperature in the feed tank, T1 is the crystallization temperature in the D-Tank, T2 is the crystallization temperature in L-Tank, Blue and red filled circles symbolize growing enantiopure seeds of D-asparagine monohydrate (D-$AsnH_2O$) and L-asparagine monohydrate (L-$AsnH_2O$) in the D- and L-Tank, respectively. The filters (grey boxes) in the D- and L-Tank are used to retain solids. 59

Figure 4.2 Comparison of model simulations (solid lines) with experimental data for the mass fractions of D- and L-Asn in the D-Tank (left) and the L-Tank (right) (symbols). Error bars for experimental data are also shown. At time equals zero seeding is performed. Conditions are the same as in Table 4.2. 72

Figure 4.3 Comparison of model simulations (solid lines) with experimental data for the supersaturation ratios and the mass growth rates of the preferred enantiomer in the D-Tank (top) and the L-Tank (bottom) (symbols). Error bars for experimental data are also shown. At time equals zero seeding is performed. Conditions are the same as given in Table 4.2. 73

Figure 4.4 Model simulations of the concentration of enantiomers in the D-Tank (left) and the L-Tank (right) for the mean residence time of the liquid phase, τ, between 15 (base case) and 60 minutes. The remaining process parameters are the same as given in Table 4.2. At time equals zero seeding is performed. Note the difference in the scale of the abscissa. 74

Figure 4.5 Model simulations of the concentration of enantiomers in the D-Tank (left) and the L-Tank (right) for the enantiomeric excess of D-Asn, ee_D, of 0 (base case) to 6%. The concentration of the enantiomer in the feed solution is changed to 2.5 wt%. The remaining process parameters are the same as given in Table 4.2. At time equals zero seeding is performed. Note the difference in the scale of the abscissa. 76

Figure 4.6 Model simulations of the supersaturation ratio of the preferred enantiomer in the D-Tank (top) and the L-Tank (bottom) for a crystallization temperature, T_{cryst}, of 19 °C (base case) and 30 °C. The remaining process parameters are the same as given in Table 4.2. At time equals zero seeding is performed. 78

Figure 4.7 Model simulations of the supersaturation ratio of the preferred enantiomer in the D-Tank (top) and the L-Tank (bottom) for the fraction of feed solution entering the crystallizers, δ, between 0.5 (base case) and 0.6. The remaining process parameters are the same as given in Table 4.2. At time equals zero seeding is performed. The solubility is indicated at supersaturation ratio of unity. Note the difference in the scale of the abscissa. 80

Figure 4.8 Model simulations of the concentration of enantiomers in the D-Tank (left) and the L-Tank (right) for the mass of seeds, m_{seed}, between 0.5 g (base case) and 5 g. The remaining process parameters are the same as given in Table 4.2. At time equals zero seeding is performed. Note the difference in the scale of the abscissa. 82

Figure 4.9 Model simulations of the concentration of enantiomers in the D-Tank (left) and the L-Tank (right) for the different sieve fractions of the seeds, SF_{seed}, of 250-355 μm (base case), 200-250 μm, and 150-200 μm. The remaining process parameters are the same as given in Table 4.2. At time equals zero seeding is performed. Note the difference in the scale of the abscissa. 84

Figure 4.10 Model simulations of the concentration of enantiomers in the D-Tank (left) and the L-Tank (right) for the different values of the pre-exponential factor for the growth rate, k_0, i.e. 25 m/s (base case) and 50 m/s. The remaining process parameters are the same as given in Table 4.2. At time equals zero seeding is performed. Note the difference in the scale of the abscissa. 86

Figure B.1 Photograph of experimental setup for the preferential crystallization experiments. The small insert (lower left corner) shows the instrumentation in the crystallization vessels. Six individual pumps are necessary to run the setup in a continuous mode. B-3

Figure B.2 Schematic diagram of the CC-PC process for the preferential crystallization experiments. TF symbolizes the temperature in the feed tank, TF1 is the temperature of feed entering the D-Tank, T1 is the temperature in the D-Tank (C1), T2 is the temperature in the L-Tank (C2), TE1 is the temperature of mother liquor effluent from the D-Tank, T1-2 is the temperature of exchange stream from the D-Tank to the L-Tank and T2-1 is the temperature of exchange stream from the L-Tank to the D-Tank. Blue and red filled circles symbolize growing enantiopure seeds of D-AsnH_2O and L-AsnH_2O in the D- and L-Tank, respectively. The grey boxes in the D- and L-Tank represent filters for mother liquor exchange. B-4

Figure B.3 Assembling the parts of the crystallization units. B-4

Figure B.4 Components in the crystallization units. B-5

Figure B.5 Cooling unit and the connected tubes. B-6

Figure B.6 Control board on cooling unit. B-6

Figure B.7 Computer screen showing the interface of Logger Lite 1.6.1 software for temperature logging through the GO!Link thermocouple connection sensor. B-6

Figure B.8 Feed system. B-7

Figure B.9 Heating unit for feed system. B-8

Figure B.10 Purge system. B-9

Figure B.11 The polarimeter and the accompanied 1 mL cell used. B-10

Figure B.12 The densitometer with 1 mL sampling cell. B-10

Figure B.13 The SEM microscope at CEN, DTU. B-12

Figure C.1 Calibration curve and linear fit for the mass fraction difference between D-Asn and L-Asn in aqueous solution as function of the observed optical rotation. C-2

Figure C.2 Calibration curve and linear fit for the liquid density as function of the total concentration of enantiomers in aqueous solutions. C-3

Figure C.3 Calibration curve and linear fit for the mass fraction of L-AsnH_2O in aqueous solution as function of the observed optical rotation. C-4

Figure D.1 DSC and TGA thermograms for the solid product from the D-Tank in Exp 1 ((a) and (b), respectively). D-1

Figure D.2 DSC and TGA thermograms for the solid product from the L-Tank in Exp 1 ((b) and (d), respectively). D-2

List of Tables

Page

Table 1.1 Examples of APIs in pharmaceuticals and their biological activity. Trade names of pharmaceuticals approved by the Food and Drug Administration (FDA) in 2012 are given in parenthesis[25,48]. 2

Table 1.2 Sales of small-molecule chiral APIs in 2011. Sales are given in billion US$[59]. 4

Table 2.1 Crystallization modes commonly employed. The influence of solute solubility on the selection of crystallization mode is addressed[3]. 24

Table 3.1 Operational conditions for experiments conducted in triplicates. 42

Table 3.2 Summary of the results of the productivity, yield, and purity of solid product produced in experiments Exp 1-3 in both D-Tank and L-Tank and the additional experiment (Exp 4). Note the units. 49

Table 3.3 Summary of some statistical results of the productivity, yield, and purity for experiments Exp 1-3 in the D- and L-Tank. Note the units. 50

Table 4.1 Summary of the results of the U-value, yield based on feed solution, Y_L, productivity, Pr, the accumulated yield of solid products, and the yield in crystal size from the D- and L-Tank obtained by the simulation and experimental data[11], Y_S and Y. Note the units. Standard deviations for the experimental results are also given. 68

Table 4.2 Physical and chemical parameter values required for the mathematical model. 69

Table 4.3 Summary of the results of the U-value, yield based on feed solution, Y_L, productivity, Pr, the accumulated yield of solid products, Y_S, and the yield in crystal size, Y, from the D- and L-Tank obtained by the simulations for changing the mean residence time, τ, between 15 (base case) and 60 minutes. Note the units. 75

Table 4.4 Summary of the results of the U-value, yield based on feed solution, Y_L, productivity, Pr, the accumulated yield of solid products, Y_S, and the yield in crystal size, Y, from the D- and L-Tank obtained by the simulations for an enantiomeric excess of D-Asn, ee_D, between zero (base case) and 6%. Note the units. 77

Table 4.5 Summary of the results of the U-value, yield based on feed solution, Y_L, productivity, Pr, the accumulated yield of solid products, Y_S, and the yield in crystal size, Y, from the D- and L-Tank obtained by the simulations for different crystallization temperature, T_{cryst}, of 19 °C (base case) and 30 °C. Note the units. 79

Table 4.6 Summary of the results of the U-value, yield based on feed solution, Y_L, productivity, Pr, the accumulated yield of solid products, Y_S, and the yield in crystal size, Y, from the D- and L-Tank obtained by the simulations for the change in the feed fraction into the D-Tank, δ, between 0.5 and 0.6. Note the units. 81

Table 4.7 Summary of the results of the U-value, yield based on feed solution, Y_L, productivity, Pr, the accumulated yield of solid products, Y_S, and the yield in crystal size, Y, from the D- and L-Tank obtained by the simulations for the change in the mass of seeds, m_{seed}, between 0.5 g and 5 g. Note the units. 83

Table 4.8 Summary of the results of the U-value, yield based on feed solution, Y_L, productivity, Pr, the accumulated yield of solid products, Y_S, and the yield in crystal size, Y, from the D- and L-Tank obtained by the simulations for the different sieve fractions of the seeds, SF_{seed}, of 250-355 μm (base case), 200-250 μm, and 150-200 μm. Note the units. 85

Table 4.9 Summary of the results of the U-value, yield based on feed solution, Y_L, productivity, Pr, the accumulated yield of solid products, Y_S, and the yield in crystal size, Y, from the D- and L-Tank obtained by the simulations for the different values of the pre-exponential factor for the growth rate, k_0, of 25 m/s (base case) and 50 m/s. Note the units. 86

Table A.1 Features of fluidized bed crystallizers and stirred vessel crystallizers[87]. A-3

Chapter 1

Introduction

This chapter provides a concise introduction to the underlying motivations for the production of pure chiral active pharmaceutical ingredients (APIs) and outlines the potential and challenges of continuous processing in the pharmaceutical industry. Finally, the objectives of this thesis are outlined.

1.1 Background and motivation

Activity in biological systems, in terms of the specific interaction with a biological molecule, such as a receptor or enzyme, and the resulting physiological effects of chiral pharmaceuticals, depends strongly on the stereochemical configurations[17,58]. The term *chiral* is used to describe the three-dimensional property of a molecule which is nonsuperimposable with its mirror image, i.e. a molecule which lacks a plane of symmetry (Figure 1.1)[48,58].

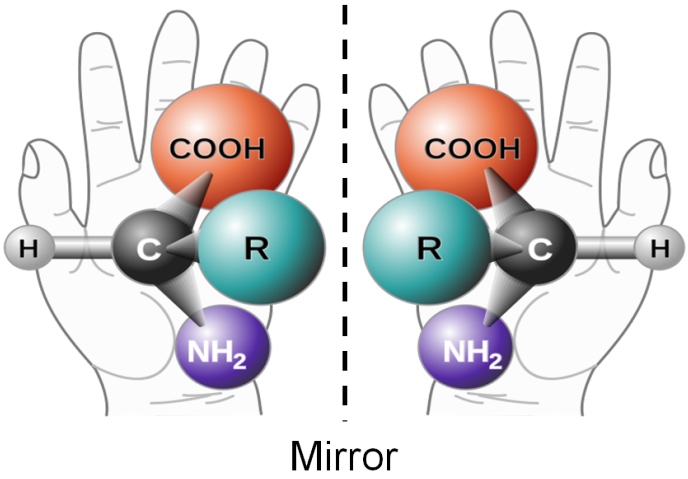

Figure 1.1: Amino acid molecules representing chirality, i.e. they are nonsuperimposable with their mirror images[64]. Only the backbone of the chemical structure of amino acids is shown. The C-atom in the backbone structure is regarded here as chirality center or stereocenter. R refers to the side groups of the amino acids and can also include chiral moieties.

A pair of chiral molecules are called *enantiomers* (from Greek '*enantios*' meaning

'*opposite*' and '*méros*' meaning '*part*')[48,58]. *Optical isomers* also refer to enantiomers due to the ability of rotation of the plane of polarized light according to the investigations of the French physicist Jean-Baptiste Biot in the early 19th century. Counterclockwise rotation of the plane of light is said to be *levorotatory*, denoted by L, and is by convention given a minus (–) sign. Clockwise rotation is said to be *dexorotatory*, denoted D, and is given a plus sign (+). Another notation based on the three-dimensional arrangement of substituents at a stereocenter is also commonly used. The stereocenter can either have either the (*R*) configuration (from Latin '*rectus*' meaning '*right*') or the (*S*) configuration (from Latin '*sinister*' meaning '*left*') depending on the priority of substituents[58].

A large number of chiral APIs are commercialized as mixtures of the enantiomers, so-called *racemic mixtures*. Side effects caused by different therapeutic, toxicological, and pharmacological properties of the enantiomers are in many cases attributed to the presence of the undesired enantiomer in the final pharmaceutical[48,71,79]. Table 1.1 lists examples of chiral substances in pharmaceuticals and their biological activity[25,48].

Table 1.1: Examples of APIs in pharmaceuticals and their biological activity. Trade names of pharmaceuticals approved by the Food and Drug Administration (FDA) in 2012 are given in parenthesis[25,48].

Chiral substance	**Biological activity**
Ethambutol (Myambutol)	Tuberculostatic effect is provided by the (*S*,*S*)-isomer; Optical neuritis, which can lead to blindness, is caused by the (*R*,*R*)-isomer
Penicillamine (Cuprimine, Depen)	Antiarthritic activity against joint disorder is provided by the (*S*)-isomer; Extreme toxicity is ascribed to the (*R*)-isomer
Thalidomide (Thalomid)	The desired antinausea effect (sedative) is provided by the (*R*)-isomer to treat morning sickness; Teratogenic effect causing fetal abnormalities, such as severely underdeveloped limbs, is ascribed to the (*S*)-isomer

The evident and dramatic consequence of administering thalidomide as racemic mixture in the 1960s has attracted great attention to the development of chiral pharmaceuticals[9]. This resulted in issuing guidelines in 1992 by the Food and Drug Administration (FDA) followed by the Japanese and Chinese authorities and the European Medicine Agency (EMA). The guidelines can be summarized in two main points[24]:

1. Specifications for the final chiral pharmaceutical should assure stereoisomeric composition regarding chemical identity, quality, and purity. This should be performed by the use of appropriate manufacturing and control procedures

2. Methods to quantify single enantiomers or mixture of enantiomers and evaluation of the pharmacokinetics of these should be available early in product development

Strict regulatory requirements, increasing public demand, and nevertheless, the fierce competition between pharmaceutical companies have initiated the intensive research devoted to the development of reliable and cost-efficient production processes to produce pure chiral APIs. These appreciated efforts can result in the following merits of producing pure enantiomers[48]:

- The pure enantiomer may have more than double the biological activity as the racemic mixture. Thus, the dosage for a patient is automatically halved and the side effects become less or diminish completely

- The unwanted enantiomer can be considered as waste in manufacturing comprising 50% of the mixture. Through chiroselective technologies, the yield of the production process can be doubled and the generation of waste reduced

- The physical properties, e.g. morphology, of pure enantiomer can improve downstream processing and formulation

- The opportunity of 'Racemic switching', i.e. the introduction of a pharmaceutical of pure enantiomer to market by redevelopment of existing pharmaceutical commercialized as racemic mixture, can be useful for extending patents

The above mentioned guidelines and the economic, environmental, and health concerns regarding the production and administration of pure enantiomers have to be strongly considered in the early stages of pharmaceutical discovery and process development. The reason is the possibility to reduce the time for product release to the competitive and new emerging markets by having a more biologically effective and safe pharmaceutical which reduces the risk of rejection during clinical trials and the approval process[48].

In 2000, about one-third of pharmaceutical sales were single-enantiomer pharmaceuticals comprising 133 billion US$ and expected to hit 200 billion US$ in 2008[81]. About 40% of the pharmaceuticals in use in 2006 were chiral. In 2011, small-molecule chiral pharmaceuticals comprised about 43% (57.2 billion US$) of the sales of top 20

global pharmaceutical products (Figure 1.2)[59]. Table 1.2 lists the sales of chiral small-molecule APIs in 2011[59]. Geographically, the consumption in the United States of chiral fine chemicals, including pharmaceuticals, comprises 60% of the worldwide total consumption. This makes USA the World's largest market for chiral fine chemicals[48].

Table 1.2: Sales of small-molecule chiral APIs in 2011. Sales are given in billion US$[59].

Rank	Brand	API	Manufacturer	Sale
1	Lipitor	**Atorvastatin**	Pfizer	**12.5**
2	Plavix	**Clopidogrel**	Bristol-Myers Squibb	**9.3**
3	Seretide	**Fluticasone**	GlaxoSmithKline	**8.7**
4	Crestor	**Rosuvastatin**	AstraZeneca	**8.0**
5	Nexium	**Esomeprazole**	AstraZeneca	**7.9**
11	Singulair	**Montelukast**	Merck & Co.	**6.1**
17	Cymbalta	**Duloxetin**	Eli Lilly & Co.	**4.7**

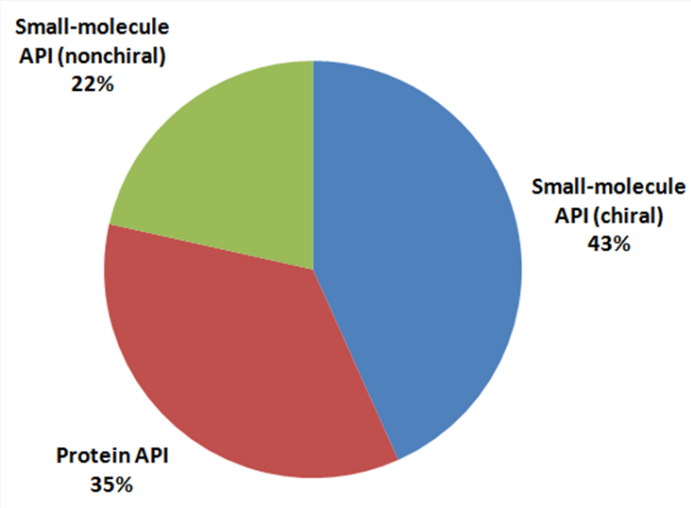

Figure 1.2: Distribution in percentage of 2011 sales of chiral and nonchiral small-molecule APIs and protein APIs of the top 20 global pharmaceutical products[59]. Racemic APIs are included in chiral small-molecule APIs segment. Note that protein APIs are often chiral in nature and consist of amino acids of the naturally occurring L-form. Total sales of top 20 pharmaceuticals in 2011 was 132.1 billion US$.

In this respect, strategic decisions have to be made in order not to lose market while implementing Lean manufacturing principles to ensure sustainability and long-term viability. An important issue to consider in the decision-making process is the full or partial conversion from batch to continuous production of APIs, chiral as well as nonchiral. It is essential to consider the fact that existing batch processes have already been approved by the demanding authorities, and converting to continuous operation,

either by retrofitting or new establishments, has to be documented and approved once again[65]. Additionally, the existing infrastructure in the pharmaceutical industry is designed for batch processing and needs to be fitted for continuous manufacturing. Nevertheless, increasing demand, strict regulatory requirements, and the strong competition have forced the pharmaceutical industry to strongly consider the continuous alternative in product and process development as a mean for the reduction of manufacturing cost, environmental impact, and social responsibility[3,12,65].

1.2 Batch vs. Continuous

Continuous operation provides many advantages and is highly attractive from an environmental, economical, and regulatory point of view compared to batch processes. For instance, in theory, a continuously stirred tank reactor (CSTR) ensures ideal mixing in the reactor. This means that all molecules in the reactor experience the same reaction conditions. In practice, there exist differences due to residence time distribution effects, which have to be taken into account in the design stage of a CSTR[23]. Critical process parameters are easily controlled in time-invariant, steady-state operation compared to the time-dependent batch operation[87]. Higher yields and reproducible product quality are achievable due to the reduction of batch-to-batch variations by the implementation of online measurement techniques, as part of Process Analytical Technology (PAT) tools, to reduce the time delay between offline measurements and corrective actions. Continuous operation also allows for reduction of large processing volumes of potentially volatile and flammable or toxic compounds. Thus, the costs associated with adopting expensive risk management tools and protection measures can be significantly reduced. Finally, as part of Lean manufacturing principles, continuous operation can significantly reduce the environmental footprint and manufacturing costs or cost of goods (COGs). Figure 1.3 shows the distribution of the costs and revenue as percentage of sales in 2008 averaged over 17 major pharmaceutical companies[3]. As shown in Figure 1.3, the COGs comprises 27% of sales[3]. The application of continuous processing in API manufacturing can potentially reduce the COGs. All in all, the results are a cheaper and a more safe manufacturing process. Because of the mentioned, and other equally important reasons, research in continuous processing in general has been ranked as first in key green research areas[44].

Nevertheless, there are some pronounced disadvantages of continuous manufacturing. Processes run in batch mode are often less complex and process understanding level of batch processes are typically high. Continuous processing therefore requires a higher level of process understanding, especially when complex hazardous reactions are in-

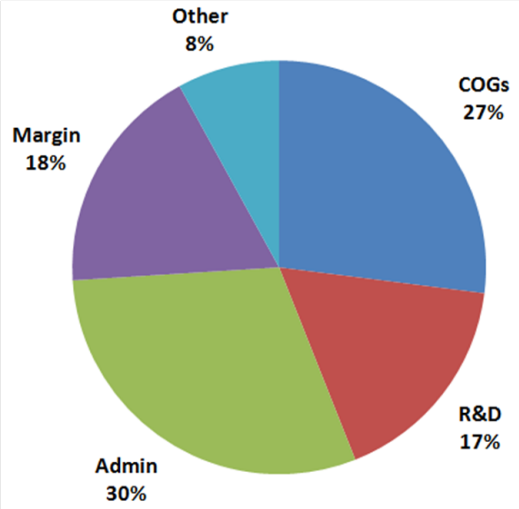

Figure 1.3: Distribution of the average costs as percentage of sales in 2008 for 17 major pharmaceutical companies[3].

volved. Batch processes provide higher level of flexibility and versatility compared to continuous processes. A continuous process, once developed and implemented, is dedicated for a certain reaction or separation and therefore changes in equipment setup, inventory, and operation protocols are necessary when considering another reaction or separation. In this respect, flexibility of the continuous process should be strongly considered in the early stages of process development. For these reasons, and the fact that in the pharmaceutical industry, where often a very small amount of product is required, it is difficult to justify the effort connected to startup and shutdown, and the amount of material required for the establishment of steady-state conditions, the above mentioned advantages of continuous operation can often be lost. Furthermore, collection of the product at equilibrium conditions is permitted in batch operation and not in a continuously operated process. Finally, frequent cleaning of the equipment without disturbing the system is allowed in batch operation, which adds to the advantages of interest in the pharmaceutical industry[3,87].

Having in mind the mentioned advantages and disadvantages of batch and continuous operation, it should be noted that even when batch operation is considered the most attractive choice in the fine chemicals industry, including the pharmaceutical industry, there are some reactions and separations for which batch operation is impractical. Reactions involving hazardous chemicals at exceptionally high or low temperatures and pressures and separation of chiral compounds are examples for which continuous operation is the only suitable choice[3,87].

1.3 Project objectives

The strict regulatory requirements and the increased public demand for the development and production of pharmaceuticals consisting of pure enantiomers have resulted in extensive research to find potential sustainable alternatives to existing production processes. The current production processes in the fine chemical industries, including the pharmaceutical industry, are mainly dominated by batch mode operation. An increased understanding of process complexity regarding chemical reactions and transport phenomena in continuous operation, and the change in the infrastructure of manufacturing are essential in order to convert to the potentially more sustainable continuous operation. The objectives of the work presented in the subsequent chapters are to gain insight into the separation of enantiomers from racemic mixtures by preferential crystallization (PC), and to investigate the performance of a newly developed continuous preferential crystallization process for the separation of enantiomers from a racemic mixture. It is furthermore the objective of this project to develop a model of the continuous PC process to increase the understanding of the complex behavior of preferential crystallization in the continuous PC process.

1.4 Outline of thesis

In chapter 2, a literature survey concerning the methods currently available for the production of pure enantiomers, crystallization process objectives and constraints in the pharmaceutical industry, the underlying fundamentals of crystallization and thermodynamics of racemic mixtures are presented. The insight into the fundamental aspects of preferential crystallization as a chiroselective separation method for the separation of enantiomers from racemic mixtures provides the theoretical foundation for the subsequent investigation of the continuous PC process.

The experimental realization of the separation of enantiomers by preferential crystallization in the newly developed continuous PC process is presented and discussed in chapter 3. In this respect, special attention is paid to the achievement of simultaneous separation of enantiomers by crystal growth and the maintenance of racemic composition in the liquid phase. The process is evaluated in terms of productivity, yield, purity, and the fraction of unutilized enantiomer in the purge. The robustness of the process is also assessed.

In chapter 4, the development of a transient one-dimensional model describing the continuous PC process is provided. Furthermore, the validation of the model against experimental data is presented and an investigation of the influence of the different process parameters on the predictability of the model and performance of the process

is provided.

Finally, in chapter 5 conclusions and suggestions for future work are presented.

1.5 Conclusions

In this chapter, the background and motivations for the production of pure chiral APIs were highlighted. Additionally, the potential and challenges of the conversion from conventional batch processing to continuous processing in the pharmaceutical industry were outlined and discussed. Finally, the objectives of the work, presented in the thesis, were outlined.

Chapter 2

Literature survey

In this chapter, a concise overview of the current methods for the production of pure enantiomers is provided. Emphasis is placed on the design criteria and constraints of crystallization processes in the pharmaceutical industry. The underlying thermodynamic aspects of solid-liquid phase equilibria of chiral systems and crystallization theory are also presented. The content of this chapter provides the basis for the work presented in the remaining part of the thesis.

2.1 Methods for the production of pure enantiomers

Currently, several methods exist for the production of pure enantiomers depending on the chemical and physical nature of the raw material used (Figure 2.1). It should be emphasized that enantiomers are considered pure at an enantiomeric excess above 90%[78,79].

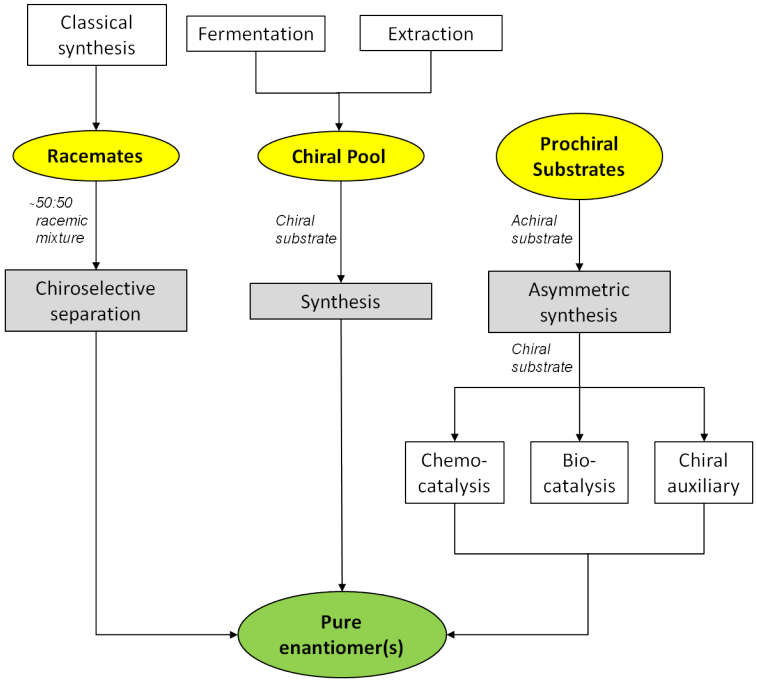

Figure 2.1: Current methods for obtaining pure enantiomers[78,79].Racemates refer to racemic mixtures consisting of equal quantity of enantiomers.

As shown there are three main routes for obtaining pure enantiomers. The first option is the conversion of a prochiral substrate by asymmetric synthesis. The synthesis can be performed either chemocatalytically, enzymatically, or by chiral auxiliary, e.g. chiral additive. The reactions involved are often complex and most commonly divided into four types depending on the controlling mechanism: 1) Auxiliary-controlled, 2) catalyst-controlled, 3) reagent-controlled, and 4) substrate-controlled[51]. A strong constraint to the commercial application remains in the economical aspect of such selective synthesis processes due to difficulties in fulfilling required success criteria in terms of time-to-process (labor), cost-to-process (development), and production costs[3,71]. In this respect, the use of expensive chiral auxiliaries as well as catalysts or enzymes requires efficient recovery systems to essentially improve process economy[78].

The second option is the utilization of a chiral substrate from a chiral pool followed by synthesis. The substrate is obtained from either *de novo* fermentation of e.g. sucrose or extraction of naturally occurring chiral compounds, e.g. amino acids, where one single enantiomer often exists in nature. This is probably the easiest and cheapest method because of two reasons: 1) Chiral substrates from the chiral pool are most often present in large amount, and 2) process and production costs are low[79].

The chiroselective separation of enantiomers from racemates, i.e. mixture of equal quantity of enantiomers, comprises an attractive option for the production of pure enantiomers. The reason is that the yields of asymmetric synthesis are often low, while chiral separation techniques can provide higher yields of each enantiomer. However, chiral separation techniques are considered expensive and inefficient in case the unwanted enantiomer is not utilized[71]. The most commercially utilized technique is chiral chromatography with its wide selection of chiral stationary phases. This allows the separation of a wide range of racemic mixtures[26,27,82]. A version of chiral chromatography successfully applied in industrial scale is continuous countercurrent Simulated Moving-Bed (SMB) Chromatography realizing the goal of achieving optically pure enantiomers[26,27]. However, highly expensive chiral stationary phases, high pressure equipment, and use of substantial amount of solvent have initiated the search for relatively cheaper alternatives, e.g. PC technology[14,21,28,41,54,66,67,91]. In this respect, process economical considerations and regulatory requirements concerning optical purity and operation safety have to be taken into account in order to assess the economical and technical feasibility of each alternative or a combination thereof, e.g. PC combined with chiral membrane technology[83].

2.2 Crystallization in the pharmaceutical industry: Objectives and constraints

In the fine chemical industries, including the pharmaceutical industry, crystallization is used to accomplish two main objectives: 1) Separation and purification of the API, and 2) the achievement of physical attributes of the produced crystals suitable for subsequent downstream processing, formulation, and bioavailability. The constraints underlying the design of the crystallization process to achieve these objectives comprises economic and manufacturing considerations, such as throughput, yield, scaleability, and environmental impact[3,87].

2.2.1 Separation and purification

The initial point in the design of the overall API production process is the understanding of where in the production process it is necessary to meet purification requirements for the isolated intermediates. Normally, the production of an API involves a multistep synthesis procedure to convert raw materials to the desired API compound in high purity (typically above 99%)[3,4]. In this multistep procedure, a number of intermediate crystallization processes is usually used to achieve the desired purity of the separated intermediates, whereas the final crystallization step is mainly focusing on the control of the final physical attributes of the API crystals[3]. In this respect, it should be addressed that thermodynamics is often regarded as the primary control for achieving separation and purification, while crystallization kinetics, and the mechanisms involved, are often the primary determinant of the physical attributes of the produced API crystals[3,62,87].

2.2.2 Product attributes and performance

The influence of the physical attributes of the solid product of an API on subsequent downstream processing, e.g. filtration, formulation, and bioavailability, are of outmost importance for designing the appropriate crystallization processes. Attributes of the API product of particular concern include[8,38,42,43,46,53,84,87]:

- Solubility
- Melting point
- Dissolution rate and bioavailability
- Chemical and physical stability
- Powder properties, such as flowability, bulk density, and compressibility

Different solid forms of an API exhibiting different crystal structures, particle size distribution (PSD) of the API, the morphology of solid product, and its flow properties, e.g. suspendability, are important to consider to achieve the above mentioned attributes of the final API product[8,38,42,43,46,53,84,87,88]. In this respect, the involved crystallization processes should be studied in conjunction with subsequent downstream processes as depicted in Figure 2.2.

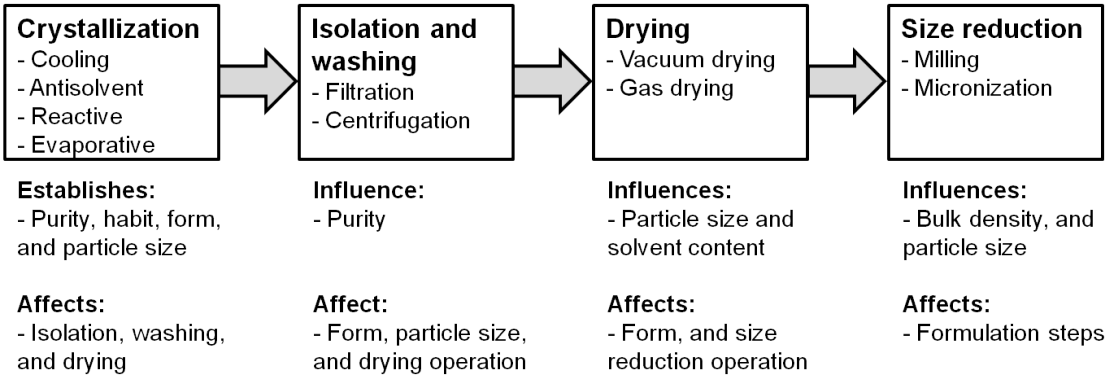

Figure 2.2: A schematic diagram showing the crystallization process in conjunction with the subsequent downstream processing steps and their effects on solid product attributes[3].

Often an API intermediate is produced with properties that are based on considerations regarding chemical and physical stability, flowability, and ease of manufacture. In contrast, performance in the host system in terms of dissolution rate, bioavailability, and chemical and physical stability together with manufacturability, e.g. compressibility, melting point, and bulk density, are of outmost importance for a final API[10,30].

2.2.2.1 Solid forms of an API

Solids of pharmaceutical compounds can have two different solid forms. They can be either amorphous or crystalline depending on the crystallization conditions. Figure 2.3 shows the different classes and subclasses of solid forms an API can exhibit[1,3,87,88]. Amorphous solids, such as the polymeric pharmaceutical substance sevelamer hydrochloride[6], can be produced by very rapid crystallization[3,62,87]. Pharmaceuticals produced as amorphous solids are primarily made to improve the solubility and dissolution rate in the host, but at the expense of chemical and physical stability of the pharmaceutical[49]. Besides solid state instability of the amorphous solid, it has complications with impurity rejection and difficulties in downstream processing, e.g. filtration, and formulation. Amorphous solids also cause difficulties with the analysis methods usually used for solid phase analysis such as X-Ray Powder Diffraction (XRPD), microscopy, and Differential Scanning Calorimetry (DSC). It should be emphasized that even when a stable crystalline solid is formed it can loose its crystallinity

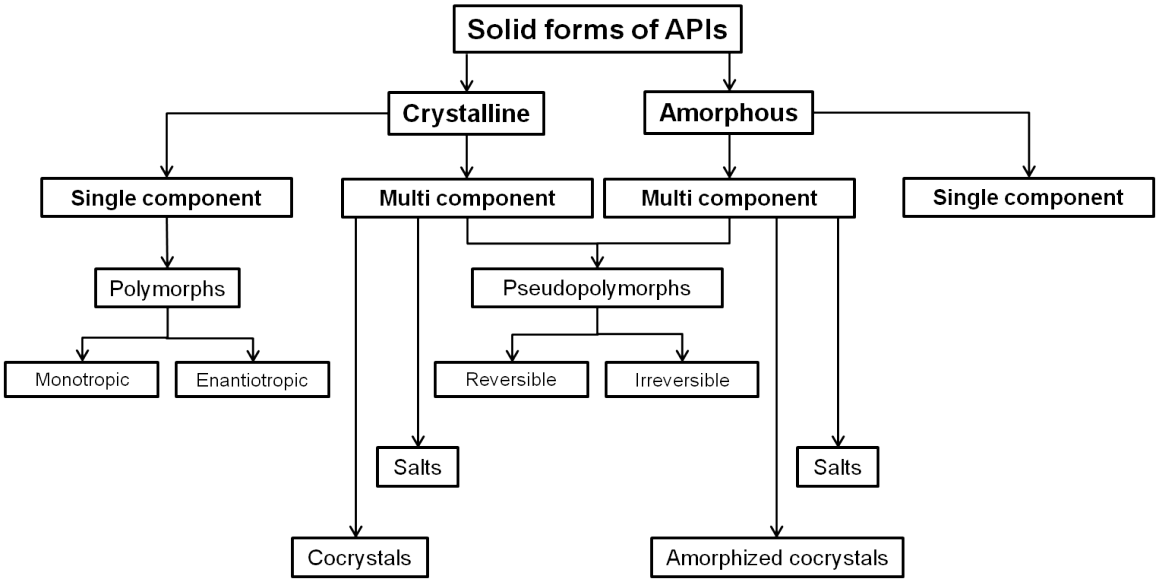

Figure 2.3: A schematic diagram showing the different solid forms an API can exhibit. Note that for multicomponent forms different polymorphs and pseudopolymorphs can also exist[1,3,87].

forming amorphous solid if it is hygroscopic, i.e. absorbs water, or exposed to heat or pressure in subsequent drying or comminution, respectively. For instance, crystalline carbamazepine dihydrate becomes amorphous anhydrate upon dehydration[50]. Therefore, attention should be paid to storage conditions and conditions of downstream processing[87,88].

APIs can crystallize in different crystal structures. This phenomenon is referred to as *polymorphism*. The different crystal structures are called *polymorphs*. Polymorphs crystallizing as mirror-images of each other are referred to as enantiomorphs, e.g. enantiomers[62]. Polymorphs exhibit different chemical and physical properties, and can either be monotropic or enantiotropic as in the case of polymorphs I and III of a reverse transcriptase inhibitor[87,88]. Polymorphs having a monotropic relationship have only one polymorph as the stable form at all temperatures considered. In contrast, an enantiotropic relationship between polymorphs implies that the different polymorphs are stable at different temperatures. In this respect, the polymorph exhibiting the lowest solubility at the conditions employed is the stable form[62]. It is therefore essential to control the conditions of crystallization to obtain the desired polymorph. Then it is necessary to prevent the transformation of the desired polymorph to another polymorph. This transformation is referred to as *polymorphic transition*[3,62,88]. Therefore, the stable polymorph of an API should be identified in the early stages of pharmaceutical development to avoid the time consuming reevaluation of previous development results, and in worst case, the recall of the pharmaceutical[73].

Crystalline and amorphous solids can also form pseudopolymorphs, i.e. solvates or hydrates (the organic solvent is replaced with water), as in the case of dirithyromycin acetone solvate[99] and asparagine monohydrate, respectively. Pseudopolymorphs form different forms of crystals with distinct chemical and physical properties. The formation occurs when one or more solvent or water molecules are incorporated into the crystal lattice of the crystalline solid by noncovalent bonds to the API molecules. Noncovalent bonds comprise hydrogen bonding, π-stacking, or van der Waals interactions[3,62,87,88]. Pseudopolymorphs can be either reversible or irreversible. Reversible pseudopolymorphs can loose solvent or water molecules from the crystal lattice without significant change in the crystallinity of the solid[90]. In contrast, for irreversible pseudopolymorphs the removal of solvent or water molecules results in nonsolvated or anhydrous crystalline or amorphous solid[62,87].

Cocrystals are regarded as a special case of pseudopolymorphs where solvent or water molecules in the crystal lattice are replaced by a nonvolatile species bonded noncovalently to the parent crystal lattice of the API crystal[1,3,88]. An example is the cocrystal of ciprofloxacin and norfloxacin[89]. Cocrystals can also form different polymorphs and different solvates or hydrates as shown in Figure 2.4.

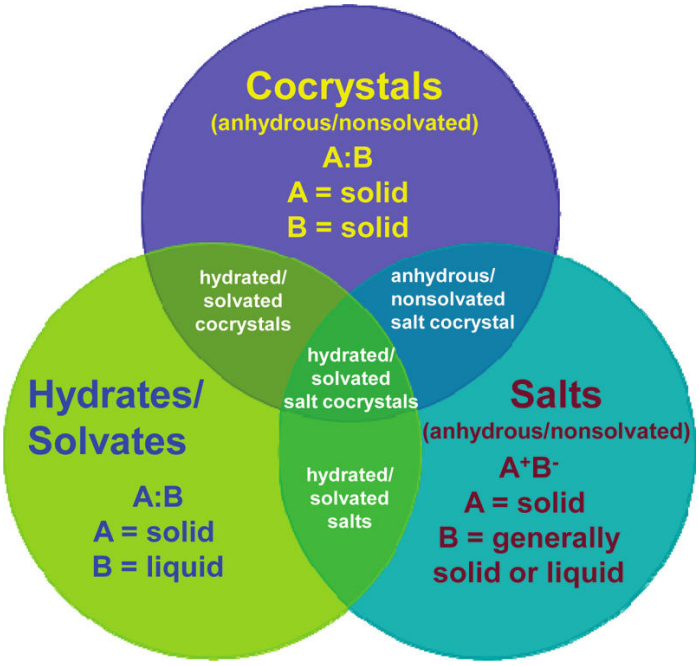

Figure 2.4: The different multicomponent solid forms of an API and the overlap between them[1].

If the nonvolatile species incorporated are removed, e.g. by exposing the cocrystals to pressure, the cocrystals can loose its crystallinity and form an amorphous solid. Amorphous solids can also form amorphized cocrystals with different chemical and physical properties. If the nonvolatile species is removed, the amorphized cocrystal

can be converted to a crystalline solid or remains amorphous[1,88].

Organic molecules, such as APIs, have often poor water solubility. To improve their water solubility, salts of APIs are often produced. Thereby, the bioavailability of the API is also improved. In some cases, however, it is the only way to achieve a solid product of the desired API or API intermediate, e.g. diastereomeric salt of (*S*)-ibuprofen-(*S*)-lysine[87]. Salts of APIs are normally produced by reactive crystallization in which neutralization of the API by an acid or a base occurs[87]. The acid or base may be an ionic compound, e.g. sulfate in crixivan sulfate salt[87], or another organic compound, e.g. (*R*)-mandelic acid in (1*S*,4*S*)-sertraline-(*R*)-mandelic acid[36]. The produced salt of an API exhibit different chemical and physical properties. Therefore, the desired salt and its chemical and physical stability should essentially be considered early in API development[3,87].

2.2.2.2 Particle size and PSD

An important concern in the production of APIs is the particle size and PSD. The particle size in the pharmaceutical industry is commonly estimated through PSD measurements by laser diffraction techniques such as Lasentec FBRM®. The PSD measurements are used to evaluate the particle size based on the x_{90}, x_{50}, and x_{10} measures corresponding to the particle size at which the cumulative mass or volume is 90%, 50%, and 10%, respectively[3].

The importance of particle size lies in its impact on the performance of the final pharmaceutical product because:

- *in vitro* specifications, e.g. solubility and dissolution rate, can be significantly affected by particle size. Assuming spherical particles, the solubility increases for decreasing particle size and vice versa, according to Gibbs-Thomson equation[62]. With respect to the dissolution rate, a decrease in particle size increases the dissolution rate and vice versa. The reason is the lower surface area to volume ratio[52].
- The final pharmaceutical product from formulation, e.g. mixing with excipients, tabletting, or capsule filling, can be affected by particle size through e.g. suspendability and compressibility. Furthermore, particle size affects uniformity of the final pharmaceutical product, i.e. the amount of API in each unit of final product, and product appearance, such as color and shape[3].

Additionally, the PSD of the produced API has great influence on the production cost due to its effects on the efficiency of downstream unit operations such as filtration

and drying. Thus, to meet the requirements for an economical API production, the defined objective regarding the final PSD of an API should be pursued by controlling all the variables affecting the crystallization process within an acceptable range which is determined by the chemical and physical nature of the product, solvent used, and impurities present. In this respect, seeding provides an excellent way for controlling particle size along with PSD and morphology[62,87].

2.2.2.3 Morphology and flow properties

A property of crystals that make them unique and distinct from gaseous or liquid materials is *crystal habit* or *morphology*. Thus, only the appearance of crystals is reflected by the morphology, and not the internal structure[87]. In the pharmaceutical industry, the most commonly used techniques for the elucidation of the morphology are optical microscopy or Scanning Electron Microscopy (SEM). The frequently observed crystal morphologies are shown in Figure 2.5[3].

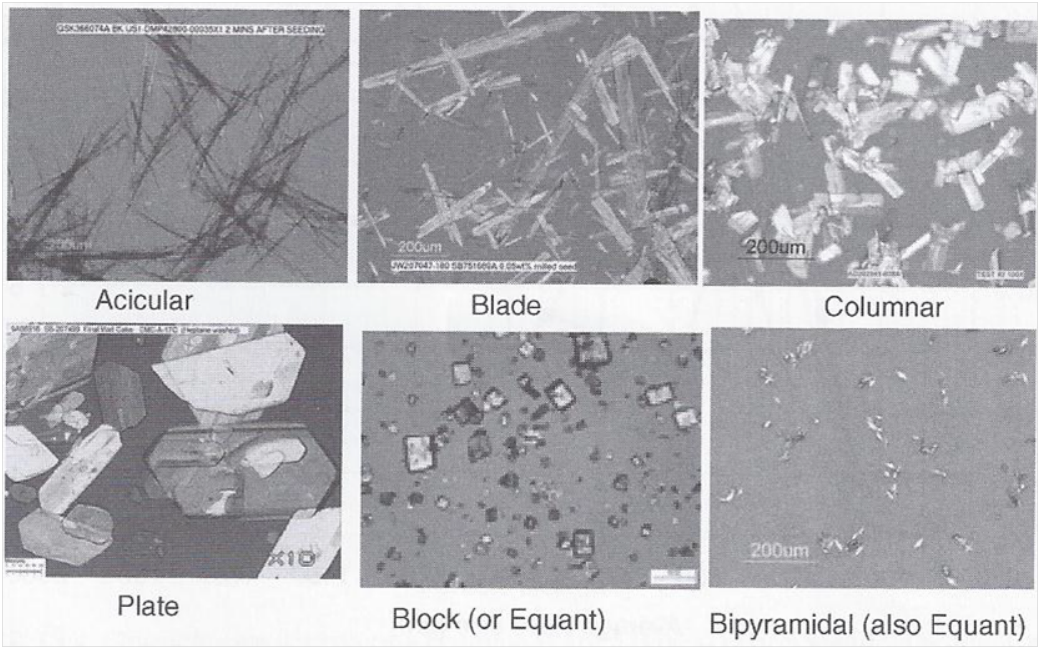

Figure 2.5: Crystal morphologies frequently observed in the pharmaceutical industry[3].

Essentially, the morphology of the solid product affects flow characteristics of powder or slurry of the product. The reason is that particles with different morphologies have different characteristic lengths affecting the PSD of the product. Crystal morphology affects the rheological properties of the crystallizing suspension, the efficiency of downstream processing such as filtration or centrifugation, the bulk density of the solid, and the flow properties of the solid measured by the Hausner ratio[62,74,84,87]. In this respect, acircular, thin blade, and plate-like crystals, with a Hausner ratio greater than 1.4, poses difficulties in downstream processing resulting in long isolation times,

agglomeration, crystal breakage or attrition, and poor flowability and solid transport properties. Columnar, block-like, and pyramidal crystals, with a Hausner ratio less than 1.2, are in contrast easier to isolate, dry, and handle. The reason is the relatively low surface area to volume ratio, which in turn affects the solubility and dissolution rate of the API[3]. Impurities, solvent used, mixing, and supersaturation levels influence the final morphology of the product crystals along with the particle size and PSD. Therefore, the control of these critical crystallization process variables are an important and integral part of the assurance of target product quality attributes. A way of controlling crystal morphology is thus the use of seed crystals as a template for the desired target morphology. However, seeding solely does not ensure the achievement of the target morphology because growing seed crystals can change morphology due to supersaturation fluctuations and impurity incorporation[3,84,87].

2.3 Solid-liquid phase equilibria of chiral systems

As for any crystallization process, the knowledge to thermodynamics and kinetics, and their interconnections, is essential for API crystallization, where requirements for purity, particle size, and morphology are determining for biological activity of the active compound[54,62,88,93]. It is well-known that chiral active ingredients are able to form three different types of solid-liquid phase equilibria[41,54,62,93]:

1. Conglomerate forming system
2. Racemic compound forming system
3. Pseudoracemate forming systems

Describing the solid-liquid phase behavior of a racemic mixture of two enantiomers is usually illustrated by a binary melting point phase diagram. In the presence of an additional phase created by solvent(s), a ternary solubility diagram is useful to illustrate the solid-liquid phase behavior[54,62,93]. These systems and their relation to PC, for which the determination of the thermodynamically stable phase and key solubility data are essential for design and operation, are described in the following sections.

2.3.1 Conglomerate forming systems

Solid-liquid phase behavior of conglomerate forming systems include the formation of a *conglomerate*, which is an eutectic mixture of pure crystals of the two enantiomers[41,54]. The fraction of racemic mixtures of organic compounds that exist as conglomerates is estimated to 5-10%[20,54,93]. Examples are 4-hydroxy-2-pyrrolidone,

an important intermediate in the synthesis of many active compounds[92], modafinic acid, an intermediate in the synthesis of modafinil[97], and the amino acids threonine[20] and asparagine monohydrate[86] used in food supplements. The ternary solubility phase diagram for a nonsolvated conglomerate forming system is shown in Figure 2.6 for the simplest case of two enantiomers crystallizing from a solution[54,62,93].

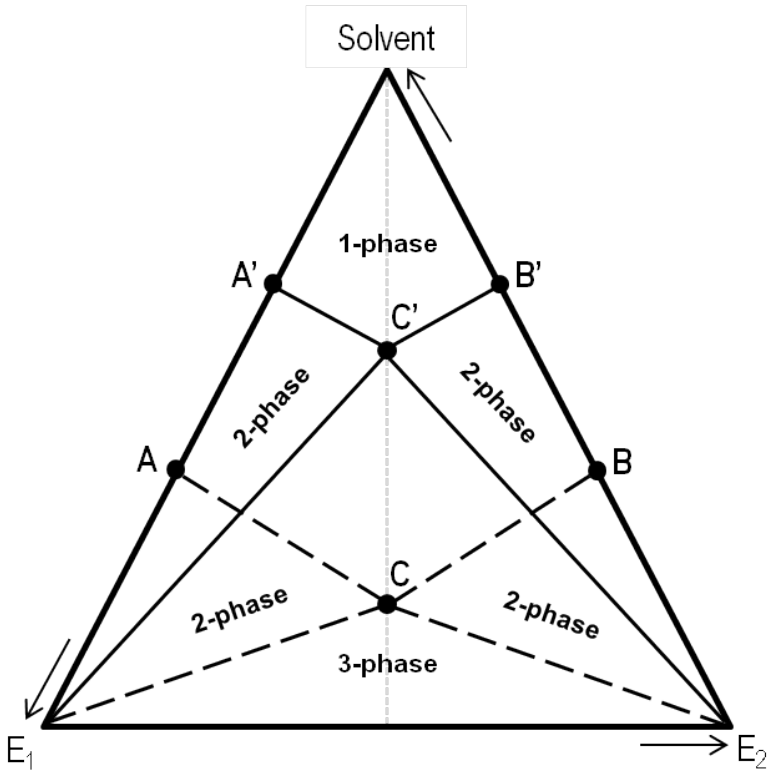

Figure 2.6: Ternary phase diagram of a simple nonsolvated conglomerate forming system[62,93]. E_1 and E_2 represent enantiomer 1 and enantiomer 2, respectively. The dashed and solid lines correspond to the composition dependent solubility curves at one temperature and at a lower temperature, respectively.

Points A and B correspond to the solubility of E_1 and E_2, respectively, at one temperature, and points A' and B' correspond to the solubility of E_1 and E_2, respectively, at a lower temperature. Points C and C' correspond to the eutectic composition, i.e. the solubility of the conglomerate, at one temperature and at a lower temperature, respectively. The 1-phase region consists of undersaturated solution of enantiomers in solvent. The 2-phase regions E_1AC and E_1A'C' consists of solids of pure E_1 and saturated solution at one temperature and at a lower temperature, respectively. Similarly for E_2, the 2-phase regions E_1BC and E_1B'C' consists of solids of pure E_2 and saturated solution at one temperature and at a lower temperature, respectively. Finally, the 3-phase region consists of a liquid phase racemic mixture of the two enantiomers and a solid phase existing as a conglomerate of the two pure enantiomers[20,62,93].

For solvated or hydrated conglomerate forming systems, where the two pure enan-

tiomers and the racemate or only the two pure enantiomers form solvate or hydrate with the solvent, the phase behavior definitely changes. The formation of solvated solids of pure enantiomers can have significant effect on the chemical stability of the solid. Furthermore, solvated solids of enantiomers can have significant effects on downstream processing, such as filtration, and bioavailability[93].

Some of the chiroselective separation technologies developed suitable for the separation of enantiomers forming conglomerates are PC in batch crystallizers coupled via crystal-free mother liquor exchange[20,21,66], and pilot and commercial scale continuous fluidized-bed crystallizers with sonication[28,87]. A common prerequisite is that the solubility of the conglomerate is sufficiently higher than the solubility of pure enantiomer. In the former, the liquid solutions in the crystallizers, each seeded with seed crystals of pure enantiomer, are maintained at a nearly racemic composition to suppress or completely avoid the nucleation of the unwanted enantiomer in the crystallizers. This is achieved by the crystal-free liquid exchange streams coupling the crystallizers presuming that crystallization kinetics of the enantiomers are identical in the crystallizers. A drawback is, however, the decrease in the crystallization driving force due to the consumption of the crystallizing species for crystal growth[21,66]. This problem can be solved by manipulating the crystallization temperature profile to enhance the crystallization driving force, thereby improving process performance[21]. A continuous process is however desirable and in this respect the fluidized-bed technology provides an excellent solution. In the continuous process, seed crystals are continuously generated by sonication of the crystallizing suspension while racemic liquid feed solution is continuously supplied. The grown seed crystals are removed by elutriation and the removed mother liquor is transferred back to the feed solution. The nucleation of the unwanted enantiomer is suppressed by controlling the supersaturation level of the enantiomer. This is performed by controlling the PSD of the seed crystals in the crystallizing suspensions[28,87]. Features of stirred vessels crystallizers and fluidized-bed crystallizers are listed in Appendix A.1.1.

2.3.2 Racemic compound forming systems

Racemic compound forming systems are the most common type of racemic mixtures corresponding to about 90-95% of chiral API. The formed racemic compound, also referred to as *true racemate*, corresponds to a crystalline racemic mixture in which the two enantiomers are present in a 1:1-ratio in a well-defined arrangement within the same crystal lattice[41,54]. Examples are the APIs ketoprofen[56] and sertraline[7]. The ternary phase diagram of a simple nonsolvated racemic compound forming system is shown in Figure 2.7[54,62,93].

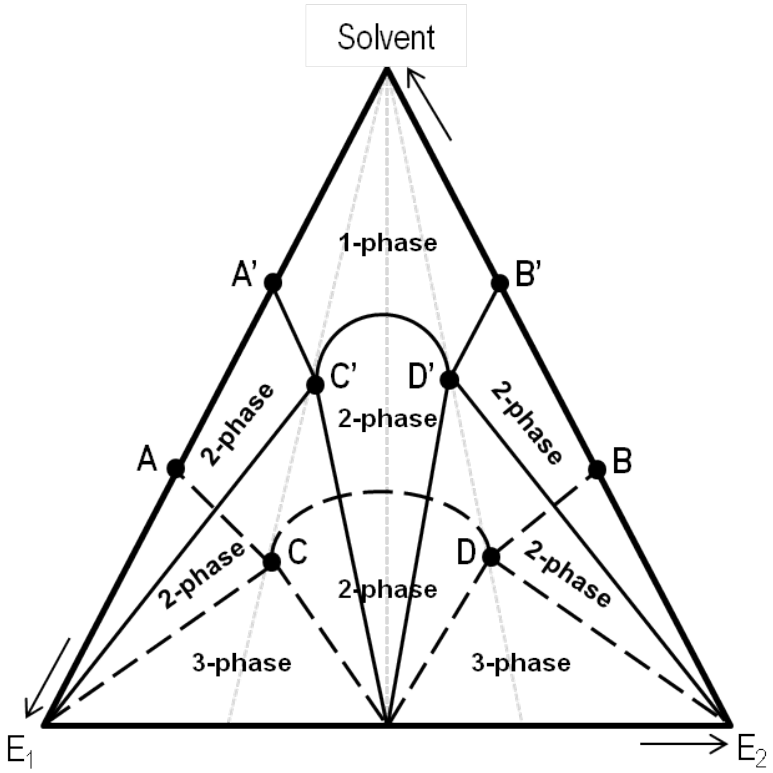

Figure 2.7: Ternary phase diagram for a simple nonsolvated racemic compound forming system[62,93]. E_1 and E_2 represent enantiomer 1 and enantiomer 2, respectively. The dashed and solid lines correspond to the composition dependent solubility curves at one temperature and at a lower temperature, respectively.

In the ternary phase diagram, the solubility of the racemic compound corresponds to the point at the maximum between the two eutectic points, e.g. C and D. Point C represents the eutectic composition consisting of solids of enantiomer E_1 and racemic compound in equilibrium with a saturated solution enriched with E_1. Similarly, D represents the equilibrium conditions for E_2. The regions defining the presence of pure enantiomers and the width of these regions are defined by the position of the eutectic points. If the crystallization process is performed with solution composition between the eutectic points, e.g. C and D, the racemic compound will crystallize as solid. In the regions to the left and right of the middle region, where the racemic compound can be formed, an equilibrium occurs between crystals of one of the pure enantiomers and a saturated solution. Crystallization of the pure enantiomers is achievable in these regions, but the feasibility of the crystallization process depends strongly on the position of the eutectic composition points, i.e. the width of the middle region, and the solubility of the racemic compound, i.e. the position of the point at the maximum between the eutectic points[41,54,55,62].

The main differences between the ternary phase diagram of a conglomerate forming system and racemic compound forming system are[41,54,93]:

- Change in the shape of 1-phase region of unsaturated solution
- Shrinkage of the 2-phase regions, i.e. solid and saturated solution
- An additional 2-phase region where the solid phase of the racemic compound appears with saturated solution
- Two separated 3-phase regions where the solid phases appear as physical mixtures of pure enantiomers and racemic compound and saturated solution

The borders of the different regions in the ternary solubility phase diagram are strongly dependent on temperature. For evaluation of the feasibility of crystallization of one pure enantiomer from a racemic compound forming system, the eutectic enantiomeric excess (*ee*) plays a major role. This factor is dependent on temperature and solvent used in the system. Typically, if the initial enantiomeric solution has a lower initial *ee* than the eutectic *ee*, a certain degree of enrichment of the desired enantiomer in solution is required to facilitate crystallization of this particular enantiomer. This enrichment has to be provided before the actual crystallization and can be provided by e.g. SMB chromatography. If the initial enantiomeric solution has a higher initial *ee* than the eutectic *ee*, pure enantiomer can be obtained in the solid phase if enough solvent is added to alter system composition to enter the 2-phase region[54,93].

As in the case of conglomerate forming system with solvate, racemic compound forming system forming solvate exhibit three different ternary phase diagrams, where only the racemic compound forms a solvate, or only the pure enantiomers forming solvates, or both the racemic compound and the pure enantiomers form solvates[93]. As in the case of solvated or hydrated conglomerates, the presence of solvent molecules in the enantiopure solids and racemic compound can have significant effects on chemical stability, bioavailability, and further treatment such as filtration and formulation of the API[62,93]. It is also possible that one enantiomer exist as a stable racemic compound at one temperature and as conglomerate at another temperature, and vice versa as in the case of crystallization of mandelic acid, or a halogenated derivative thereof, which is known to be a racemic compound, from an aqueous solution[37,68]. In such a case, it is advantageous to perform the crystallization process at a temperature allowing the formation of conglomerate rather than a racemic compound, if possible[93]. Otherwise, for the separation of enantiomers from a racemic compound forming system can be formed, large scale SMB chromatography and diastereomeric salt crystallization have been used extensively in the pharmaceutical industry[5,39]. Other developments for potential use in large scale separation of enantiomers are liquid-liquid separation by

chiral extractants[76] and chiral selective membranes[33].

2.3.3 Pseudoracemate forming systems

A third type of solid-liquid equilibria systems for chiral mixtures is the pseudoracemate forming system. *Pseudoracemate* refers to the formation of a solid solution between the two enantiomers coexisting in a completely random distribution in the crystal lattice. This type of solid solution systems is relatively rare and three classical cases of such systems occur. These are referred to as type I, II, and III depending on the melting point of the pure enantiomers compared to that of the pseudoracemate[93].

The difference between a racemic compound, which requires an equal fraction of the two enantiomers, and a pseudoracemate is that a pseudoracemate is a special case of continuous series of different chiral solid solutions. From a crystallization point of view, a slight increase in final enantiomeric excess (*ee*) can be achieved in the case of type II, where a maximum melting point exists for the racemate, and III, where a minimum melting point exists for the racemate. But in the case of type I, where the enantiomers over the whole composition range melt at the same temperature as the racemate, no increase in final *ee* can be achieved. However, because difficulties in achieving true equilibrium in systems of type II and III, the reproducibility of increase in final *ee* in industrial applications is unlikely[93].

The formation of solid solutions of enantiomers over the whole range of composition is rarely observed. However, a more common observation is the formation of conglomerate or racemic compounds with partial solid solution formation in a limited composition range close to the region of pure enantiomer or racemic compound as in the case of ethanolamine mandelate[93,96].

2.4 Crystallization theory

2.4.1 Crystallization driving force: Supersaturation

Crystallization is a rate process which depends on a driving force. The fundamental driving force for all crystallization processes is supersaturation. Frequently used expressions of supersaturation are given below[3,62]:

$$\sigma = C - C_{eq} \tag{2.1}$$

$$S = \frac{C}{C_{eq}} \tag{2.2}$$

$$s = \frac{C - C_{eq}}{C_{eq}} \tag{2.3}$$

where σ is the supersaturation, S is the supersaturation ratio, and s is the relative supersaturation. C is the actual concentration of solution and C_{eq} is the saturation (solubility) concentration[3,62]. It should be emphasized that the above given definitions are only valid for ideal solutions, i.e. solutions wherein the molecular interactions between solute and solvent(s) are identical to the interactions between solute molecules and solvent molecules themselves[62]. Such solutions are unlikely to exist and to extend the application of the definitions above to nonideal systems, activity coefficients are often used in the following dimensionless expression[62]:

$$\frac{\mu - \mu^*}{RT} = \ln \frac{\gamma c}{\gamma^* c^*} \tag{2.4}$$

where μ is the chemical potential, c is the concentration of solute, and γ is the activity coefficient. The asterix represents the property at saturation[62]. In this respect, and especially when solvent mixtures are employed in a solvent-solute system, the solid-liquid phase behavior can be predicted by a variety of group-contribution methods such as UNIFAC[40,62,77].

2.4.1.1 Crystallization modes

The first step in any crystallization process is the generation of supersaturation to achieve crystallization. There are commonly four modes used in the pharmaceutical industry to achieve crystallization in a solution. The modes are employed either solely or in combination (Table 2.1)[3,62,87]. Reactive crystallization, commonly known as precipitation[62], can for instance be employed if the solubility concentration of the solute in a solvent is below 0.01 g/g solvent. If the solubility concentration is above 0.2 g/g solvent and the change of the solubility concentration with temperature is below 0.005 g/(g solvent °C). Otherwise antisolvent or cooling crystallization should be employed[47]. To meet the predefined yield requirements of a crystallization process and to control the physical attributes of the final solid product such as PSD, it could be advantageous to consider a combination of the listed crystallization modes such as vacuum crystallization, i.e. combined evaporative and cooling crystallization[62], or combined antisolvent and cooling crystallization[63,102].

2.4.2 Metastable region

In order to achieve crystallization, supersaturation greater than unity, i.e. greater than equilibrium solubility, is required. Figure 2.8 illustrates the different crystallization phenomena corresponding to the level of supersaturation[87].

Table 2.1: Crystallization modes commonly employed. The influence of solute solubility on the selection of crystallization mode is addressed[3].

Crystallization mode	Description	Solubility behavior
Cooling	Solute solubility is reduced to achieve crystallization by cooling the solution from a high temperature to a low temperature at constant solvent composition	Solute is soluble in a solvent at high temperature, but below the normal boiling point of the solvent, and is relatively insoluble at low temperatures
Antisolvent	An antisolvent is added to reduce the solubility of the solute in a solvent in which the solute is soluble. Crystallization is achieved by composition change	Yield constraints cannot be achieved by cooling crystallization at reasonable dilutions. The solubility of the solute in a solvent can be reduced by more than 50%
Reactive	Changing the ionic composition or structure of the solute through reaction can induce crystallization by change in the solubility behavior. The concentration of the product is changed by reaction to exceed the solubility limit	Reactants used are often readily soluble in the solvent with the produced solids by reaction being completely insoluble
Evaporative	Crystallization is induced by increasing the concentration of the solute in a solvent above the solubility limit by the evaporation of solvent	Evaporative crystallization is commonly used in combination with cooling crystallization to meet yield requirements. Concentration through distillation allows for additional mass of solute to be recovered

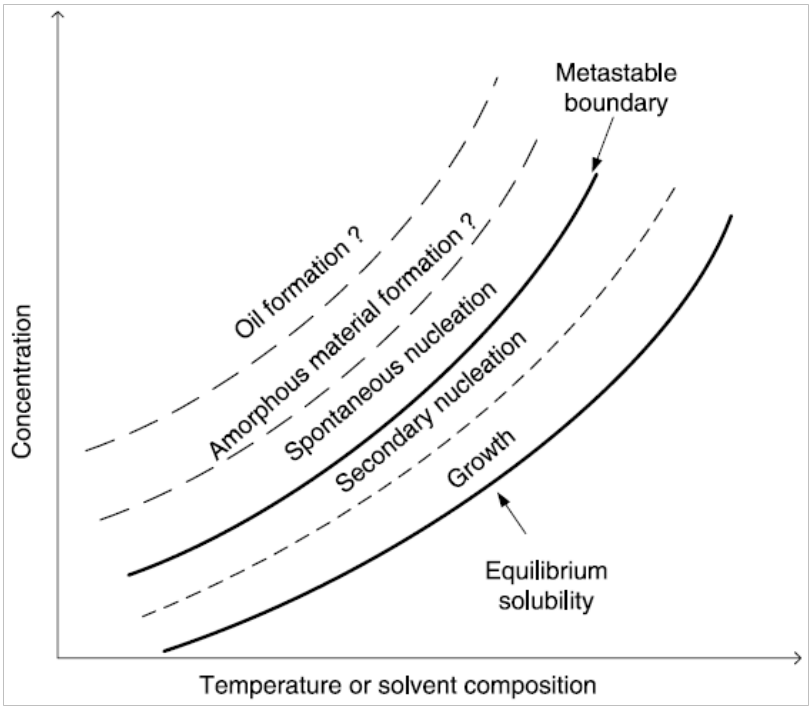

Figure 2.8: A hypothetical map between supersaturation and possible crystallization phenomena[87]. Note that the metastable boundary is only kinetically determined and is dependent on process conditions, such as amount and size of seed crystals or stirring rate. The region between the metastable boundary and equilibrium solubility is the metastable region.

Between the equilibrium solubility and the metastable boundary, a metastable region exists. Beyond the metastable boundary, any change to the system will result in a mixture having a lower Gibbs-free energy than in the initial condition. Within the metastable region, nuclei from secondary nucleation may form or growth on existing crystal surface, i.e. seed crystals, may occur. In order to control the crystallization process and thereby crystal attributes, such as particle size and PSD, it is desirable to maintain the crystallization process in the metastable region to allow for growth of already existing crystals previously formed by nucleation or supplied externally as seed crystals[3,87].

The metastable region may be narrower or wider than that illustrated above and this will have a great influence on the selection of the strategy for operating the crystallization process. The width of the metastable region is essentially controlled by the position of the metastable boundary, which is kinetically controlled, while the equilibrium solubility is a constant thermodynamic property at the given conditions, e.g. temperature or solvent composition. Thus, the width of the metastable region may be influenced by[3,62,87]:

- Cooling rate employed (cooling crystallization)

- Rate of antisolvent addition (antisolvent crystallization)
- Rate of addition of reactants (reactive crystallization)
- Rate of solvent evaporation (evaporative crystallization)
- Stirring rate
- Amount and size of seeds, if any
- Nature and concentration of impurities
- Storage of solution prior to crystallization

Two methods exist for the measurement of the metastable boundary: 1) Cooling rate method, and 2) nucleation induction time method[3,62,87]. The first method is primarily applicable for cooling crystallization, but can also be used for evaporative crystallization. The main principle of the method is cooling a solution at very low cooling rate until particles are detected by the online measurement devices such as Lasentec FBRM®. The experiment is repeated several times with faster cooling rates. For evaporative crystallization, the evaporation rate is varied. In the second method, supersaturation is initially generated rapidly by cooling, evaporation, reaction, or antisolvent addition. The supersaturated solution is then held isothermally until the formation of particles is detected by e.g. Lasentec Focused-Beam Reflectance Measurement (FBRM®) device. The experiment is repeated for different conditions, e.g. different amount of antisolvent used, different temperatures (cooling and evaporative crystallization), and different amount of reactants added. The most general method is the second method because it is applicable for all crystallization modes and gives a better estimation of the time window available for e.g. addition and growth of seeds or mixing of antisolvent or reactants with the supersaturated solution[3].

2.4.3 Nucleation

As a result of the generation of supersaturation, new crystals may be formed. The formation of crystal nuclei can be spontaneous and occurs without the presence of crystalline surfaces. This process is called *primary nucleation*. This process can either be *homogeneous* or *heterogeneous*[61,62,87].

2.4.3.1 Primary homogeneous nucleation

Primary homogeneous nucleation is believed to be based on sequences of collisions and interactions between molecules in a supersaturated fluid resulting in the association of molecules to form *clusters*, which may dissociate or grow, because they may or may

not achieve thermodynamic stability, i.e. minimum Gibbs-free energy, depending on their size[62,87]. If the cluster becomes large enough to have the appearance of a lattice structure, it becomes an *embryo*. Further growth results in stable crystalline *nucleus* and is basis for crystal growth[61,62,87]. The rate of primary homogeneous nucleation, B_0, is theoretically given by the following expression[61,87]:

$$B_0 = A_0 \exp\left[\frac{-16\pi\phi^3\nu^2}{3k_B^3T^3(\ln S)^2}\right] \tag{2.5}$$

where A_0 is the pre-exponential factor containing solute diffusivity, supersaturation, molecular diameter and volume, equilibrium solute concentration, and Avogadro's number. A_0 has a theoretical value of 10^{30} nuclei/(cm^3 s). This value generally differ from observed values due to the unavoidable presence of impurities or low surface integration rates, which is exhibited by many organic molecules[87]. The exponential term reflects the energetics of phase change.

The development of equation (2.5) is based on thermodynamic consideration of the free energy involved in solid-phase formation and in creation of an arbitrarily spherical crystalline body of a certain size. It is thus observed in equation (2.5) that if a very high degree of supersaturation is obtained and thereby a supersaturation rate beyond a critical value of S is achieved, the nucleation rate explosively increases. However, below a certain optimal temperature the liquid becomes too viscous to allow nucleation. In contrast, at conditions above that temperature, molecular motion prevents crystal formation. In this respect, an additional thermodynamic term is added to the exponential term in equation (2.5) to count for these practically important effects[15,62,72].

The limitations in the classical nucleation theory, represented by equation (2.5) lies in the assumptions made to achieve this expression. Firstly, the assumption that only one molecule is added to the growing cluster at a time is an extreme simplification. Certainly, clusters or embryos aggregate and rearrange while growing to critical size. This building process is in practice also affected by local supersaturation fluctuations[87]. Secondly, the rate of addition of the molecules to form the solid phase can exceed the ability of the molecules to orient themselves properly. This is especially relevant for organic compounds, which create complex crystal lattices connected by relatively weak forces. The result is a partially or totally amorphous solid, which can easily be formed[87]. In industrial crystallizations, the following empirical expression, relating the primary nucleation rate to the supersaturation, ΔC is commonly used[15,72]:

$$B_0 = K_0\,(S-1)^a \tag{2.6}$$

where K_0 is the primary nucleation rate constant, and a is the order of the nucleation process, which is usually between 1 and 2, depending on the physical and hydrodynamic properties of the crystallizing process[15,72].

2.4.3.2 Primary heterogeneous nucleation

In contrast to primary *homogeneous* nucleation, primary *heterogeneous* nucleation is facilitated by the presence of foreign particles or heteronuclei. This presence causes a reduction in the Gibbs-free energy required for nucleation by the adsorption on the surface of the foreign particle. Thus, heterogeneous primary nucleation occurs generally at a lower degree of supersaturation than homogeneous nucleation (Figure 2.9)[62,72].

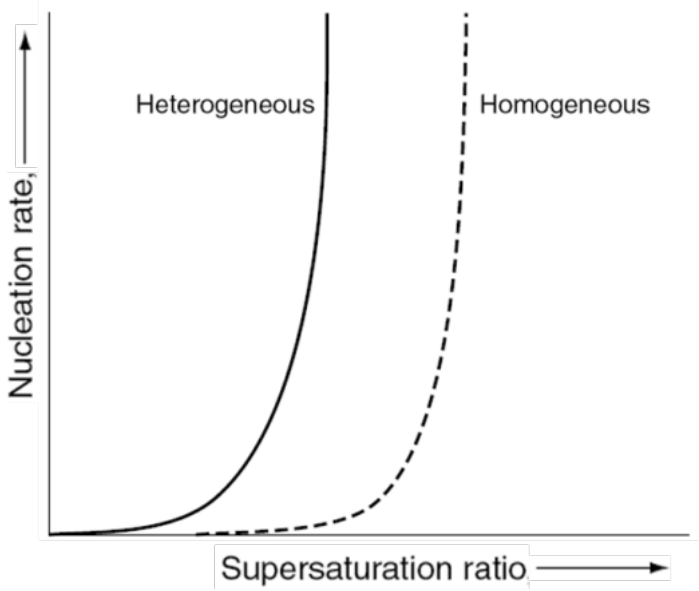

Figure 2.9: Homogeneous and heterogeneous nucleation rate versus supersaturation ratio[72].

In fact, the degree of lowering the Gibbs-free energy for nucleation, and thereby supersaturation, is dependent on the contact angle of the foreign particle and its surface energy. Thus, the extent to which the foreign particle mimics the structure of the compound to be crystallized undoubtedly influences the nucleation process[62,72,87].

2.4.3.3 Secondary nucleation

The process of *secondary nucleation* is, in contrast to primary nucleation, not spontaneous, but follows primary nucleation by the development of crystals formed by either primary homogeneous or heterogeneous nucleation. This development results in uneven growth of crystals on crystal surface of the species considered even at lower degree of supersaturation compared to primary homogeneous and heterogeneous nucleation. Secondary nucleation can occur through several ways[61,62,87]:

- Dust breeding
- Polycrystalline breeding
- Attrition breeding
- Contact nucleation
- Impurity concentration gradient
- Shear nucleation

Thus, secondary nucleation can be induced by vibrations, mixing or the presence of seeds or impurities. The process of secondary nucleation, although poorly understood, is important for industrial crystallizations because it enables the control of particle size and PSD[62,72].

An expression of the rate of secondary nucleation, B_{sec}, is purely established based on the power law correlation of many experimental data due to the absence of a theory describing the complex phenomena of secondary nucleation. In this respect, the most widely used correlation is the following empirical expression[62,72,87]:

$$B_{sec} = k_{sec} M^r P^l (\Delta C)^b \tag{2.7}$$

where k_b is the empirical secondary nucleation constant, M is the density of slurry, P is the agitation rate, and ΔC is the supersaturation. The exponents r, l, and b are experimentally determined according to operating conditions. Thus, it is observed that factors that affect the secondary nucleation are the rate of cooling, the rate of agitation, the presence of impurities, and supersaturation[62,72,87].

2.4.4 Crystal growth

Primary and secondary nucleation are followed by *crystal growth*, which is a diffusion and integration process influenced by the effect of solid surface on which it occurs[62,72,87]. Figure 2.10 illustrates the driving forces for crystal growth in solution[72].

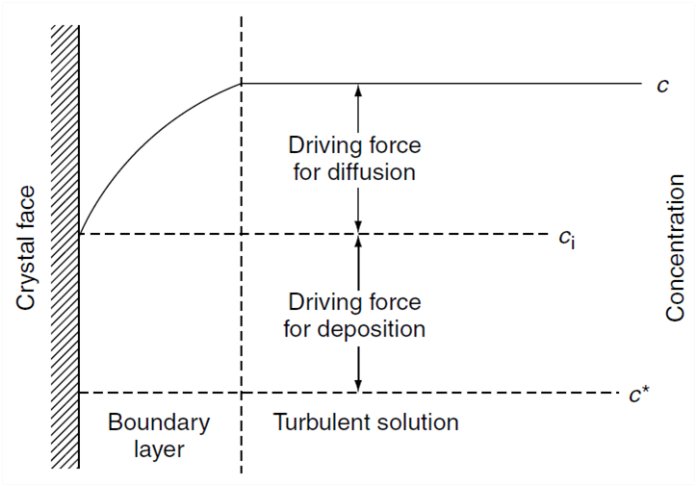

Figure 2.10: Driving forces for crystal growth[72]. c denotes the concentration of solute in the bulk solution, c_i is the concentration of solute at the crystal surface-solution interface, and c^* is the saturation concentration.

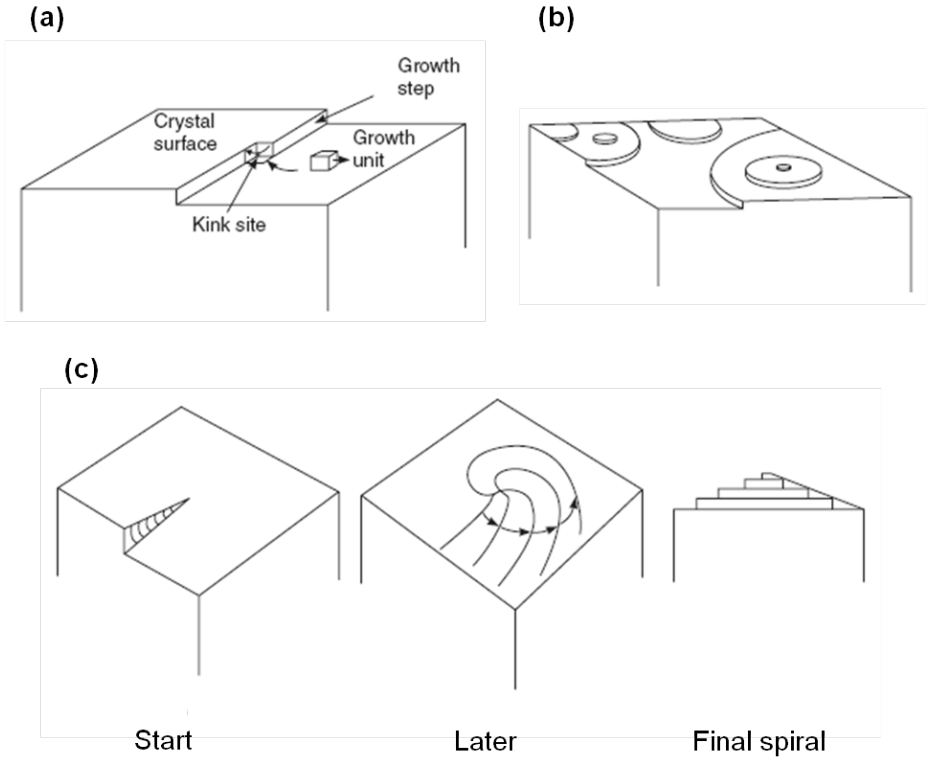

Figure 2.11: Proposed crystal growth mechanisms. (a) illustrates the attachment of a growth unit into a kink site, (b) illustrates crystal growth arising from surface nucleation, and (c) the development of growth spiral starting from a screw dislocation[15,62,87].

Crystal growth may occur by several mechanisms (Figure 2.11) for which a variety of theoretical models have been proposed[45,62,87]. The proposed models describing crystal growth are[15,62,87]:

- The Diffusion-Reaction Model

- Surface Integration Models including Continuous Growth Model, Screw Dislocation Model, and Birth and Spread Model

In most cases more than one mechanism is involved in crystal growth. Hence, these mechanisms have great influence on the growth rate of crystals. If the mechanisms occur in parallel, then the mechanism resulting in the faster growth controls the overall growth rate. If the growth mechanisms occur in series, then the slower mechanism controls the overall rate of crystal growth[15,62].

The process of crystal growth consists of two important kinetic steps[62,72]:

1. Diffusion of solute ions or molecules through liquid interface from solution to crystal surface
2. Ordering and integration of solute ions or molecules into the crystal lattice

The driving force in mass transfer, i.e. diffusion, from mother liquor to crystal surface is given by the concentration driving force, i.e. the difference between the concentration of the surrounding supersaturated solution and saturation concentration at the same temperature[61,62,72]. The second kinetic step of integration can be divided into a number of stages[45]:

1. Adsorption of the growth unit (ion or molecule) on the crystal surface
2. Part of the unit's solvation shell is released
3. The growth unit diffuses into the adsorption layer until it is either incorporated into the crystal lattice, thereby loosing the remaining of its solvation shell, or leaves the adsorption layer and returns to the solution

These kinetic processes occur in a consecutive manner and this causes the solution concentration to adjust itself resulting in an equal rates of the steps at steady state[45,62].

Analogous to similar mass transfer phenomena, the diffusion is improved by the following options[45,61,62]:

- Increase the degree of supersaturation
- If the resistance of the laminar liquid film surrounding the crystal surface comprises a significant part of the total resistance to mass transfer, the increase of turbulence is essential to reduce the thickness of the laminar liquid film, thereby

increasing the mass transfer number

- Increase the mass transport area, i.e. area of crystal surface, by increasing the number of growing crystals
- A combination of the above mentioned options

These options for the improvement of crystal growth should be carefully practiced. The reason is that fast crystallization (precipitation) could result in many very small crystal nuclei resulting in impure crystals of undesired morphology and size. For instance, rapid diffusion to each crystal would result in one-dimensional growth giving needle-like crystals or dendrites. Therefore, it is important to control the relation between the degree of nucleation-to-crystal growth that determines the product crystal size and morphology. For instance, if a mass of very small crystals with a wide PSD is desired, then the dominant kinetic mechanism should be nucleation. In contrast, if small amounts of large crystals are desired, then the crystal growth mechanism should be the dominant[62]. The benefits of a growth-driven crystallization process are[16]:

- Larger average crystal size
- Predictable dry solid flow characteristics
- Reduction of aggregation and/or agglomeration
- Control of hydration, solvation, and polymorphism
- Control of PSD
- Decreased sensitivity to mixing
- Improved reproducibility on scale-up
- Easier transformation to continuous operation

Thus, the balance between the nucleation and growth determines the resulting physical and chemical characteristics of the produced solids and also establishes the basis for evaluation of whether a crystallization process is successful or not[62].

2.4.4.1 Size-dependent growth and growth rate dispersion

In modeling of crystallization processes, it is common to assume that crystal growth obeys the classical McCabe ΔL law, i.e. size-independent growth, in which the growth rate is expressed as the linear velocity perpendicular to the growing characteristic dimension or face. According to the Gibbs-Thomson equation, however, there

is a difference in the solubility of very small particles (below 1 μm) and larger particles. Consequently, supersaturation becomes a function of particle size. Thus, the growth of the small particles becomes slower than the larger particles due to a lower supersaturation of the small particles[62,87].

For larger particles (above 1 μm), if the growth controlling mechanism is surface integration, the particles will become larger, their total surface area increases, and consequently the probability for the occurrence of dislocations on the surfaces increases due to higher mechanical stresses, collision energy, and impurity inclusion. It is thus more likely that larger particles grow faster than smaller ones. Similarly, if the growth rate is diffusion-controlled, larger particles can grow faster than smaller particles under certain mixing conditions due to higher settling velocity. The dependence of the growth rate on the size of the growing particles is referred to as *size-dependent growth*[62,87]. In this respect, several empirical growth rate expressions that include size dependence have been developed[70].

Experimental investigations have also shown that even if particles having the same size and are of the same material are exposed to identical conditions of supersaturation, temperature, and mixing, they do not necessarily grow at the same rate. This phenomenon is known as *growth rate dispersion*. Two different mechanisms have been proposed to describe the behavior of growth rate dispersion. The first mechanism suggests that there exists a distribution of growth rates among particles in a population, but each individual particle grows with a constant growth rate. The second mechanism proposed suggests that the time-averaged growth rate over a certain time period is the same for all particles while there exist fluctuations in the growth rate of each individual particle with time. It should be emphasized that in both cases growth rate dispersion is dependent on the occurrence of dislocations on the surface of a particle. The primary cause of these dislocations is the surface integration step in crystal growth. Changes in the density and locations of dislocations on the surface of a particle caused by e.g. collisions of particle with impeller or impurity inclusion can cause large changes in crystal growth rate[62,87].

2.5 Conclusions

In this chapter, a concise introduction to the methods currently available for the production of pure enantiomers was provided. Chiroselective separation technologies provide a potentially cheaper alternative to other available techniques for the production of pure enantiomers. Additionally, a review on the design objectives and criteria for crystallization processes in the pharmaceutical industry was provided. Solid prod-

uct attributes are of great importance in the pharmaceutical industry and therefore crystallization processes involved in the production of an API should be considered in conjunction to downstream processing and formulation. Moreover, a review on the solid-liquid phase equilibria of chiral systems was given and in relation to that the application of chiroselective separation methods were discussed. Finally, the fundamentals of crystallization theory, which provide the basis for the work presented in the subsequent chapters, were highlighted and discussed.

Chapter 3

Separation of enantiomers by continuous preferential crystallization: Experimental realization using a coupled crystallizer configuration

This chapter presents the experimental realization of separation of enantiomers of the conglomerate forming system of the amino acid asparagine monohydrate in aqueous solution by preferential crystallization using a lab-scale coupled crystallizer process. The setup was designed and built by the author of the thesis and comprises the main objective of the PhD project. The work will be submitted for publication in the journal *Organic Process Research and Development* (Authors: Joussef Chaaban, Kim Dam-Johansen, Tommy Skovby, and Søren Kiil). Modeling of the process presented in this work and sensitivity analysis to improve process understanding are presented and discussed in chapter 4.

Abstract

The experimental realization of a continuous preferential crystallization process, consisting of two mixed flow crystallizers coupled via crystal-free liquid exchange streams and with only the liquid phases operated continuously, is addressed. Experiments in triplicate, using the conglomerate forming system of DL-asparagine monohydrate (DL-AsnH_2O) in water, were conducted and the achievement of nearly racemic composition of the liquid phase in the crystallizers was verified. An experiment was also carried out using seed crystals of a smaller average particle size than used in the reference experiments. Successful enantioseparation by crystal growth, with the repeatability being within ±10% deviation, was obtained. However, slow crystal growth, due to a low surface integration rate, led to a negligible consumption of the desired enantiomer in the feed solution added resulting in low productivities. Productivities, yields, and purities of solid products were influenced by the morphological differences in the seed crystals. Due to irregularly shaped seed crystals, increase in the productivities and

yields were achieved in the L-Tank. Lower purities of solid products from the L-Tank compared to solid products from the D-Tank were obtained. This could be due to surface nucleation of D-AsnH_2O, ascribed to the surface structure of the seeds of L-AsnH_2O supplied. Improvements in productivity, yield, and purity in the L-Tank, for the same process duration, were realized using seed crystals of lower average particle size having a smoother surface structure. The main advantages compared to other separation processes are low capital cost, high crystal purity and yield, ease of upscaling, increased safety, and reduced environmental impact due to reduction in amount of solvent used. The application is currently limited to conglomerate forming systems, but the separation concept may open new possibilities for process improvements regarding enantioseparation of racemic compound forming systems as well.

3.1 Introduction

Continuous pharmaceutical production and separation processes in minireactors are receiving increasing attention as a mean of efficient and safe manufacturing[12,60]. Continuous crystallization also has a great potential in this respect. A substantial number of active ingredients in the pharmaceutical, agrochemical, food, and cosmetic industries are racemic mixtures, i.e. conglomerates and racemic compounds. Usually, only one enantiomer is biologically effective and the other enantiomer can be considered as an impurity comprising 50% of the mixture. Human and environmental side effects are in many cases attributed to the presence of counter enantiomers. A clear evidence of the potential consequences of administering racemic drugs is e.g. the dramatic incident of the pharmaceutical thalidomide in the last century, which caused fetal abnormalities, such as severely underdeveloped limbs[9,48]. During the last decade, the commercialization of chiral active ingredients attracted great attention, which has resulted in new guidelines for the commercialization of chiral ingredients by the FDA, the Japanese authorities, and the European Community[13,80,98]. Strict regulatory requirements and increasing public demand for the production of chiral active ingredients in optically pure form have sparked intensive research devoted to the development of reliable and cost-efficient production processes. In this context, two options are available: 1) Enantioselective synthesis (chemical or enzymatic asymmetric synthesis) or 2) Enantioselective separation of racemic mixtures.

As a result of intensified efforts put into the development of enantioselective synthesis, remarkable progress has been achieved, chemically as well as enzymatic[13,14]. However, an obstacle to the wide commercial application is the cost of such selective synthesis processes. Among other reasons, the use of expensive chemical auxiliaries and reagents as well as enzymes must be considered. Therefore, separation of enan-

tiomers from racemic mixtures comprises an attractive alternative for the production of optically pure enantiomers[13].

The technique most utilized commercially is chiral chromatography with its wide selection of chiral stationary phases. This allows the separation of many racemates[26,27,82]. A version of chiral chromatography successfully applied in industrial scale is continuous countercurrent SMB chromatography enabling an increase in productivity and realizing the goal of achieving optically pure enantiomers[34]. Nevertheless, highly expensive chiral stationary phases and a dilute separation product have initiated the search for and development of alternative technologies which, among others, include 1) diastereomeric (or classical) resolution[5,22,41], 2) chiral membranes[32,33,100], 3) dynamic resolution[14,57,94,95], 4) liquid-liquid extraction[75,76,85,101], and 5) preferential crystallization[14,19–21,54,66,67,91]. Preferential crystallization, in particular, has attracted great attention, the reason being that the majority of chiral pharmaceutical, agrochemical, food, and cosmetic products, and their intermediates are produced as highly pure solids.

3.1.1 Coupled-Batch Preferential Crystallization

A thoroughly studied preferential crystallization process is the Coupled-Batch Preferential Crystallization (CB-PC) process[19–21,66]. It consists of two batch crystallizers coupled via crystal-free mother liquor exchange streams between the crystallizers. The process can be operated either isothermally throughout the duration of separation[21,66] or with a transient decrease in crystallization temperature[21]. Both operations are performed with external supply of enantiopure seeds to facilitate selective crystal growth. Both operation modes for the CB-PC process have proven to be feasible for the simultaneous separation of enantiomers by crystallization[20,21,66] with improved productivity and yield compared to preferential crystallization in a single batch crystallizer. Because of the crystal-free liquid exchange streams, the delay or even the suppression of the nucleation of excess counter enantiomer is possible due to the nearly racemic composition of the mother liquors. However, a characteristic drawback is the decrease in the crystallization driving force, i.e. supersaturation of desired enantiomer, with time in the crystallizing solutions.

The CB-PC process is applicable for conglomerate forming systems[21,66] and racemic compound forming systems as well[20]. In case of conglomerate forming systems, the enantiomers are separated simultaneously (one in each crystallizer) by seeding. Enrichment of initial racemic solution is not necessary. An essential requirement allowing for separation is a sufficiently higher solubility of the racemate compared to that of

the pure enantiomers. For a racemic compound forming system the process is feasible only if 1) sufficient enrichment of the desired enantiomer beyond the eutectic composition is present in the initial racemic solution, and 2) the solubility of the racemic compound is sufficiently higher than that of pure enantiomers[41,67]. In this case, the simultaneous separation of the racemic compound and the desired enantiomer in excess can be performed. A loss in the yield of pure solid product of the desired enantiomer is unavoidable in this process due to the consumption of that enantiomer in the formation of solid racemic compound.

A detailed theoretical study followed by experimental investigation of the parameters influencing the enantioseparation performance of the CB-PC was performed by Elsner et al.[19,21]. The study was conducted on the conglomerate forming system of the amino acid threonine using water as solvent. The study highlighted that an increase in productivity can be achieved by manipulating critical process parameters such as flow rate of crystal-free liquid exchange between crystallizers, initial enantiomeric excess in solutions, mass of seeds supplied, time for initiating liquid exchange (switching time), process duration time, and crystallization temperature.

3.1.2 Coupled Continuous Preferential Crystallization

In the present study, the continuous preferential crystallization apparatus called Coupled-Continuous Preferential Crystallization (CC-PC) process is investigated. This newly developed process is based on the thoroughly investigated CB-PC apparatus developed by Elsner et al.[20,21], and a proof-of-concept investigation of a continuous isothermal version of the process is conducted. The objectives are to assess the potential achievement of simultaneous separation of the enantiomers by crystal growth and the achievement of a nearly racemic composition of the liquid phase in each crystallizer. Due to the nearly racemic composition of the mother liquor, the crystal-free liquid exchange could ensure the suppression of crystallization of the counter enantiomer. The stages and decisions made during the development of the CC-PC process are provided in Appendix A.

The newly developed continuous process is evaluated with respect to productivity, yield, and purity of the solid product produced. To evaluate the robustness of the process, experiments in triplicates with almost identical experimental conditions were conducted. Furthermore, to investigate the flexibility of the process, an experiment where seed particles with smaller size were used was also conducted.

3.1.3 Chemical model system

The investigation is performed as a case study of enantioseparation of the enantiomers of the amino acid asparagine monohydrate from an aqueous racemic mixture by preferential crystallization. The selection of the asparagine monohydrate system as model compound for the investigation in this study was based mainly upon two reasons:

1. Aqueous solution of the compound belongs to the conglomerate forming systems[86]
2. Solubility data and data for crystallization kinetics are available in the literature[66]

The solubility of the asparagine monohydrate compound in water decreases with decreasing temperature[66]. This facilitates the application of cooling crystallization as separation method in the continuous preferential crystallization process considered. Enantioseparation of the enantiomers of the selected model compound in the isothermal CB-PC process was also investigated by Petruševska-Seebach et. al[66]. It was concluded that the crystallization process is controlled predominantly by surface integration at the given experimental conditions. In general, surface integration rate exhibited by many organic molecules is known to be rather low[87] leading to a slow consumption of the enantiomer from the liquid phase. It was also found that the growth rate of the desired enantiomer is dependent on the concentration of the counter enantiomer which can inhibit the growth of the desired enantiomer[66]. The low rate of crystal growth means that the consumption of the desired enantiomer from the continuously added feed solution in the CC-PC process considered in this study is, for any practical uses, expected to be negligible. Therefore, the purpose of this work is not to demonstrate a quantitative separation of the two monohydrate enantiomers in the feed streams, but, as an initial step, to show that it is possible to grow only one of the enantiomers in each of the two crystallizers. Thus, the estimated productivities of the solid product produced are expected to be low. However, it is believed that process parameters influencing the growth rate of the seed crystals, such as crystallization temperatures, can be manipulated so that feasible separation of the enantiomers of quantitative scale can be realized.

3.2 Experimental section

3.2.1 Materials

The chiral compounds used as enantiopure seeds in the present study were D-(+)-Asparagine monohydrate (D-$AsnH_2O$) ($\geq$99%) and L-(-)-Asparagine monohydrate (L-$AsnH_2O$) ($\geq$99%) purchased from Sigma-Aldrich (Copenhagen, Denmark). DL-(±)-Asparagine monohydrate (DL-$AsnH_2O$) ($\geq$99%)) was also obtained from Sigma-Aldrich (Copenhagen, Denmark) and dissolved in demineralized water (solvent) and used as racemic feed for the experiments.

3.2.2 Experimental setup and procedures

3.2.2.1 Continuous Preferential Crystallization (CC-PC) process

The schematic diagram of the experimental setup is shown in Figure 3.1 and a picture of the setup is shown in Figure 3.2.

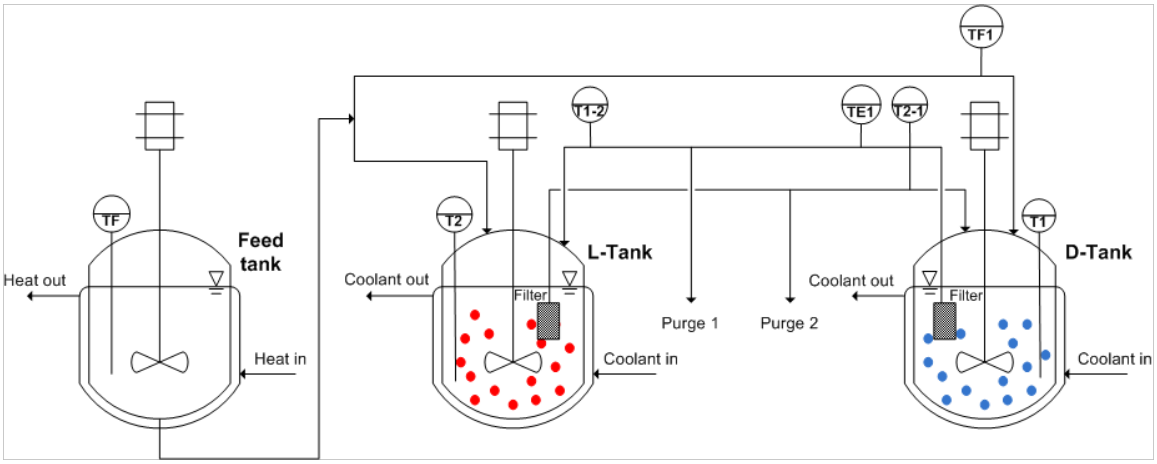

Figure 3.1: Schematic diagram of the CC-PC process for the preferential crystallization experiments. TF symbolizes the temperature in the feed tank, TF1 is the temperature of feed entering the D-Tank, T1 is the temperature in the D-Tank, T2 is the temperature in the L-Tank, TE1 is the temperature of mother liquor effluent from the D-Tank, T1-2 is the temperature of exchange stream from the D-Tank to the L-Tank and T2-1 is the temperature of exchange stream from the L-Tank to the D-Tank. Blue and red filled circles symbolize growing enantiopure seeds of D-$AsnH_2O$ and L-$AsnH_2O$ in the D- and L-Tank, respectively. The grey boxes in the D- and L-Tank represent filters for mother liquor exchange.

The CC-PC process in Figure 3.1 is a modification of the CB-PC. The modification consists of the addition of two feed streams consisting of undersaturated racemic solution, one to each crystallizer, and two purge streams from the crystal-free liquid exchange to maintain constant volumes in the crystallizers. It should be emphasized that the process is operated continuously with respect to the liquid phase only.

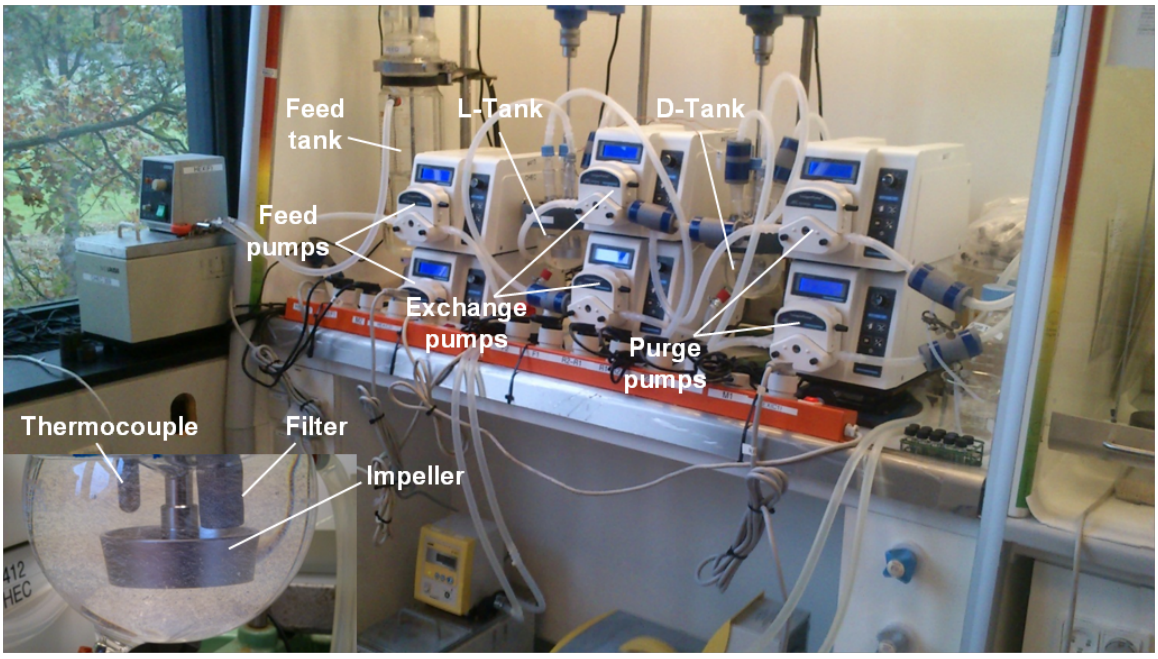

Figure 3.2: Photograph of experimental setup for the preferential crystallization experiments. The small insert (lower left corner) shows the instrumentation in the crystallization vessels. Six individual pumps are necessary to run the setup in a continuous mode.

Each of the crystallizers (D-Tank and L-Tank) consisted of jacketed round-bottom glass vessels of 250 mL in total volume with 75 mm ID flange and lid with five necks. The stirrer used in each crystallizer was a 45 mm ringed propeller-type impeller (Heidolph PR 32 Ringed Propeller, Schwabach, Germany) mounted on a motor (IKA Eurostar Digital, Staufen, Germany). Two separate thermostated circulation water baths (LAUDA Alpha RA 8 for the D-Tank and LAUDA Ecoline Star Edition RE 104 for the L-Tank, Lauda-Königshofen, Germany) were used for cooling the crystallizers. The liquid solutions from and into the crystallizers were transported by six separate peristaltic pumps (Longer Pump LP-BT-100-1F, pump head YZ1515x, Baoding Longer Precision Pump Co. Ltd., Hebei, China). A detailed instruction manual for the CC-PC process is provided in Appendix B.

3.2.2.2 Preparation of undersaturated racemic feed solution

The racemic feed solution was prepared by dissolving 100 g of solid DL-AsnH_2O in 1.90 kg of demineralized water in a jacketed cylindrical glass vessel with total volume of 2.5 liters (Feed tank). An in-house made stirrer shaft fitted with a half-moon impeller of PTFE mounted on a motor (IKA Eurostar Power Control-Visc, Staufen, Germany) was placed in the center of the feed vessel. The feed slurry was heated up to about 31 °C by a thermostated circulation water bath (LAUDA M3, Lauda-Königshofen, Germany) and maintained for 1 hour for complete dissolution. The solution was maintained at that temperature throughout the duration of the experiment. The

temperature of feed solution was recorded via the Vernier Software package Logger Lite 1.6.1 using the thermocouple sensor connected to Go! Link interface (Vernier Software and Technology LLC, Beaverton, OR, USA).

3.2.2.3 Continuous Preferential Crystallization (CC-PC) experiments

The first experiments were performed with almost identical experimental conditions according to Table 3.1. An additional experiment was conducted with the experimental conditions given in Table 3.1, but using enantiopure seeds with a smaller average particle size (i.e. a sieve fraction of 150-250 μm).

Table 3.1: Operational conditions for experiments conducted in triplicates.

Parameter	**Value**	**Unit**
Feed tank		
Feed temperature	304	K
Concentration	5	wt% DL-AsnH_2O
Total mass of feed solution	2000	gram
Stirring rate	250	rpm
Heating rate	14	K/h
D-Tank and L-Tank		
Inlet feed temperature	300	K
Saturation temperature	296	K
Crystallization temperature	292	K
Effective volume	220	mL
Residence time of liquid phase	15	min
Inlet feed flow rate	7.3333	mL/min
Liquid exchange flow rate	7.3333	mL/min
Effluent flow rate	14.6667	mL/min
Mass of seeds	0.4648	gram
Sieve fraction of seeds	250-355	μm
Cooling rate	14	K/h
Stirring rate	250	rpm

Initially, 220 mL of undersaturated racemic solution from the feed vessel was transferred into each crystallizer by two separate peristaltic feed pumps (Longer Pump LP-BT-100-1F, YZ1515x, Baoding Longer Precision Pump Co. Ltd., Hebei, China). Stirring of solutions was initiated and maintained at about 250 rpm. A liquid sample of about 4 mL was withdrawn from the feed solution for offline polarimetric analysis

and density determination. The racemic solutions in the crystallizers were then cooled with constant cooling rate about 14 K/h to a crystallization temperature of about 19 °C and maintained throughout the duration of the experiments. The temperatures were recorded via the Vernier Software package Logger Lite 1.6.1 using Al-Cr thermocouples type K (0.1 K in resolution) connected to thermocouple sensors which in turn were connected to Go!Link interface (Vernier Software and Technology LLC, Beaverton, OR, USA).

The experiments were initiated by starting the peristaltic pumps at a flow rate of 7.333 mL/min. The liquid phase was separated from the solids by *in-situ* sintered metal filters with pore size of 10 μm (IDEX Health and Science, Wertheim-Mondfeld, Germany) fitted in each crystallizer. When the temperature of the solutions in the crystallizers was stabilized, dry homochiral seeds of pure enantiomer were externally supplied to each crystallizer. The mass of seeds was collected from a certain sieve fraction and analyzed offline for the particle size distribution with laser diffraction particle size analyzer (Malvern Mastersizer 2000, Malvern Instruments Ltd.). Liquid samples of about 4 mL were withdrawn from the respective purge stream from each crystallizer every 15 minutes after seeding. The samples were analyzed offline for optical rotation at about 23 °C and 589 nm in 1 mL glass cell (PerkinElmer 341 Polarimeter, PerkinElmer Life and Analytical Sciences, Shelton, CT, USA) with a reproducibility of $\pm 0.002°$. Additionally, the liquid density of the liquid samples was measured offline at about 23 °C using Density Meter DMA 35 (Anton Paar GmbH, Graz, Austria) with a reproducibility of ± 0.0005 g/mL.

After each experiment, the pumps and the heating and cooling water baths were turned off and the slurries were filtered using ashless cellulose filter paper with 7.0 cm in diameter and pore size of 3 μm placed on a Büchner funnel with vacuum suction. The filtered solids were washed with 50 mL ice cold ethanol to remove mother liquor adhering to the crystal surface. A short time delay occurred between the filtration tasks. The solids were dried for 24 hours in a ventilated cupboard and weighed for yield and productivity estimation. The solids were also analyzed for optical purity using offline polarimetry and STA consisting of DSC and TGA (STA 409, NETZSCH-Gerätebau GmbH, Selb, Germany) using Pt/Rh crucibles with lids. The STA analysis was conducted at a heating rate of 5 K/min and up to 300 °C with purge gas flow of 100 mL N_2/min. Furthermore, samples of the seeds and harvested solids were coated with gold particles and analyzed by SEM imaging at Center for Nanoscopy (CEN) in the Technical University of Denmark (DTU).

3.3 Process Metrics

To quantify the efficiency of the present preferential crystallization process, productivity, yield, and purity of the solid product have been considered. Additionally, the liquid phase concentration (mass fraction) change during the crystallization experiments has been assessed to observe the performance of the process.

3.3.1 Analysis

3.3.1.1 Concentration of enantiomer in the liquid phase

The concentration (mass fraction) profiles for each enantiomer in the mother liquor in each crystallizer during the crystallization process are calculated by a combination of the polarimetric analysis and the density analysis of samples of the mother liquor[18]. The polarimetric analysis determines the difference in the concentrations of D-Asn and L-Asn in the mother liquor according to the calibration curve obtained for different aqueous solutions with known concentrations of each enantiomer. The density analysis determines the total concentration of enantiomers in the mother liquor by using the calibration curve of liquid density for known concentrations in a series of aqueous solutions. The detailed calibration procedure and data for polarimetry and densitometry analyses are provided in Appendix C.1 and C.2, respectively.

3.3.1.2 Supersaturation ratio

The crystallization driving force, i.e. supersaturation, in terms of the supersaturation ratio of the desired enantiomer in each crystallizer is also estimated. The supersaturation ratio of the desired enantiomer is defined as the ratio between the mass fraction of the desired enantiomer and the equilibrium mass fraction of the desired enantiomer. The equilibrium mass fraction is in turn a function of the crystallization temperature and the concentration of the counter enantiomer in the crystallizing suspensions[21,66].

3.3.1.3 Productivity and yield

The productivity is defined as the product of the optical purity of the solid product and the ratio between the mass of solid product produced and the mass of the desired enantiomer in feed solution fed into the crystallizing suspension per unit time. The mass of the solid product produced is estimated as the difference between the mass of dry solids harvested and the initial mass of the supplied seeds. The mass of the desired enantiomer in the feed solution is estimated by the product of the density of the feed solution, the volumetric flow rate of the feed inlet and the mass fraction of the desired enantiomer in the feed solution.

The solid product yield is in turn defined as the product of the optical purity and the ratio between the mass of the solid product produced and the initial mass of seeds supplied.

3.3.1.4 Optical purity

The optical purity of the solid product was determined quantitatively by polarimetry. Solid samples were dissolved in water and the solutions were analyzed for optical rotation and compared to the reference solutions of the pure enantiomer estimated from a linear fit of the calibration curve. The optical purity was then calculated as the ratio between the actual observed optical rotation of a solution of the solid product with a certain concentration and the expected observed optical rotation of a solution of the pure enantiomer with the same concentration. The procedure and calibration data are provided in Appendix C.3.

3.4 Results and Discussion

Results of the crystallization process, namely crystallization temperature and optical rotation of the liquid phase are now presented and discussed. Estimations of the liquid phase compositions, supersaturation ratios, and growth rates of crystals are also given and discussed. Moreover, the results obtained of the solid phase analysis in terms of purity, productivity, and yield of solid products produced are evaluated.

3.4.1 Crystallization temperature and observed optical rotation

Crystallization temperatures in the D- and L-Tank and the observed optical rotation of the mother liquors are shown in Figure 3.3 for all three initial experiments.

Minor fluctuations in the crystallizer conditions are due to heat transfer limitations, the efficiency of mixing in the crystallizers, and the placement of the thermocouple. Nevertheless, under isothermal conditions the process performed with a reasonable repeatability.

The reason for the selection of 19 °C as crystallization temperature in the present investigation is that a crystallization temperature lower than the surrounding air temperature enables natural heating of the liquid exchange streams and thereby avoid the nucleation of the counter enantiomer in the tubing between the crystallizers. The liquid exchange temperature achieved was about 23 °C, which is the saturation temperature of the pure enantiomer[66]. Operating at crystallization temperature higher than the temperature of the surroundings requires a heating system to avoid cooling

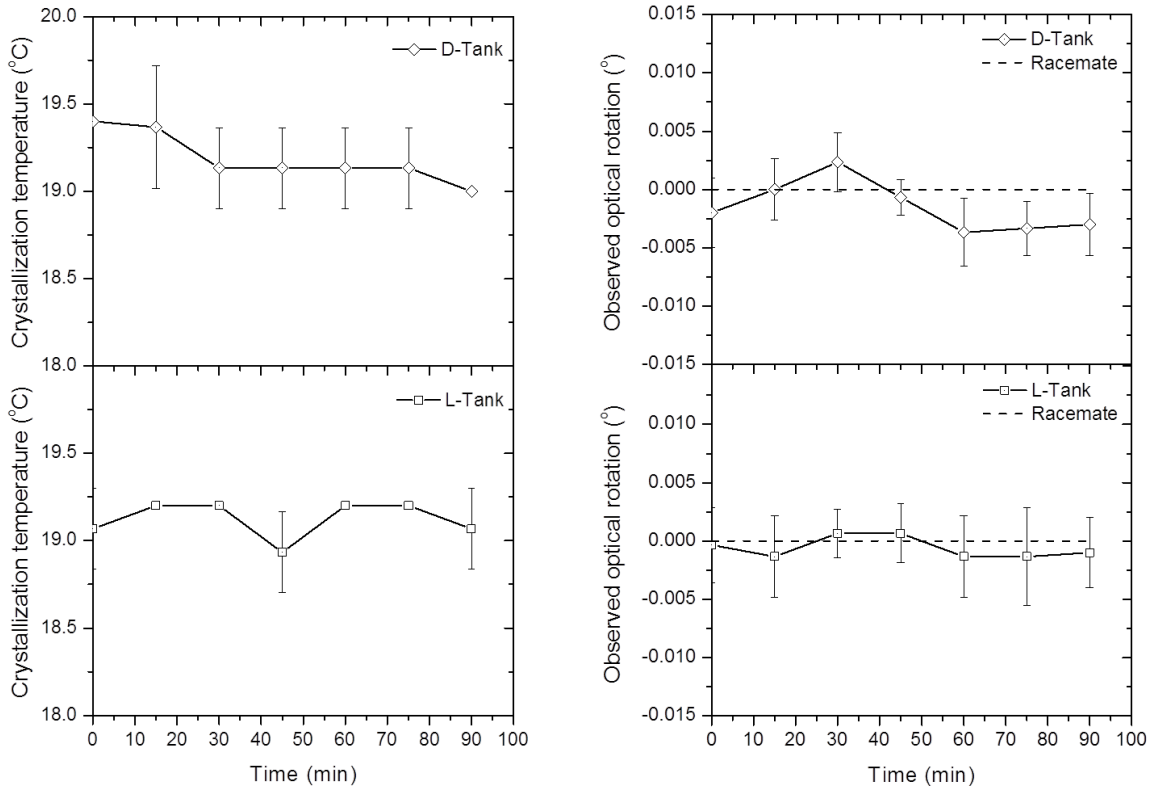

Figure 3.3: Temperatures and observed optical rotations of the mother liquors in the D- and L-Tank during preferential crystallization experiments. Error bars represent the standard deviation. Where error bars cannot be seen, a standard deviation of zero was found. The racemate has an optical rotation of zero. At time equal zero, enantiopure seeds are introduced. The experimental conditions are provided in Table 3.1.

of the liquid exchange streams. Due to limited space, such a heating system was problematic to implement.

The observed optical rotations over time indicate that the composition of the mother liquor is nearly racemic because of values very close to zero.

3.4.2 Liquid phase concentration profiles of enantiomers

The estimated liquid phase concentrations of D-Asn and L-Asn in each tank as a function of time, calculated from the polarimetric and the liquid density measurements, are shown in Figure 3.4.

As shown above by the observed optical rotation, the liquid phase composition is nearly racemic and this is due to the crystal-free liquid exchange streams between the two crystallizers. Furthermore, as shown in Figure 3.4 a nearly constant concentration of the preferred enantiomer in each crystallizer is achieved and that the

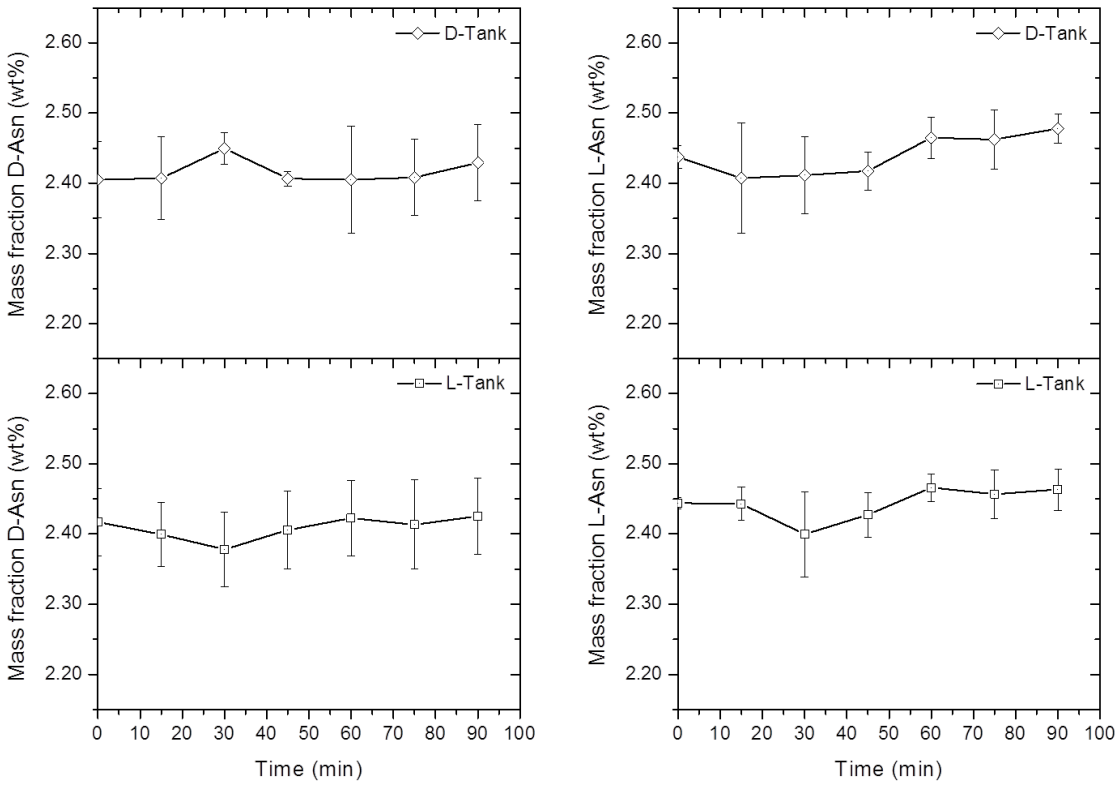

Figure 3.4: Liquid phase concentrations of enantiomers in each tank as a function of time. Error bars represent the standard deviation. At time equal zero, enantiopure seeds are introduced.

concentration of enantiomers is the same as the concentration in the feed solution. Because of the slow rate of surface integration, negligibly low consumption of the desired enantiomer in each crystallizer occurs. It is thus expected that the crystallization driving force, i.e. supersaturation, and thereby the rate of crystal growth, is constant for the desired enantiomer in each crystallizer and can be determined only by knowing the concentration of the enantiomers in the feed solution.

3.4.3 Supersaturation and crystal growth

The estimated supersaturation ratio of the preferred enantiomer in each crystallizer is given in Figure 3.5.

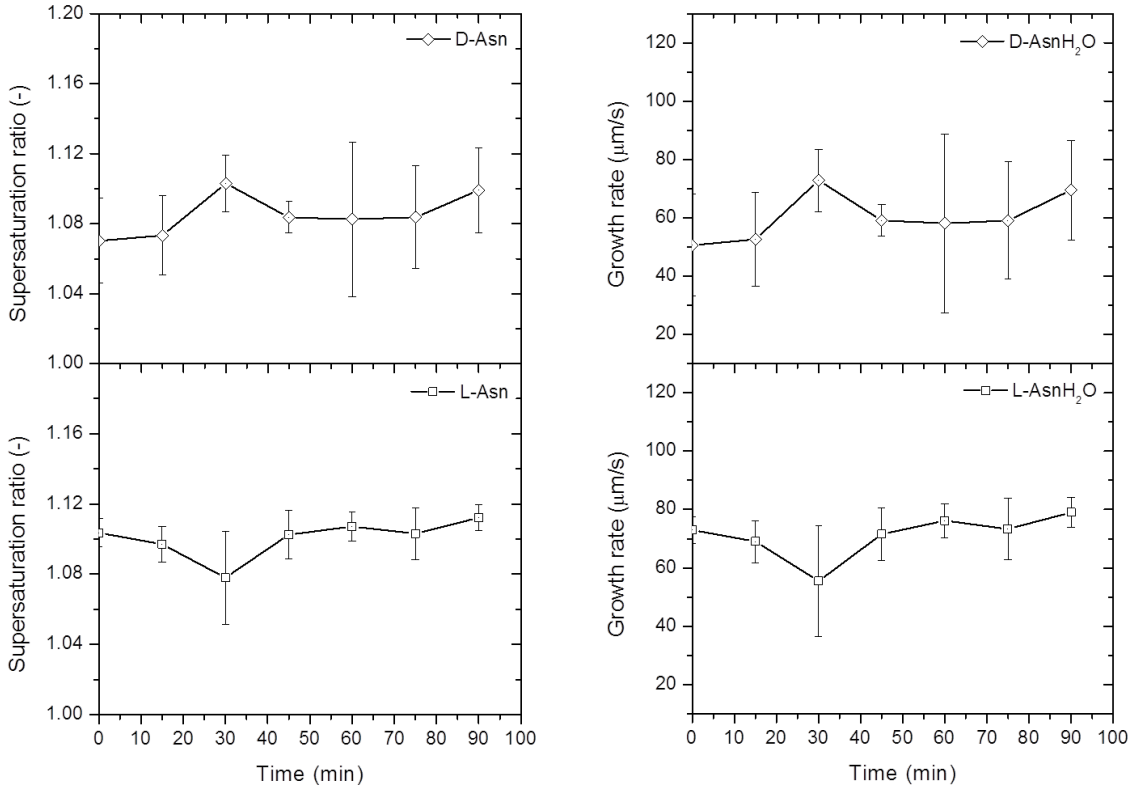

Figure 3.5: Transient development in the supersaturation ratio for the preferred enantiomer in each tank. At time equal zero, enantiopure seeds are introduced.

Indeed the crystallization driving force of the preferred enantiomer is almost constant in the respective crystallizers. Obviously, there exists a slight difference in the supersaturation driving force of the crystallizing enantiomer which could be explained by the difference in the morphology and the size of the enantiopure seed crystals supplied[21,69] and the minor fluctuations in the temperature of the crystallizing solutions.

An inherent consequence of the above mentioned constant driving force is a constant crystal growth rate of the enantiopure seeds in each tank throughout the duration of the crystallization experiments. This is desirable because of the possibility for improving the control of the purity and the particle size of the growing crystals.

3.4.4 Analysis of the solid product

A summary of the results of the analysis of the solid product produced in terms of productivity, yield, and purity for the triplicate experiments (Exp 1-3) conducted and the additional experiment (Exp 4) are listed in Table 3.2. Some statistics are given in Table 4.1. With respect to the size and the mass of the seed crystals used in this study

Table 3.2: Summary of the results of the productivity, yield, and purity of solid product produced in experiments Exp 1-3 in both D-Tank and L-Tank and the additional experiment (Exp 4). Note the units.

Experiment	**Exp 1**		**Exp 2**		**Exp 3**		**Exp 4**	
Tank	**D**	**L**	**D**	**L**	**D**	**L**	**D**	**L**
Sieve fraction of seeds [μm]	250-355	250-355	250-355	250-355	250-355	250-355	150-250	150-250
Purity [%]*	100.0	93.4	100.0	92.2	100.0	93.9	100.0	100.0
Productivity [$\times 10^{-4}$ g/(g min)]†	0.97	1.71	1.24	1.57	1.39	1.80	1.82	2.31
Yield [%]‡	31.2	54.5	39.0	50.8	43.2	57.0	57.7	76.8
Fraction of solids produced [%]§	23.8	36.8	28.1	35.5	30.2	37.2	36.6	43.4

$*$ The optical purity is defined as the ratio between the actual observed optical rotation of a solution of the solid product with a certain concentration and the expected observed optical rotation of a solution of the pure enantiomer with the same concentration.

† The productivity is defined as the product of the optical purity of the solid product and the ratio between the mass of solid product produced at the end of experiment and the mass of the desired enantiomer in feed solution fed into the crystallizing suspension per unit time.

‡ The solid product yield is defined as the product of the optical purity and the ratio between the mass of the solid product produced and the initial mass of seeds supplied.

§ The fraction of solids produced is defined as the ratio of the mass of solids produced by growth of seed crystals to the total mass of solids harvested (seeds and solids produced) at the end of the experiment.

(see Table 3.1), the selection was mainly based upon the amount of the seed crystals of each enantiomer available for performing three identical experiments, taking into account the increase in the risk of agglomeration and secondary nucleation caused by attrition and breakage when using a large amount of seed crystals.

Table 3.3: Summary of some statistical results of the productivity, yield, and purity for experiments Exp 1-3 in the D- and L-Tank. Note the units.

Tank	**D**	**L**
Purity [%]	100.0±0.0	93.9±2.0
Productivity [$\times 10^{-4}$ g/(g min)]	1.20±0.21	1.69±0.12
Yield [%]	37.8±6.1	54.1±3.1
Fraction of solids produced [%]	27.4±3.3	36.5±0.9

SEM photomicrographs in Figure 3.6 show the difference in the growth of the seed crystals in both the D- and L-Tank for the experiments Exp 1 and 3.

3.4.5 Productivity and yield

As shown in Table 3.2, the productivity and yield of solid product are low due to the slow crystal growth controlled by low surface integration rates. However, slightly higher values are obtained for the product from the L-Tank, in which L-AsnH_2O seed crystals were grown, compared to the D-Tank. This could be explained by the difference in the morphology and the size of enantiopure seed crystals acquired[21,69]. The enantiopure seed crystals of L-AsnH_2O have a more random structure with many irregularities compared to seeds of D-AsnH_2O. These irregularities could be a result of attrition and abrasion in the manufacturing process and the sieve analysis performed prior to introduction to the crystallizing solution in the L-Tank. The stirring of the crystallizing suspensions does not cause any attrition or breakage of the enantiopure seed crystals introduced during the experiments performed. The rougher and irregular morphology of the seed crystals of L-AsnH_2O (Figure 3.6 (b)) allows for rapid and more random crystal growth (Figure 3.6 (d) and (f)) compared to the more systematic growth of seed crystals of D-AsnH_2O (Figure 3.6 (a), (c), and (e)). The reason is the higher number of nearest neighboring molecules accompanied with the irregular grow sites such as kink sites on the seed crystals of L-AsnH_2O, which promote rapid crystal growth[62].

The PSDs of the enantiopure seeds used in the experiments are shown in Figure 3.7. The PSDs are plotted as $dF_v/d\log(d_p)$ versus $\log d_p$ in order to normalize the area under the differential curve to 1 which make the PSDs comparable[2]. The seed crystals

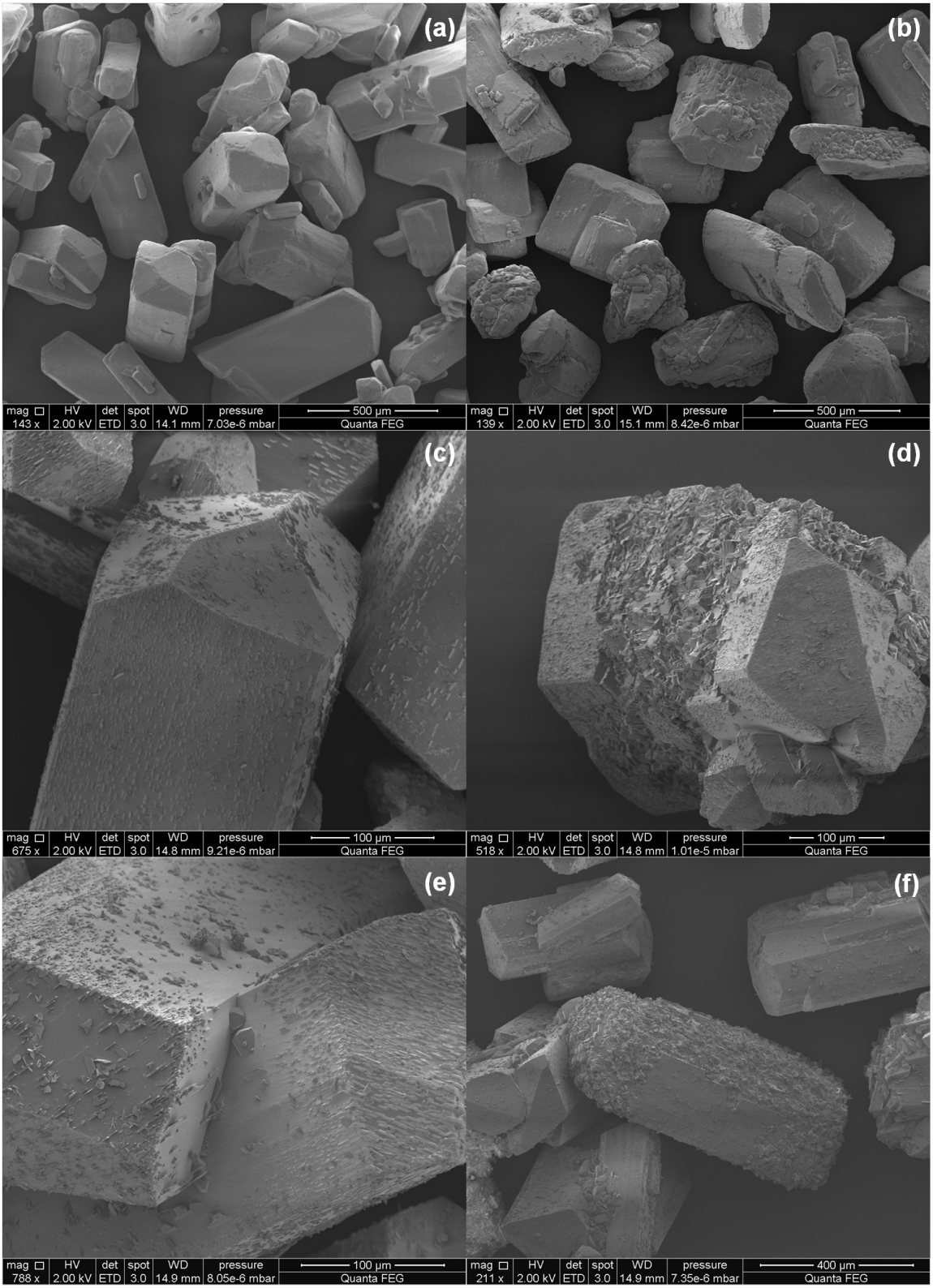

Figure 3.6: SEM photomicrographs of the seeds of D-$AsnH_2O$ ((a)) and L-$AsnH_2O$ ((b)) and the final solid products showing the growth of the seed crystals of D-$AsnH_2O$ in the D-Tank for experiments Exp 1 and 3 ((c) and (e)) and the growth of the seed crystals of L-$AsnH_2O$ in the L-Tank for experiments Exp 1 and 3 ((d) and (f)). Note the scale of the images.

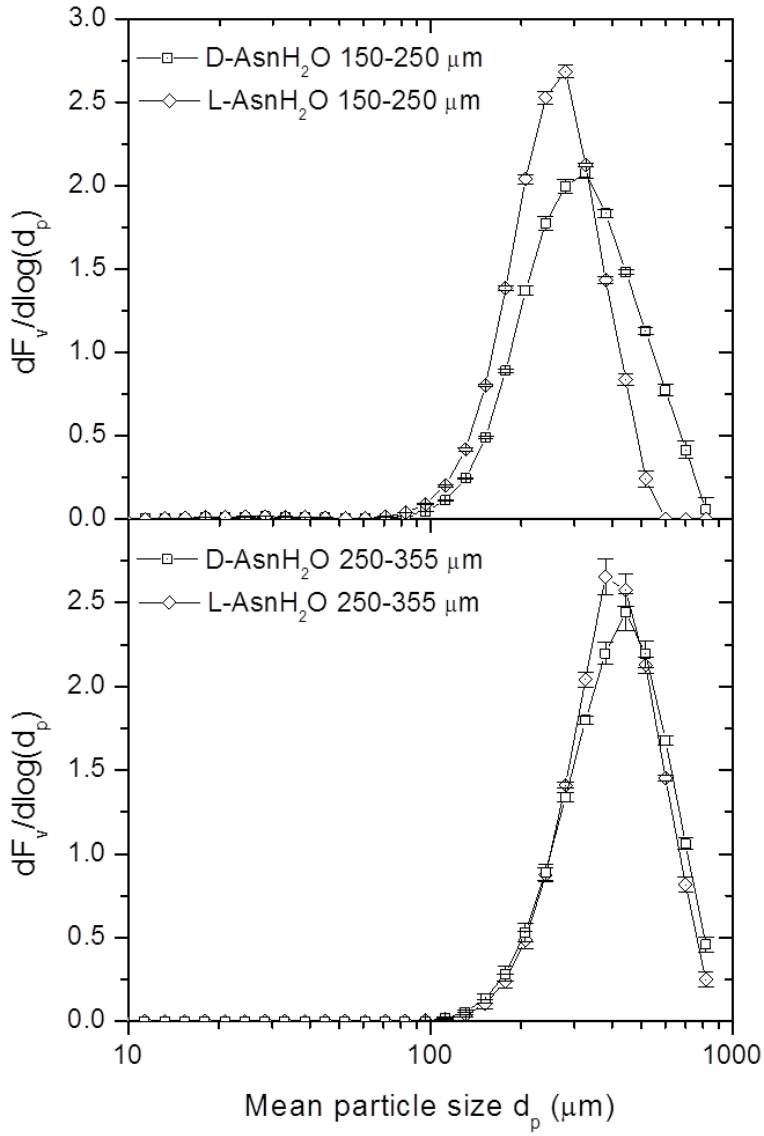

Figure 3.7: Normalized frequency functions of the PSDs for the enantiopure seeds of D- and L-$AsnH_2O$ supplied in experiments Exp 1-3 (sieve fraction 250-355 μm) and Exp 4 (sieve fraction 150-250 μm). Note the logarithmic scale on the abscissa.

of L-$AsnH_2O$ in both sieve fractions have a more narrow PSD with larger average particle size compared to the seeds of D-$AsnH_2O$. This could possibly be due to the manufacturing of the respective seeds and the subsequent sieve fraction analysis. The result is more uniform and larger seeds of L-$AsnH_2O$. This means a larger surface area available for the crystal growth of L-$AsnH_2O$, which could contribute to the higher yield and slightly higher productivity achieved in the L-$AsnH_2O$ in Exp 1-3. Additionally, the seeds used in Exp 4 have a smaller average particle size compared to the larger sieve fraction used in Exp 1-3 (Table 3.2). Thus, the higher yield and

productivity in this case could be due to the larger surface area available for crystal growth in the crystallizing solutions.

In the present study, the duration of the crystallization experiments of 90 minutes was limited by the volume of the feed solution and the mean residence time of the liquid phase in the crystallizers. A mean residence time of the liquid phase of 15 minutes was chosen to ensure that the flow rate of the crystal-free liquid exchange is sufficiently high to obtain a racemic composition in the mother liquor in both crystallizers, because identical crystallization kinetics of the monohydrate enantiomers are assumed. The supersaturation ratio of the preferred enantiomer in each crystallizer could be maintained constant (Figure 3.5) thereby obtaining a constant growth rate. In this context, a longer duration could be realized by a longer mean residence time of the liquid phase in order to improve the utilization of the mass of enantiomers in the feed solution thereby improving the productivities and the yields of the solid product in each crystallizer.

In Table 3.2 it is shown that the mass of seed crystals supplied comprises the major fraction of the mass of solids harvested at the end of each experiment. Increasing the mean residence time of the liquid phase could increase the fraction of the solids produced of the total amount of the harvested solids.

3.4.6 Optical purity

The optical purity estimated is lower than the desired 100% for the solid product from the L-Tank as listed in Table 3.2. The reason for the purity drop in the L-Tank could be explained by the surface structure and size of the seed crystals at which surface nucleation of the counter enantiomer could occur[69]. The rougher surface morphology of the seed crystals of L-AsnH_2O and the larger surface area available for growth of the seeds of L-AsnH_2O in the L-Tank could result in a relatively higher growth rate of the seeds of L-AsnH_2O (Figure 3.5) and thereby the observed purity drop in the L-Tank[69]. The randomly oriented particles observed on the irregular locations on the surface of the grown seed crystals of L-AsnH_2O (Figure 3.6 (b), (d) and (f)) suggest the surface nucleation of the counter enantiomer D-AsnH_2O in the L-Tank. In contrast, due to the more uniform and smoother surface structure of the smaller seed crystals of L-AsnH_2O supplied to the L-Tank in Exp 4, 100% purity was achieved. This fact could explain the effect of the surface morphology of the seed crystals supplied on the purity of the solid product achieved in the preferential crystallization experiments[21,69]. However, it should be emphasized that in general the purity drop in preferential crystallization is unavoidable due to the changes of the surface structure of the seed crystals during

the crystallization process. The purity drop can be delayed by controlling the surface morphology of the seed crystals and the process duration[21,69].

To qualitatively assess whether the nucleation of the counter enantiomer D-$AsnH_2O$ on the surface of the seed crystals of L-$AsnH_2O$ in the L-Tank occurred or not, STA measurements were conducted. The thermograms from the STA measurements of the solid products from Exp 1 are provided in Appendix D. The STA measurements showed that the decomposition of D- and L-$AsnH_2O$ occurs simultaneously at about 215 °C. Therefore, it was not possible to distinguish between the racemate and the pure enantiomer. However, a difference in the stage of the dehydration of crystal water occurred, but it was not possible to confirm the presence of the counter enantiomer D-$AsnH_2O$. The reason is that the difference in the surface structure, crystallinity, crystal defects due to grinding, aging etc. of the crystals in both pure form and the solid products from the crystallization experiments allow for different dehydration kinetics[29,31].

3.4.7 Unutilized enantiomer in purge

From a simple steady-state total mass balance for both enantiomers for a control volume of the CC-PC process, the fraction of unutilized enantiomer in the purge can be estimated. It was found that the growth rate of the desired enantiomer is very low at the given experimental conditions and therefore practically no consumption of the enantiomer in the feed occurs in the crystallizer. As mentioned, this is due to the nature of the controlling mechanism for crystal growth comprising slow surface integration of the asparagine monohydrate molecules onto the surfaces of the supplied seed crystals. Furthermore, rarely do all crystal faces have the same growth rate[87] and therefore growth rate differences between the crystal faces of the growing seed crystals could slow down the overall growth kinetics. Additionally, the inhibitory effect of the presence of the counter enantiomer[66], which is also supplied by the liquid feed solution, could also contribute to lower the rate of surface integration.

To increase the separation potential of this particular chemical system, a modification of the crystal surfaces of the seed crystals could alter the surface integration rates and thereby enhancement of the crystal growth can potentially be realized[21]. Additionally, a prohibitive long residence time (days), high crystallization temperature (evaporation of water), or large amount of seed crystals (risk for agglomeration) would be required. Therefore, it seems more beneficial to recycle the purge streams and to continuously add seed crystals and remove solid product. In this respect, enantiopure seed crystals of could be produced in a separate MSMPR crystallizer or by a technique called

the impinging jet[42]. This approach could result in higher productivity and yield due to the larger surface area of the continuously supplied seed crystals available for growth. This fully continuous process, however, requires a substantial extension and modification of the present setup and will be explored in a future investigation.

For other conglomerate forming chemical systems, with higher rates of crystallization, the setup has great promise as a continuous separation unit.

3.5 Conclusions

In the present work, an experimental realization of the newly suggested continuous preferential crystallization process has been performed using the conglomerate forming system DL-asparagine monohydrate in water. It can be concluded that enantioseparation by the continuous process developed is achievable and that the experiments performed are repeatable. This confirms that the process is robust.

It has been proven that a nearly racemic composition is achieved throughout the duration of the experiments taking into account the effects of morphological differences in the initially supplied seed crystals. Furthermore, separate growth of the supplied seed crystals of the desired enantiomer in each crystallizer was verified.

It can be concluded that reasonable productivities, yields, and purities are achieved, taking into account the short process duration of 90 minutes and the morphological differences in the enantiopure seeds supplied. The lower purity achieved for the solid product from the L-Tank is ascribed to the surface nucleation of counter enantiomer D-AsnH_2O due to the morphology of the enantiopure seeds of L-AsnH_2O. An increase in the productivity, yield and purity can be achieved in the L-Tank for the same duration time of 90 minutes only by using smaller particle size of enantiopure seeds of both enantiomers with a smoother surface structure of the L-AsnH_2O crystals.

The present continuous process has potential for further development into a fully continuous process to increase the efficiency of enantioseparation for conglomerate forming systems having slow growth rates controlled by surface integration. Further work is therefore required to develop and implement proper solid feeding systems for the continuous supply of enantiopure seeds, efficient downstream units necessary for the continuous harvest of solid product, and effective recycle systems for the recycle of the purge streams.

Chapter 4

Separation of enantiomers by continuous preferential crystallization: Mathematical modeling of a coupled crystallizer configuration

In this chapter, a theoretical investigation of the lab-scale CC-PC process experimentally investigated in chapter 3 is presented. A dynamic one-dimensional model to describe the overall behavior of the CC-PC process was established, and model validation against experimental data was conducted. Sensitivity analysis to improve process understanding are presented and discussed together with the validity of the assumptions made. The work will be submitted for publication in the journal *Organic Process Research and Development* (Authors: Joussef Chaaban, Kim Dam-Johansen, Tommy Skovby, and Søren Kiil). The program developed to solve the model discussed was written in MATLAB R2009b, and consists of three separate m-files.

Abstract

A mathematical model describing the continuous separation of enantiomers by simultaneous preferential crystallization in a coupled crystallizer configuration is developed. The model was validated against experimental data for a chemical model compound, the conglomerate forming system of asparagine monohydrate in water. The kinetic parameters required were taken from available literature sources and simulations compared to experimental data. Simulations were found to be in good agreement with experimental data. Additional model simulations suggest that the separation process can be improved by increasing the mean residence time of the liquid phase in the crystallizers, the crystallization temperature, and the mass of seeds supplied. Reducing the size of seed crystals will also lead to a better separation. The model can be used to simulate the performance of the continuous crystallization process for a racemic compound forming system. The racemic compound and the pure enantiomer can be separated simultaneously in each crystallizer having sufficient enrichment of the pure

enantiomer in the feed solution. The model can also be extended to represent a fully continuous separation process taking into account the continuous supply of enantiopure seed crystals and liquid feed solution and the continuous removal of solid product and mother liquor.

4.1 Introduction

Racemic mixtures, i.e. conglomerates and racemic compounds, comprise a substantial fraction of chiral active ingredients in the pharmaceutical, agrochemical, food, and cosmetic industries[13,79]. Usually, the desired biological activity and physiological effect of the enantiomers are ascribed to only one of the two enantiomers. Thus, 50% of a racemic mixture can be considered as an impurity thereby providing the active enantiomer with undesirable side effects[9,48].

Strict regulatory requirements for the production of chiral active ingredients in optically pure form have resulted in strong efforts being put into the development of enantioselective separation technologies[13,80]. The major fraction of chiral compounds and their intermediates must be produced as highly pure solids, and therefore preferential crystallization, in particular, has attracted great attention and is successfully applied for the separation of enantiomers from conglomerate forming systems[14,54,67,91].

An interesting development in preferential crystallization technologies is the Coupled-Batch Preferential Crystallization (CB-PC) process[19,21,66]. This process consists of two batch crystallizers in which the simultaneous crystallization of each enantiomer occurs in a separate crystallizer. The crystallizers are physically coupled via crystal-free liquid exchange streams, thereby maintaining a nearly racemic composition of the mother liquors in the crystallizers. A critical parameter is the flow rate of the exchange streams which is strongly dependent on the crystallization kinetics of the compounds and must be carefully selected. In the case of enantiomers, the crystallization kinetics of the two molecules can be assumed identical. Therefore, to ensure a nearly racemic composition in the mother liquors and thereby avoid crystallization of the undesired enantiomer, the exchange flow rates should be set as high as practically possible[19].

A thorough modeling and simulation study, followed by experimental validation of some parameters influencing the performance of the CB-PC process, using the conglomerate forming system of the amino acid threonine in water was performed by Elsner et al.[19,21]. This study showed that productivity can be improved by manipulating critical process parameters such as initial enantiomeric excess in crystallizing

solutions, flow rate of crystal-free liquid exchange between crystallizers, switching time for initiating liquid exchange, mass of seeds supplied, crystallization temperature profile (isothermal or polythermal), and process duration[19,21]. Due to the slow surface integration rate of the preferred enantiomer on the seed crystals, the authors could demonstrate that simultaneous crystal growth of the preferred enantiomers in each crystallizer could successfully be carried out even though the extent of separation, and thereby the productivities, were negligible[21].

4.1.1 Continuous Coupled Preferential Crystallization

A further step in the development of preferential crystallization processes is the newly developed continuous coupled preferential crystallization (CC-PC) process[11]. The continuous setup is a modification of the coupled batch process. In this extended configuration, two feed streams, consisting of undersaturated racemic solution, one to each crystallizer, and two purge streams, taken from the crystal-free liquid exchange streams, to maintain constant volumes in the crystallizers are employed. The process is continuous with respect to the liquid phase and, at least in this first investigation, batch for the solid phase[11]. In this respect, steady-state in the liquid phase in each crystallizer can be achieved when the growth rate becomes very close to the rate of accumulation of the preferred enantiomer.

The CC-PC process is applicable for conglomerate forming systems, i.e. a physical mixture of equal amount of solid enantiomers, where the enantiomers are separated simultaneously (one in each crystallizer) by seeding. Enrichment of initial racemic solution, which would be required for a racemic compound ('true' racemate), is not necessary. An essential requirement, allowing for separation of the enantiomers, is a sufficiently higher solubility of the racemate compared to that of the pure enantiomers.

An experimental realization of the CC-PC process for the separation of asparagine monohydrate enantiomers, D-asparagine monohydrate (D-AsnH_2O) and L-asparagine monohydrate (L-AsnH_2O), using seeded cooling crystallization at isothermal conditions, was performed in Chaaban et al.[11]. In that work, it was found that the CC-PC process was suitable for enantioseparation without the undesired nucleation of the counter enantiomer. The crystallization driving force, i.e. supersaturation, could be maintained at a constant value throughout the process duration, ensuring constant growth rate of seed crystals and thereby improved productivity, yield, and purity of the final solid product.

In the present study, a transient mathematical model of the CC-PC process is set up

and solved. The objective is to investigate the influence of critical process parameters on the performance of the CC-PC process. Parameters considered are productivity, solid product yield (based on mass of enantiomer present in the feed solution), yield of solid product (based on mass of enantiopure seeds supplied), and the yield of crystal size, i.e. additional size of the growing seed crystals gained by crystal growth. Moreover, the optimal operation conditions are suggested. Simulations are validated against experimental data of the conglomerate forming system of the amino acid asparagine monohydrate in water as solvent[11].

4.2 Description of the continuous setup

The CC-PC process considered is shown schematically in Figure 4.1.

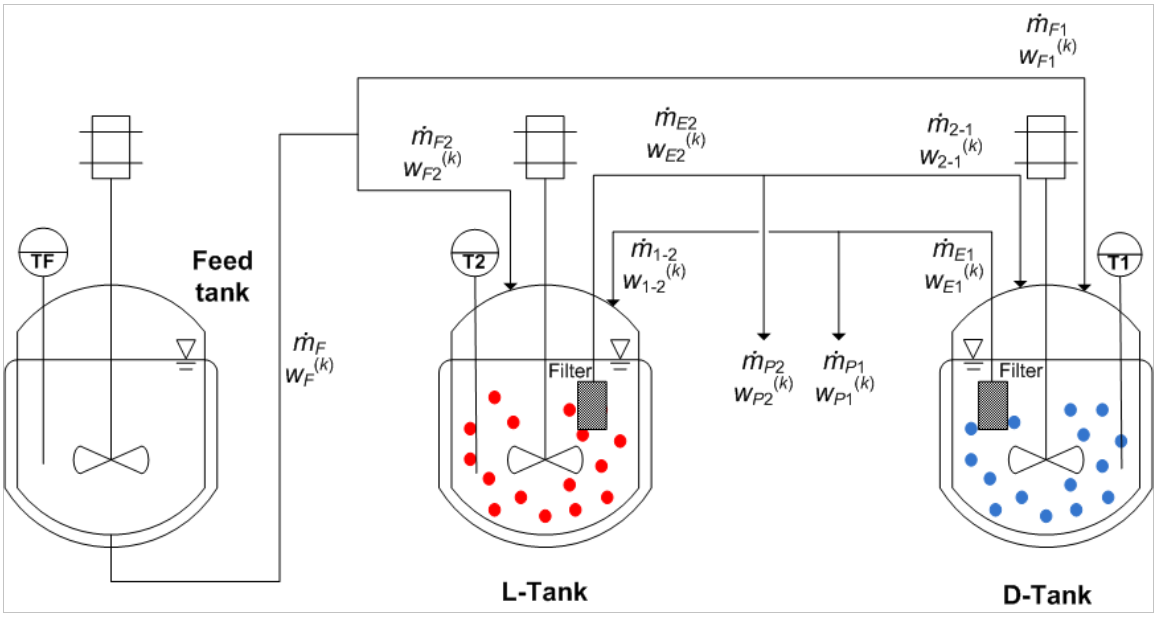

Figure 4.1: Schematic illustration of the CC-PC process for the separation of enantiomers using the conglomerate forming system of asparagine monohydrate. TF symbolizes the temperature in the feed tank, T1 is the crystallization temperature in the D-Tank, T2 is the crystallization temperature in L-Tank, Blue and red filled circles symbolize growing enantiopure seeds of D-asparagine monohydrate (D-AsnH_2O) and L-asparagine monohydrate (L-AsnH_2O) in the D- and L-Tank, respectively. The filters (grey boxes) in the D- and L-Tank are used to retain solids.

The preferential crystallization of the asparagine monohydrate enantiomers begins with the cooling of the aqueous racemic solutions present in each crystallizer to bring them into the metastable zone. The racemic feed solution of the conglomerate monohydrate enantiomers dissolved in water is supplied continuously to the crystallizers at a higher temperature. When the crystallization temperature is reached in the crystallizers, enantiopure seeds of the monohydrate enantiomers are supplied to each crystallizer. Thus, crystal growth of the D- and L-AsnH_2O seeds occurs in the D- and

D-Tank, respectively, at isothermal conditions with identical crystallization temperatures in both crystallizers (i.e. T1 = T2). The crystal-free liquid exchange streams between the crystallizers are initiated and mother liquor is transferred via a filter to the opposite crystallizer to obtain a nearly racemic composition in the mother liquors. To maintain a constant suspension volume in each crystallizer, mother liquor is withdrawn from the liquid exchange streams from the crystallizers and transferred to the purge tanks.

4.3 Mathematical modeling

In this section, the assumptions underlying the mathematical model are first presented. Then follows the development of the mathematical model.

- The crystallizers are considered ideally mixed.
- The operation of the two crystallizers is isothermal.
- Residence times and volumes of the liquid phase in the crystallizers are identical.
- No crystals are withdrawn or fed to the crystallizers. Only initial seeding is used.
- Nucleation of enantiomers, crystal breakage, attrition, and agglomeration are neglected. Only growth on the initially supplied seed crystals takes place.
- Secondary nucleation of the seeded enantiomer, caused by the presence of the seed crystals in the crystallizing suspension, is neglected in accordance with Petruševska-Seebach et al.[66].
- Crystal growth inhibition by the presence of the counter enantiomer is neglected.
- Crystallization kinetics, i.e. nucleation and growth kinetics, of the enantiomers are supposed to be identical.
- The overall growth rate of the seed crystals is independent of size[66] and morphology of the seeds and thereby time.
- The overall growth rate is controlled by surface integration kinetics as suggested by Petruševska-Seebach et al.[66].
- The size-independent crystal growth is assumed to be governed by McCabe ΔL law[70].

The validity of the above assumptions, and some additional ones to be made during the model development below, is assessed after model validation of the CC-PC process with experimental data has taken place. The mathematical model can now be developed by considering each crystallizer as a control volume.

4.3.1 Model development

4.3.1.1 Crystal population balance

During the crystallization process, only growth of the enantiopure seeds occurs in each crystallizer. The crystal population balance equation (PBE) for the preferred enantiomer in each crystallizer becomes[70]:

$$\frac{\partial n_i^{(p)}(t,L)}{\partial t} = -G_i^{(p)}(t)\,\frac{\partial}{\partial L} n_i^{(p)}(t,L), \quad i \in \{1,2\} \tag{4.1}$$

with the boundary condition:

$$n_i^{(p)}(t, L=0) = 0 \tag{4.2}$$

The initial condition is:

$$n_i^{(p)}(t=0, L) = n_{seeds,i}^{(p)}(L) \tag{4.3}$$

$n_{seeds,i}^{(p)}(L)$ is the initial number distribution of the seed crystals, which is directly linked to the mass of enantiopure seeds of the preferred enantiomer supplied into the crystallizer per unit volume of suspension:

$$m_{seeds,i}^{(p)} = k_v \rho_S \int_{L=0}^{\infty} L^3 n_{seeds,i}^{(p)}(L)\,\mathrm{d}L \tag{4.4}$$

4.3.1.2 Crystal growth kinetics

The linear overall growth rate, $G_i^{(p)}$, can be described by a power-law growth rate model expressing the relation between supersaturation ratio of the preferred enantiomer and crystal growth[62]:

$$G_i^{(p)}(t) = k_{g,i}(T_i)\left(S_i^{(p)}(t) - 1\right)^{\alpha}, \quad i \in \{1,2\} \tag{4.5}$$

The temperature-dependent rate constant for the surface integration controlled crystal growth, $k_{g,i}$, can be expressed by an Arrhenius equation[62]:

$$k_{g,i}(T_i) = k_{0,i} \exp -\frac{E_{a,g}}{RT_i} \tag{4.6}$$

4.3.1.3 Supersaturation ratio

The supersaturation ratio of the preferred, p, enantiomer as well as the counter, c, enantiomer, $S_i^{(k)}$, in each crystallizer can be expressed as[62]:

$$S_i^{(k)}(t) = \frac{w_i^k(t)}{w_{eq,i}^k(t)}, \quad k \in \{p, c\} \tag{4.7}$$

where $w_i^{(k)}$ is the mass fraction of enantiomer k and $w_{eq,i}^{(k)}$ is the solubility mass fraction of enantiomer k at the crystallization temperature.

4.3.1.4 Concentration of enantiomers

The mass fraction of the enantiomers in each crystallizer, $w_i^{(k)}$, is expressed as:

$$w_i^k(t) = \frac{m_i^{(k)}(t)}{\sum_{(k)} m_i^{(k)}(t) + m_i^{sol}}, \quad k \in \{p, c\} \tag{4.8}$$

where $m_i^{(k)}$ is the mass of dissolved enantiomer k and m_i^{sol} is the mass of solvent at the crystallization temperature.

4.3.1.5 Liquid phase mass balance for the preferred enantiomer

The liquid phase mass balance of the preferred enantiomer includes the consumption from the continuous phase leading to deposition on the surfaces of the enantiopure seed crystals resulting in crystal growth and the mass flow rates of the inlet and outlet streams:

$$\frac{\mathrm{d}m_i^{(p)}(t)}{\mathrm{d}t} = \dot{m}_{F,i}^{(p)} + \dot{m}_{j-i}^{(p)}(t) - \dot{m}_{E,i}^{(p)}(t) - \dot{m}_{g,i}^{(p)}(t), \quad i \in \{1,2\} \neq j \in \{1,2\} \tag{4.9}$$

where $m_i^{(p)}$ is the mass of enantiomer p in crystallizer i, $\dot{m}_{F,i}^{(p)}$ is the mass flow rate of the feed inlet into the crystallizer, $\dot{m}_{j-i}^{(p)}$ is the crystal-free liquid exchange from crystallizer j to crystallizer i and $\dot{m}_{E,i}^{(p)}$ is the crystal-free effluent mass flow rate from the crystallizer. It should be emphasized that the liquid mass flow rates are expressed as the product of the volumetric flow rate of solution, the density of the solution at the actual temperature and concentration, and the mass fraction of the preferred enantiomer in the solution.

The rate of the mass of solids produced by crystal growth, $\dot{m}_{g,i}^{(p)}(t)$, is given by[70]:

$$\dot{m}_{g,i}^{(p)}(t) = 3\rho_S k_v G_i^{(p)}(t) A_i^{(p)}(t) V_i \tag{4.10}$$

Equation (4.10) is derived based on the assumption that the overall growth rate is

linear, i.e. the growth rate is the same along the same characteristic dimension of all crystals, and a size-independent growth rate[62,70].

Regarding the liquid phase mass balance for the preferred enantiomer, the initial condition in the crystallizers is the initial mass of the preferred enantiomer in solution:

$$m_i^{(p)}(t=0) = m_{0,i}^{(p)} \tag{4.11}$$

4.3.1.6 Liquid phase mass balance for the counter enantiomer

Since it is assumed that neither nucleation nor growth of the counter enantiomer occurs, the liquid phase component mass balance of the counter enantiomer in each crystallizer includes only the terms relating the mass flow rates of the inlet and outlet flows:

$$\frac{\mathrm{d}m_i^{(c)}(t)}{\mathrm{d}t} = \dot{m}_{F,i}^{(c)} + \dot{m}_{j-i}^{(c)}(t) - \dot{m}_{E,i}^{(c)}(t), \quad i \in \{1,2\} \neq j \in \{1,2\} \tag{4.12}$$

where $i \neq j$.

The initial condition for the mass balance in (4.12) is given by the initial mass of the counter enantiomer in solution:

$$m_i^{(c)}(t=0) = m_{0,i}^{(c)} \tag{4.13}$$

4.3.1.7 Feed flow rates

In the above mentioned mass balances, the feed mass flow rate of enantiomer into each crystallizer is given as a function of the fraction of the feed solution entering the crystallizer. For $i = 1$:

$$\dot{m}_{F,1}^{(k)} = \delta \dot{m}_F^{(k)} \tag{4.14}$$

and for $i = 2$:

$$\dot{m}_{F,2}^{(k)} = (1-\delta)\,\dot{m}_F^{(k)} \tag{4.15}$$

It should be emphasized that the flow rate of the racemic feed solution is assumed constant and therefore is only a function of the temperature of the feed.

4.3.1.8 Crystal-free liquid exchange flow rate

The mass flow rate of the crystal-free liquid exchange between the crystallizers is given as:

$$\dot{m}_{j-i}^{(k)}(t) = \dot{m}_{E,j}^{(k)}(t) - \dot{m}_{P,j}^{(k)}(t) \tag{4.16}$$

where $i \neq j$. It should be noted that the volumetric flow rate of the purge streams is equal to the volumetric flow rate of the feed solution entering the respective crystallizer. This is based on the assumption that changes in the volume of the suspension in the crystallizer, due to the crystallization reaction, are negligible.

4.3.1.9 Effluent flow rate

The effluent mass flow rate of enantiomer from the crystallizers is given as a function of the concentration of enantiomer in the liquid phase in each crystallizer:

$$\dot{m}_{E,i}^{(k)}(t) = \frac{V_i}{\tau_i} \rho_{L,i}(T_i, w_i)\, w^{(k)} i(t) \tag{4.17}$$

4.3.2 Process metrics

4.3.2.1 Separation efficiency: U-value

To assess the efficiency of the CC-PC process, the ratio between the total concentration of the preferred enantiomer in the purge streams and the total concentration of the preferred enantiomer in the feed solution entering the crystallizers, calculated by a steady-state mass balance, is considered at time t. The ratio is denoted the U-value and is expressed as:

$$U - \text{value}(t) = \frac{w_i^{(p)}(t) + w_j^{(p)}(t)}{w_{F,i}^{(p)} + w_{F,j}^{(p)}} \times 100\%, \quad i \in \{1,2\} \neq j \in \{1,2\} \tag{4.18}$$

4.3.2.2 Yield based on feed solution

The yield, based on the feed solution, provides a measure of the amount of enantiomer supplied from the liquid feed solution which is produced as solid material deposited on the seed crystals supplied in each crystallizer. The yield is given as the ratio between the accumulated mass of the solid product produced at the end of the process duration, t_f, and the total mass of the enantiomer fed into the crystallizer:

$$Y_{L,i}^{(p)}(t_f) = \frac{m_{g,i}^{(p)}}{m_{F,i}^{(p)}} \times 100\% \tag{4.19}$$

4.3.2.3 Productivity and yield based on seeds

The productivity from the simulations of the preferred enantiomer in each crystallizer at the end of the process duration is estimated as the ratio between the accumulated mass of the solid product produced and the product of the total mass of enantiomer fed into the crystallizer and the duration of the process, t_f:

$$\mathrm{Pr}_i^{(p)}\left(t_f\right) = \frac{m_{g,i}^{(p)}}{m_{F,i}^{(p)} t_f} \tag{4.20}$$

Similarly, the yield of the solid product of the preferred enantiomer produced in each crystallizer at the end of the duration of the process, t_f, is defined as the ratio between the accumulated mass of solid product produced and the mass of the enantiopure seeds initially supplied to the crystallizer:

$$Y_{S,i}^{(p)}\left(t_f\right) = \frac{m_{g,i}^{(p)}}{m_{seeds,i}^{(p)}} \times 100\% \tag{4.21}$$

4.3.2.4 Crystal size yield

The simulations of the CC-PC process are also evaluated by the gain in the average size of the solid product. This is defined as the ratio between the average size of the final solid product and the sum of the average size of the initially supplied seed crystals and the average size of the final solid product produced at the end of the process duration, t_f:

$$Y_i^{(p)}\left(t_f\right) = \frac{L_{av,i}^{(p)}}{L_{av,i}^{(p)} + L_{seeds,i}^{(p)}} \times 100\% \tag{4.22}$$

4.4 Numerical solution procedure

The coupled partial differential equation system and the liquid phase mass balances are solved using the method of moments (MOM) according to Randolph and Larson[70]. This transformation method of the PBE is useful to obtain average quantities of the particle size distribution of the final solid product. The reason for the selection of the method of moments is the lack of knowledge of the Particle Size Distribution (PSD) of the harvested solid product due to the insufficient quantity of the solid product harvested at the end of each experiment[11]. Furthermore, in most industrial applications the representation of the PSD is sufficiently obtained by some average or total quantities[70].

Using integration by parts, the following general expression is obtained for the moments of the number density function of the crystal population of the preferred enantiomer in the crystallizing suspension[70]:

$$\frac{\mathrm{d}N_{x,i}^{(p)}(t)}{\mathrm{d}t} = xN_{x-1,i}^{(p)}(t)\,G_i^{(p)}(t) \tag{4.23}$$

where the moments are expressed as[70]:

$$N_{x,i}^{(p)}(t) = \int_{L=0}^{\infty} L^x n_i^{(p)}(t,L)\,\mathrm{d}L \tag{4.24}$$

The first four moments of the population balance, i.e. $x \in \{0,1,2,3\}$, for the preferred enantiomer in each crystallizer are derived:

$$\frac{\mathrm{d}N_{0,i}^{(p)}(t)}{\mathrm{d}t} = 0 \tag{4.25}$$

$$\frac{\mathrm{d}N_{1,i}^{(p)}(t)}{\mathrm{d}t} = N_{0,i}^{(p)}(t)\,G_i^{(p)}(t) \tag{4.26}$$

$$\frac{\mathrm{d}N_{2,i}^{(p)}(t)}{\mathrm{d}t} = 2N_{1,i}^{(p)}(t)\,G_i^{(p)}(t) \tag{4.27}$$

$$\frac{\mathrm{d}N_{3,i}^{(p)}(t)}{\mathrm{d}t} = 3N_{2,i}^{(p)}(t)\,G_i^{(p)}(t) \tag{4.28}$$

The derivation of the moments is provided in Appendix E. The first four moments of the PBE result in coupled ordinary differential equations (ODEs) together with the liquid phase mass balances. The systems of the ODEs are solved using the built-in *ode*45 function in MATLAB (The Mathworks Inc., Natick, USA). The necessary MATLAB scripts are provided in Appendix F. The model is capable of describing the transient change in the concentrations of the enantiomers in the mother liquor in each crystallizer. Furthermore, the transient change in the moments representing the particle size distribution of the crystal population of the preferred enantiomer in each crystallizer is also obtained from the model. The purpose of the model is to provide a suitable tool for the estimation of critical process parameters to enable the separation of conglomerate forming enantiomers by the CC-PC process without the loss in productivity and yield due to crystallization of the counter enantiomer. Moreover, the model can be used to elucidate effects of changes in the crystallization kinetics on the progress of the separation process to be used for optimization studies.

4.5 Estimation of physical and chemical parameters

A number of chemical and physical parameters for the asparagine monohydrate enantiomers and data for the crystallization kinetics of the conglomerate forming system of asparagine monohydrate in water are required in the model. Some of these were estimated by Petruševska-Seebach et al.[66]. The parameters are listed in Table 4.2.

4.5.1 Physical constants

The solid density was taken from Haynes[35] and the volume shape factor and the area shape factor were taken from Myerson[62] based on the observation by SEM of the enantiopure seed crystals and the solid product harvested at the end of each experiment[11].

4.5.2 Solubility concentration of enantiomer

The equilibrium mass fraction, describing the solubility of L-AsnH_2O in water at crystallization temperature, $w_{eq,i}^{\text{L-Asn}}$, is experimentally determined and is expressed as a function of the concentration of the counter enantiomer D-Asn, $w_i^{\text{D-Asn}}$, in the crystallizer[66]:

$$w_{eq,i}^{\text{L-Asn}}(t) = 0.0092 \exp 0.0443 (T_i - 273.15) + 0.030482 w_i^{\text{D-Asn}}(t) \tag{4.29}$$

where $i \in \{1, 2\}$. Equation (4.29) is assumed to be valid also for D-AsnH_2O in water.

4.5.3 Density of the liquid phase

The density of the liquid phase in the crystallizers, $\rho_{L,i}$, can be expressed by the following empirical correlation[66]:

$$\rho_{L,i}(T_i, w_i) = \frac{1}{0.9999 + 4.911 \times 10^{-6} (T_i - 273.15)^2} + 0.3572 w_i(t) \tag{4.30}$$

Note that equation (4.30) takes into account the dependence of the liquid density on the temperature of the solution and the total concentration of the enantiomers in the solution.

4.5.4 Parameters for growth kinetics

The pre-exponential factor included in the Arrhenius expression for the overall growth rate constant, $k_{0,i}$, is estimated by fitting the model to the progress curves of the concentration of the dissolved enantiomers in the mother liquor obtained from the

three experiments for continuous preferential crystallization[11].

The activation energy for crystal growth and the order of crystal growth used are estimated by Petruševska-Seebach et. al[66]. The values obtained imply that the mechanism for the control of crystal growth is predominantly surface integration[61].

The remaining parameters were taken from the experimental conditions for the experimental realization of the CC-PC process[11]. These parameters are adjustable and are investigated in the sensitivity analysis subsequent to model validation in the present study.

4.6 Results and discussion

4.6.1 Model validation using the data of Chaaban et al.[11]

The validation of the dynamic model for the continuous preferential crystallization of the asparagine monohydrate enantiomers, denoted D-AsnH_2O and L-AsnH_2O, is performed using the experimental data from the liquid and solid phase analyses of triplicate experiments carried out and presented in Chaaban et al.[11]. Initially, the input parameters listed in Table 4.2 are used. The validity of some of these parameters is also investigated subsequent to validation of the model.

4.6.1.1 Productivity and yield

A summary of the simulation and experimental results of the productivity and the accumulated yield of the solid product obtained are listed in Table 4.1.

Table 4.1: Summary of the results of the U-value, yield based on feed solution, Y_L, productivity, Pr, the accumulated yield of solid products, and the yield in crystal size from the D- and L-Tank obtained by the simulation and experimental data[11], Y_S and Y. Note the units. Standard deviations for the experimental results are also given.

	Experimental		**Simulation**	
Tank	**D**	**L**	**D**	**L**
***U*-value [%]**	100.0±1.8	100.4±2.1	100.2	100.0
Y_L **[%]**	1.08±0.19	1.52±0.11	1.08	1.52
Pr [$\times 10^{-4}$ g/(g min)]	1.20±2.10	1.69±0.12	1.17	1.65
Y_S **[%]**	37.79±6.12	54.08±3.07	37.79	54.09
Y **[%]***	N/A	N/A	51.35	51.85

$*$ Not experimentally determined due to insufficient sample size for PSD measurements.

Table 4.2: Physical and chemical parameter values required for the mathematical model.

Parameters	Symbol	Value	Unit
Physical constants			
Density of $AsnH_2O$ crystal[35]†	ρ_S	1533	kg/m^3
Volume shape factor	k_v	2	-
Area shape factor	k_a	10	-
Universal gas constant	R	8.3145×10^{-3}	kJ/(mol K)
Process variables			
Crystallization temperature‡	T_{cryst}	19	°C
Liquid volume in crystallizers	$\mathbf{V}$	220	mL
Mean residence time of liquid phase in crystallizers	τ	15	min
Fraction of feed solution inlet	δ	0.5	-
Mass of seeds of preferred enantiomer in D-Tank	$m^{(p)}_{seeds,1}$	0.4642	g
Mass of seeds of preferred enantiomer in L-Tank	$m^{(p)}_{seeds,2}$	0.4641	g
Initial sieve fraction of seeds in crystallizers	-	250-355	μm
Feed inlet temperature	T_F	27	°C
Conc. of D-Asn in feed solution into D-Tank§	$w^{\text{D-Asn}}_{F,1}$	2.4282	wt%
Conc. of L-Asn in feed solution into D-Tank¶	$w^{\text{L-Asn}}_{F,1}$	2.4607	wt%

(*continued*)

† Average of solid density of D- and D-$AsnH_2O$ at 15 °C[35].
‡ Crystallization temperature in both crystallizers, i.e. T_{cryst} = T1 = T2.
§ Average concentrations in the feed solution estimated by polarimetric analysis of feed samples for the three experiments performed[11].
¶ Average concentrations in the feed solution estimated by polarimetric analysis of feed samples for the three experiments performed[11].

Table 4.2 – (*Continued*)

Parameters	**Symbol**	**Value**	**Unit**
Conc. of D-Asn in feed solution into L-Tank‖	$w_{F,2}^{\text{D-Asn}}$	2.4282	wt%
Conc. of L-Asn in feed solution into L-Tank**	$w_{F,2}^{\text{L-Asn}}$	2.4607	wt%
Process duration	t_f	90	min
Parameters for growth kinetics			
Pre-exponential factor for growth rate of D-AsnH_2O	$k_{0,1}$	19.50	m/s
Pre-exponential factor for growth rate of L-AsnH_2O	$k_{0,2}$	23.78	m/s
Activation energy for crystal growth[66]	$E_{a,g}$	49.1	kJ/mol
Order of crystal growth[66]	α	1	-

‖ Average concentrations in the feed solution estimated by polarimetric analysis of feed samples for the three experiments performed[11].
** Average concentrations in the feed solution estimated by polarimetric analysis of feed samples for the three experiments performed[11].

The values of the process outputs obtained from the simulation are in good agreement with the experimental results. The pre-exponential factors, $k_{0,1}$ and $k_{0,2}$, used for estimation of the growth rates of the enantiomer monohydrates, were adjusted to fit simultaneously simulations of the productivity, yield of solids produced, and the transient liquid phase concentration curves for the enantiomers. The values of the pre-exponential factors are given in Table 4.2.

Using equation (4.6), the growth rate constant, $k_{g,i}\,(T_i)$, can be estimated. In the present study, the growth rate constant is calculated to 0.325×10^{-7} m/s in the D-Tank and 0.396×10^{-7} m/s in the L-Tank, both at 19 °C. A very small difference between the growth rate constants was found. This difference may be ascribed to the difference in the surface structure, the size of the growing seed crystals, and the type of crystallization process, which are all lumped into the pre-exponential factor.

The pre-exponential factor for crystal growth of L-AsnH_2O was estimated to 67.53 m/s at 30 °C by Petruševska-Seebach et. al[66]. Using this value, the calculation of the growth rate of L-AsnH_2O at the crystallization temperature of 19 °C gives 1.12×10^{-7} m/s, which is about 65 % higher than the value obtained in the present study. This may be ascribed to the difference in the surface structure and initial size of the seed crystals used. The sensitivity of the model to changes in the pre-exponential factors and the crystallization temperature is investigated and presented later in this study.

4.6.1.2 Concentration of enantiomers

In Figure 4.2, a comparison of simulations and experimental data for the mass fractions of D- and L-Asn in the D- and L-Tank are shown. The comparison shows a reasonable good agreement for the mass fractions of dissolved enantiomers in the crystallizing suspensions. Simulations also show that the composition in the mother liquors is nearly racemic.

Simulations in Figure 4.2 also suggest that the concentration of the counter enantiomer increases slightly, but this effect is within the standard deviation of the experimental data. The concentration of the preferred enantiomer in the D- and L-Tank is maintained nearly constant and is within the standard deviation of the experimental data. Steady-state concentrations of the preferred enantiomer and the counter enantiomer in the liquid phase in each crystallizer are obtained after about 60 minutes corresponding to four residence times.

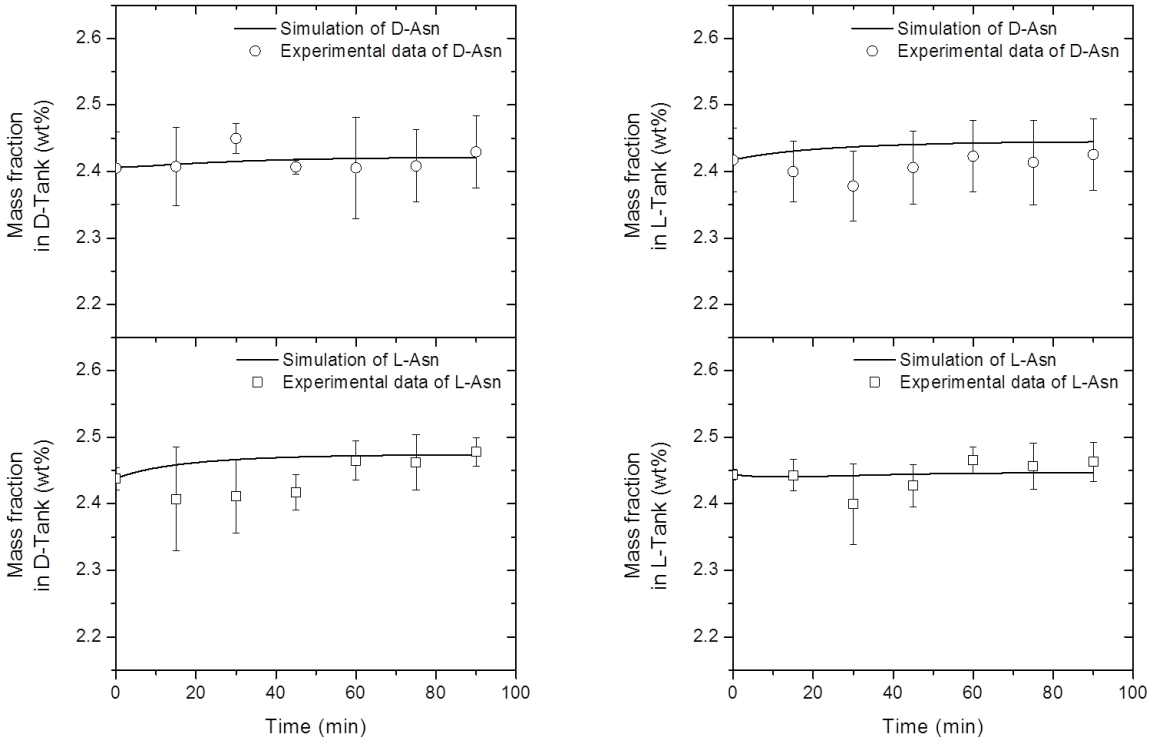

Figure 4.2: Comparison of model simulations (solid lines) with experimental data for the mass fractions of D- and L-Asn in the D-Tank (left) and the L-Tank (right) (symbols). Error bars for experimental data are also shown. At time equals zero seeding is performed. Conditions are the same as in Table 4.2.

4.6.1.3 Supersaturation and crystal growth

Comparison of experimental data and simulations of the supersaturation ratios of the crystallizing enantiomer of D-Asn in the D-Tank and L-Asn in the L-Tank and the mass growth rate of the preferred enantiomer are shown in Figure 4.3.

Simulations of the supersaturation ratio of the preferred enantiomer in each crystallizer are in reasonable agreement with the experimental data. Moreover, the tendency in the progress of the simulation is identical to that of the mass fraction of the preferred enantiomer in each crystallizer shown in Figure 4.3. This is a consequence of the dependency of the supersaturation ratio on the actual concentration of the preferred enantiomer.

In Figure 4.3, a comparison of model simulations with experimental data for the mass growth rates of the preferred enantiomer in each crystallizer shows reasonable agreement between the experimentally estimated growth rates and simulations. It is also seen that the mass growth rate of D-AsnH_2O estimated by simulations in the D-Tank is lower when compared to the growth rate of L-AsnH_2O in the L-Tank. The

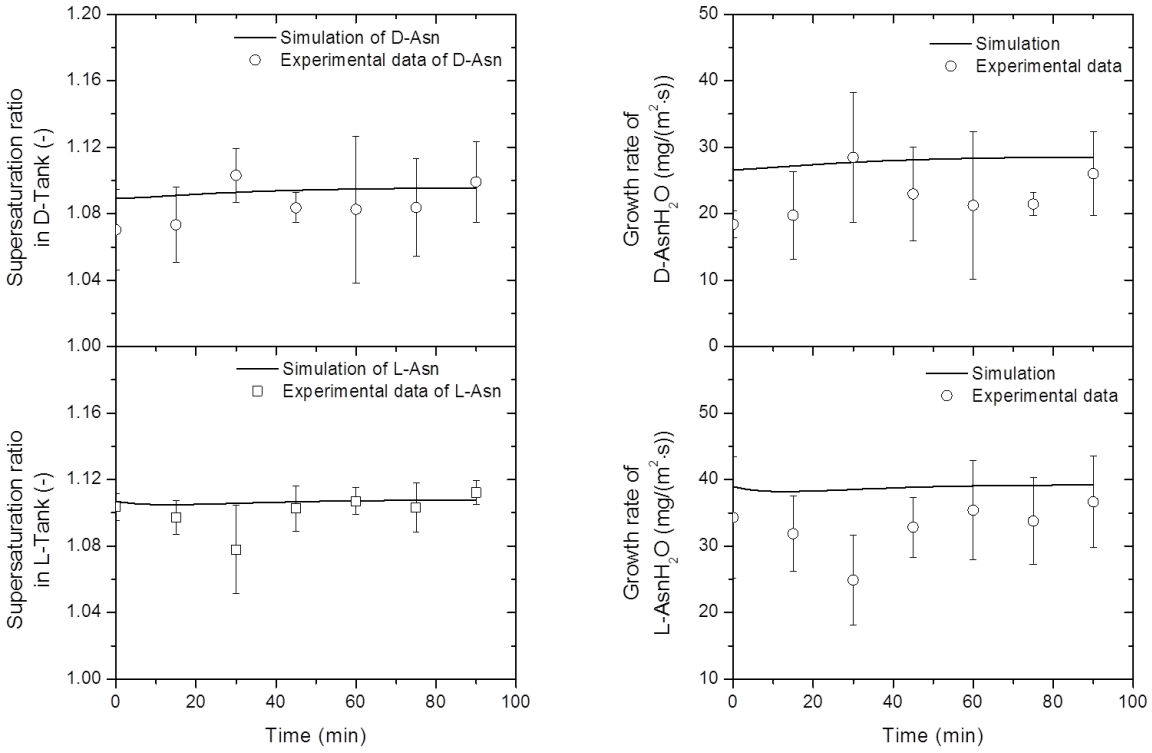

Figure 4.3: Comparison of model simulations (solid lines) with experimental data for the supersaturation ratios and the mass growth rates of the preferred enantiomer in the D-Tank (top) and the L-Tank (bottom) (symbols). Error bars for experimental data are also shown. At time equals zero seeding is performed. Conditions are the same as given in Table 4.2.

reasons for this difference are the different growth rate constants and the different overall surface area of the initially supplied seed crystals.

4.6.2 Sensitivity analysis

A sensitivity analysis is performed to investigate the effect of the different process variables and kinetic constants on the overall process performance, thereby searching for the most optimal conditions for the separation of asparagine monohydrate enantiomers by the CC-PC process. It should be emphasized that the simulations are performed assuming that the crystallizers are operated at identical conditions and only one parameter is changed at a time while all the remaining parameters are kept the same as given in Table 4.2 or as indicated in the text. Steady-state mass balance check of the simulation outputs was performed, where ever it is possible, to ensure the predictability of the model.

4.6.2.1 Mean residence time of the liquid phase

The mean residence time of the liquid phase in the crystallizers is varied between 15 (base case) and 60 minutes. The concentration of the enantiomers in the liquid phase for the simulations is given in Figure 4.4.

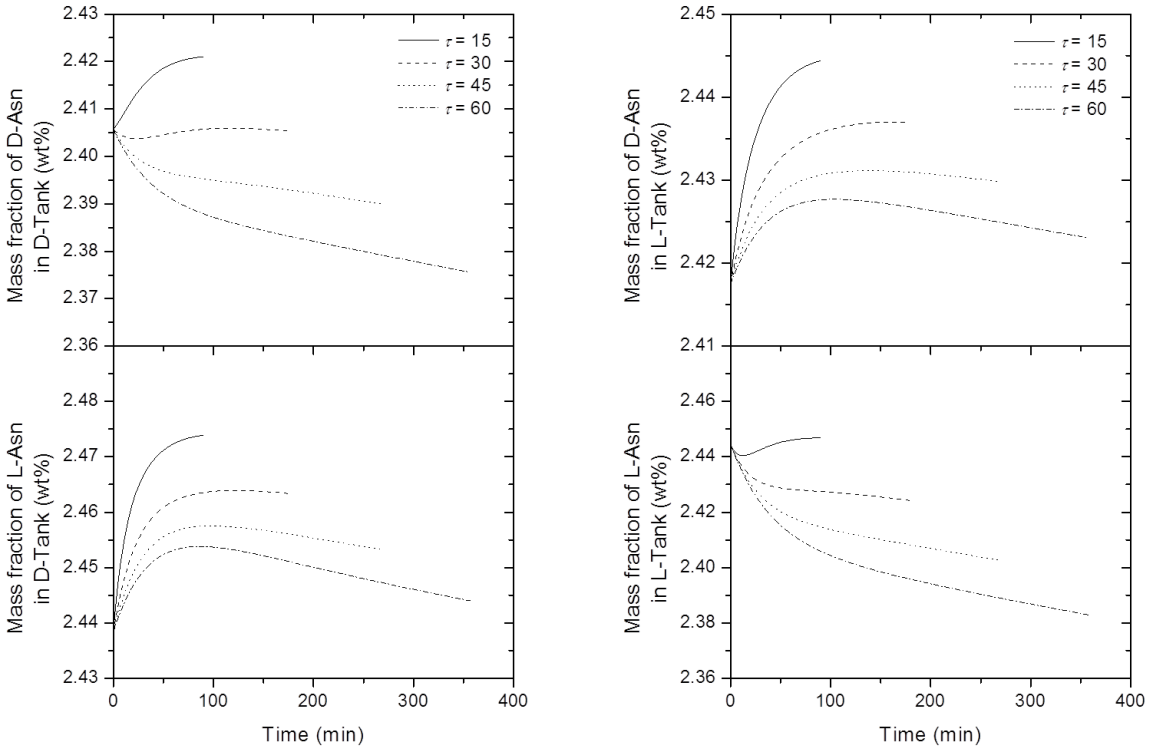

Figure 4.4: Model simulations of the concentration of enantiomers in the D-Tank (left) and the L-Tank (right) for the mean residence time of the liquid phase, τ, between 15 (base case) and 60 minutes. The remaining process parameters are the same as given in Table 4.2. At time equals zero seeding is performed. Note the difference in the scale of the abscissa.

For a mean residence time of the liquid phase of 15 minutes, the concentration of the preferred enantiomer increases indicating an accumulation of the enantiomer in the liquid phase caused by slow surface integration compared to the rate of supply of the preferred enantiomer into the crystallizers. For L-Asn in the L-Tank, the concentration decreases slightly in the beginning, but increases again. This may be due to the initial rapid growth of L-AsnH_2O seed crystals due to the initially higher supersaturation of L-Asn. At higher mean residence times, the concentration of the preferred enantiomer decreases more rapidly. This decrease is more pronounced in the first 50 minutes and begins to level out. The rapid decrease indicates an increase in the consumption of the preferred enantiomer in the crystallizing suspension due to sufficient time for the enantiomer species to integrate into the surface of the seed crystals and thereby improve the separation performance of the process.

Correspondingly, the concentration of the counter enantiomer is higher than the preferred enantiomer and decreases as the mean residence time in the liquid phase increases. This is due to the decrease of the concentration of the counter enantiomer in the opposite crystallizer in which this counter enantiomer is consumed for crystal growth of the seed crystals. This is exactly the desired effect of the coupled crystallizer configuration. Overall, however, the concentrations do not vary much with the residence time.

To evaluate the performance of the process, a summary of the estimated process metrics are listed in Table 4.3.

Table 4.3: Summary of the results of the U-value, yield based on feed solution, Y_L, productivity, Pr, the accumulated yield of solid products, Y_S, and the yield in crystal size, Y, from the D- and L-Tank obtained by the simulations for changing the mean residence time, τ, between 15 (base case) and 60 minutes. Note the units.

	15 min		30 min		45 min		60 min	
Tank	**D**	**L**	**D**	**L**	**D**	**L**	**D**	**L**
t_f **[min]**	90	90	180	180	270	270	360	360
$\boldsymbol{U}$**-value [%]**	100.2	100.0	99.71	99.31	99.24	98.66	98.80	98.06
Y_L **[%]**	1.08	1.52	2.18	3.10	3.27	4.61	4.2	5.97
Pr [$\times 10^{-4}$ **g/(g min)**]	1.17	1.65	1.19	1.68	1.18	1.67	1.21	1.69
Y_S **[%]**	37.79	54.09	76.73	110.4	114.8	164.2	150.7	212.9
$\boldsymbol{Y}$ **[%]**	51.35	51.85	52.49	53.35	53.46	54.56	54.29	55.54

From Table 4.3 it can be seen that the overall separation performance of the CC-PC process is improved compared to the base case at $\tau = 15$ min. This improvement can be ascribed to the fact the duration of the process becomes longer which gives more time for the crystallizing species to integrate into the surface of the seed crystals thereby resulting in increased yields. The U-value, however, has changed slightly due to a very slow consumption ascribed to the slow surface integration on the seed crystals. In contrast, the productivity decreases slightly, which is an inherent effect of the longer duration of the process.

4.6.2.2 Excess of enantiomer in feed solution

Sometimes preferential crystallization processes for the separation of enantiomers are carried out with an initial enantiomeric excess of the preferred enantiomer. The achievement of the desired enantiomeric excess (ee) leads to additional cost for which a higher productivity should compensate. In Figure 4.5, enantiomeric excess of the D-Asn is considered and the enantiomeric excess is varied between zero and 6% for

the same duration as the base case, i.e. 90 minutes. It should be emphasized that the concentration of enantiomers in the feed solution is changed to 2.5 wt% of D- and L-Asn compared to the values given in Table 4.2, i.e. the base case corresponding to $ee_D = 0$, to obtain a clearer picture of the effects of the enantiomeric excess.

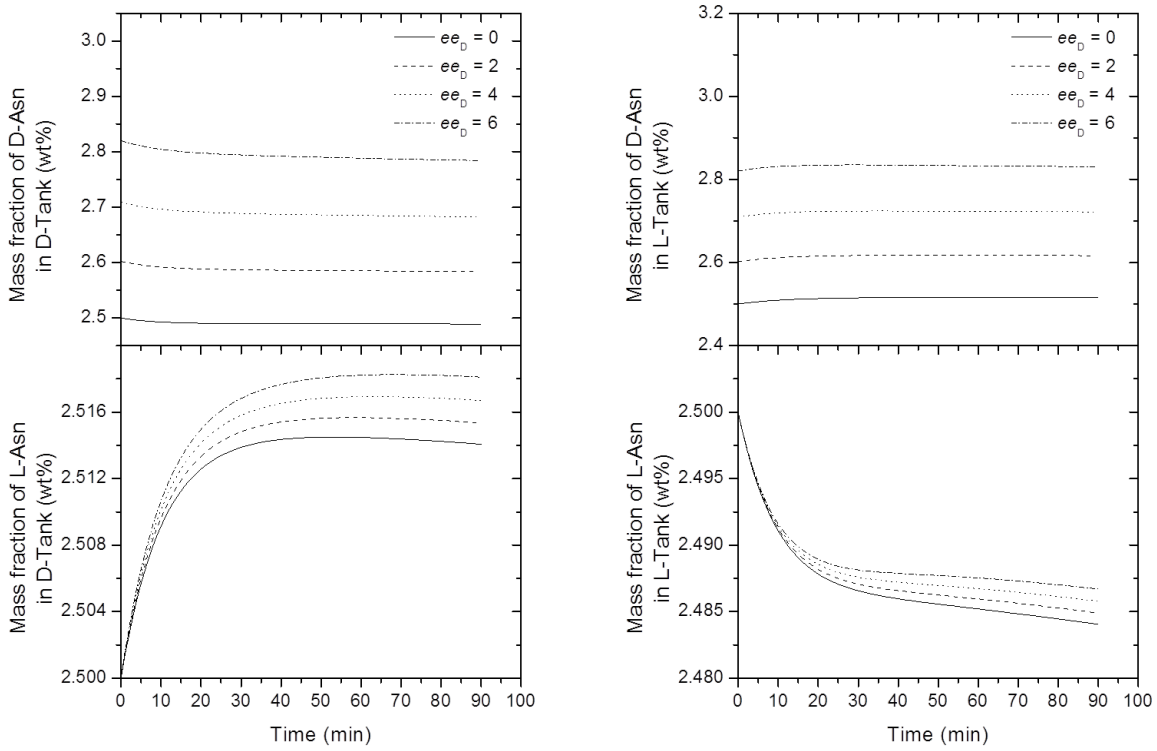

Figure 4.5: Model simulations of the concentration of enantiomers in the D-Tank (left) and the L-Tank (right) for the enantiomeric excess of D-Asn, ee_D, of 0 (base case) to 6%. The concentration of the enantiomer in the feed solution is changed to 2.5 wt%. The remaining process parameters are the same as given in Table 4.2. At time equals zero seeding is performed. Note the difference in the scale of the abscissa.

The increase in the enantiomeric excess of the D-Asn has a negligible effect on the liquid phase composition in both crystallizers. However, a slight decrease in the concentration of D-Asn is observed due to the slow surface integration on the seed crystals and is independent on the enantiomeric excess. The concentration of L-Asn is decreasing in the L-Tank, in which it is consumed for crystals growth, and is increasing in the D-Tank as expected. The change in the concentration of L-Asn in the liquid phase in each crystallizer is, however, very small as indicated by the very small scaling of the abscissa in Figure 4.5. Increasing the enantiomeric excess of D-Asn in the liquid phase increases the solubility concentration of the L-Asn as given in equation (4.29). The supersaturation ratio, i.e. the crystallization driving force, decreases for the increase in the *ee* of D-Asn. Therefore, the concentration of L-Asn in

the crystallizers increases. Additionally, the increase in the *ee* of D-Asn also increases the density of the feed solution as given in equation (4.30) when the feed temperature and total concentration of the enantiomers are considered. This results in a higher mass flow rate of the enantiomers in to and out of the crystallizers. Note that the liquid phase concentration of D-Asn in the D- and L-Tank reaches constant value after about two residence times, i.e. after about 30 minutes of operation. In contrast, the concentration of L-Asn in the D-Tank reaches constant value after about four residence times, i.e. after about 60 minutes of operation. This effect can be explained by the mentioned dependence of the solubility of L-AsnH_2O on the concentration of D-Asn in the liquid phase.

Table 4.4: Summary of the results of the U-value, yield based on feed solution, Y_L, productivity, Pr, the accumulated yield of solid products, Y_S, and the yield in crystal size, Y, from the D- and L-Tank obtained by the simulations for an enantiomeric excess of D-Asn, ee_D, between zero (base case) and 6%. Note the units.

	0%		2%		4%		6%	
Tank	**D**	**L**	**D**	**L**	**D**	**L**	**D**	**L**
***U*-value [%]**	100.1	100.0	99.9	100.0	99.7	100.1	99.5	100.1
Y_L **[%]**	1.42	1.75	1.92	1.73	2.45	1.71	3.01	1.69
Pr [$\times 10^{-4}$ g/(g min)]	1.55	1.91	2.09	1.88	2.67	1.86	3.27	1.84
Y_S **[%]**	51.54	63.49	72.45	62.78	96.21	62.04	122.88	61.28
Y **[%]**	51.80	52.15	52.40	52.13	53.00	52.11	53.61	52.09

As a consequence of the declining crystallization driving force of L-Asn, the separation performance of the process regarding L-AsnH_2O is declining for increasing *ee* of D-Asn in the feed solution, as observed in Table 4.4. In contrast, increasing the ee of D-Asn improves the separation performance of the process with respect to D-AsnH_2O as expected. However, the efficiency of the process is only slightly improved. This could again be explained by the slow surface integration on the surface of the seed crystals. It should also be addressed that the model does not account for the inhibiting effect of D-Asn on the growth of the L-AsnH_2O seed crystals as suggested by Petruševska-Seebach et. al[66]. In this case, the declining effect on the crystallization of L-AsnH_2O would be more pronounced. Similarly, changing the enantiomeric excess of the opposite enantiomer, i.e. L-Asn, would result in the same tendencies.

4.6.2.3 Crystallization temperature and subcooling

The liquid density of the crystallizing solutions, the solubility of the enantiomers, and thereby the metastable zone width, and the growth rate constant are all dependent

on the crystallization temperature. However, the influence of the crystallization temperature is more significant for the supersaturation ratio, which is dependent on the solubility of the enantiomer, and the growth rate constant, which in turn influences the overall growth rate. In order to elucidate the effect of increasing the crystallization temperature, a simulation is carried out for a crystallization temperature of 30 °C with the saturation concentration of the enantiomers in the racemic feed solution at 38 °C[66] (ΔT = 8 °C) and is compared to the base case having a crystallization temperature of 19 °C and saturation temperature of 23 °C (ΔT = 4 °C). The process duration is the same as in the base case, i.e. 90 minutes.

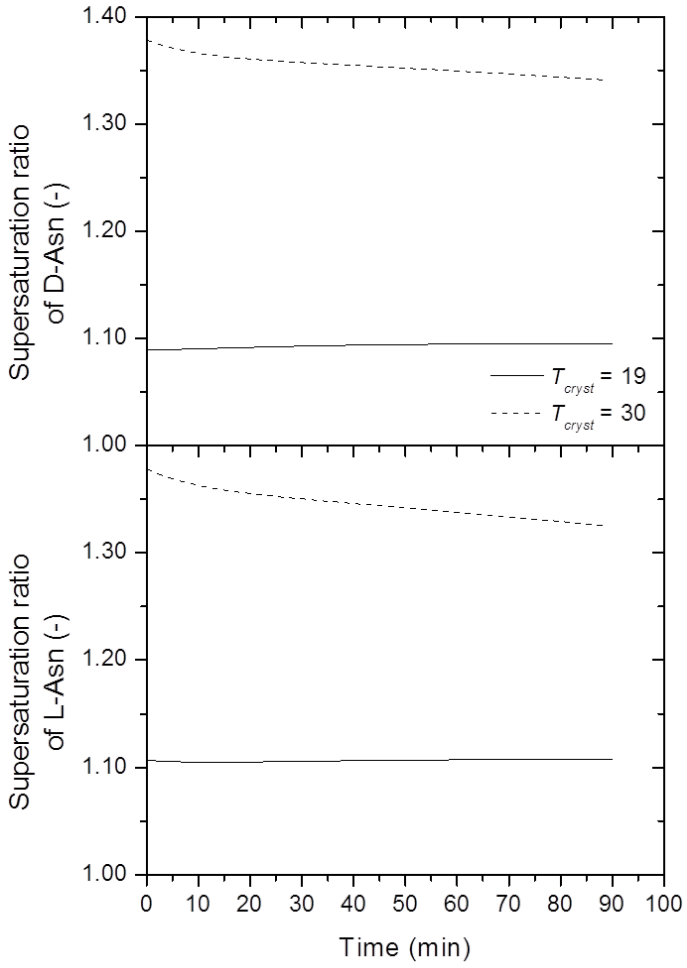

Figure 4.6: Model simulations of the supersaturation ratio of the preferred enantiomer in the D-Tank (top) and the L-Tank (bottom) for a crystallization temperature, T_{cryst}, of 19 °C (base case) and 30 °C. The remaining process parameters are the same as given in Table 4.2. At time equals zero seeding is performed.

The supersaturation ratio of the preferred enantiomer in each crystallizer increases with increasing crystallization temperature as shown in Figure 4.6. The reason for

this is the significant influence of the crystallization temperature on the solubility of the enantiomers and thereby the metastable zone width, which becomes larger when the temperature increases[66]. Additionally, the crystallization driving force decreases during the operation at the higher crystallization temperature while it remains constant for the base case temperature. The reason is the higher overall growth rate influenced by the temperature-dependent growth rate constant.

Table 4.5: Summary of the results of the U-value, yield based on feed solution, Y_L, productivity, Pr, the accumulated yield of solid products, Y_S, and the yield in crystal size, Y, from the D- and L-Tank obtained by the simulations for different crystallization temperature, T_{cryst}, of 19 °C (base case) and 30 °C. Note the units.

	19 °C		30 °C	
Tank	**D**	**L**	**D**	**L**
ΔT **[°C]**	4	4	8	8
k_g **[$\times 10^{-8}$ m/s]**	3.25	3.96	6.76	8.25
***U*-value [%]**	100.2	100.0	99.0	98.2
Y_L **[%]**	1.08	1.52	7.20	9.35
Pr [$\times 10^{-4}$ g/(g min)]	1.17	1.65	7.82	10.2
Y_S **[%]**	37.79	54.09	519.3	674.7
***Y* [%]**	51.35	51.85	58.96	60.30

As seen in Table 4.5, the performance of the process improves significantly with respect to the process metrics considered, except the U-value. The improvement in the yields and the productivity can be explained by the increase in the mass of the enantiomers present in the feed solution entering the crystallizers, the increase in the crystallization driving force of the preferred enantiomer, and the increase in the growth rate constant to more than the double. The very small change in the U-value can be ascribed to the low rate of the dominating mechanism for crystal growth, i.e. surface integration.

4.6.2.4 Fraction of the feed solution inlet

The change in the fraction of feed solution entering the crystallizers is also simulated to elucidate its influence on the outcome of the CC-PC process considered. The change in the feed fraction changes the mass of the enantiomers entering the crystallizers, which in turn affects the performance of the process. In this respect, the feed fraction δ is varied between 0.5 and 0.6. In Figure 4.7, the supersaturation ratio of the preferred enantiomer in each crystallizer is depicted.

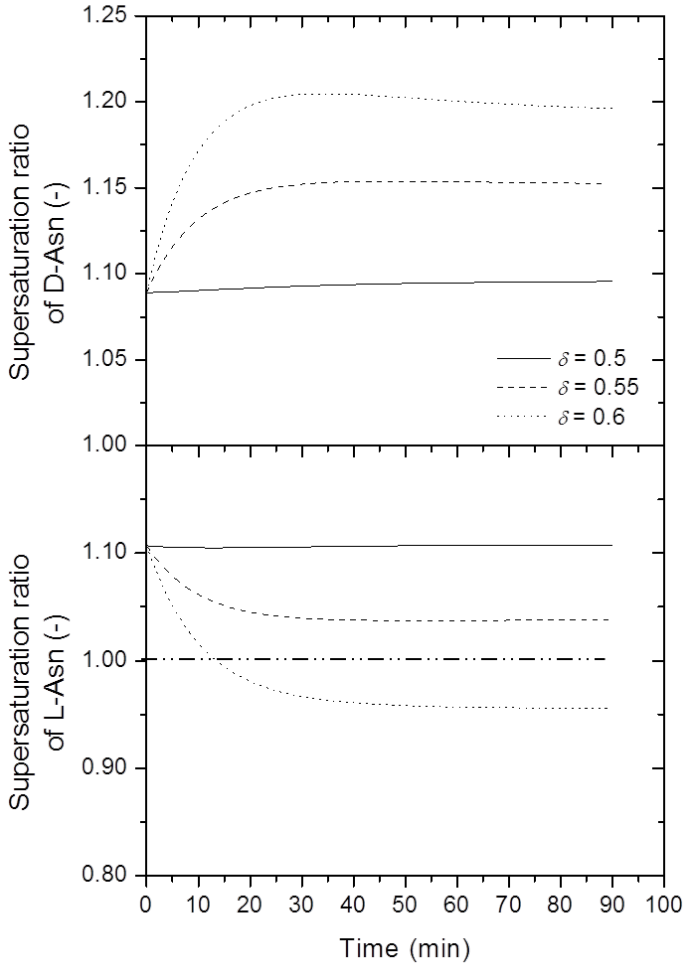

Figure 4.7: Model simulations of the supersaturation ratio of the preferred enantiomer in the D-Tank (top) and the L-Tank (bottom) for the fraction of feed solution entering the crystallizers, δ, between 0.5 (base case) and 0.6. The remaining process parameters are the same as given in Table 4.2. At time equals zero seeding is performed. The solubility is indicated at supersaturation ratio of unity. Note the difference in the scale of the abscissa.

Increasing the feed fraction allow for the supply of a higher amount of the preferred enantiomer into the respective crystallizer and the withdrawal of higher amount of enantiomers to maintain a constant volume of the crystallizing suspension. The simulations depicted in Figure 4.7 show that an increase in the feed fraction increases the concentration of D- and L-Asn in the D-Tank resulting in a higher crystallization driving force for the D-Asn. On the other hand, less feed is supplied to the L-Tank in which L-AsnH_2O is crystallizing. The decrease below the solubility of L-Asn in the L-Tank for a feed fraction of 0.6 is caused by the increase of the concentration of the counter enantiomer D-Asn, which in turn increases the solubility of the L-AsnH_2O in the L-Tank according to equation (4.29). This is due to the transfer of a higher amount of D-Asn than L-Asn in the exchange stream from the D-Tank to the L-Tank.

The increase in the solubility destabilizes the solid-liquid system in the L-Tank, and thereby the dissolution of the supplied seed crystals of L-AsnH_2O occurs to stabilize the system. Similarly, increasing the feed fraction of feed solution into the L-Tank would result in the same tendencies. Additionally, liquid phase steady-state concentrations of the preferred and the counter enantiomer are achieved after about 45 minutes of operation corresponding to three residence times.

Table 4.6: Summary of the results of the U-value, yield based on feed solution, Y_L, productivity, Pr, the accumulated yield of solid products, Y_S, and the yield in crystal size, Y, from the D- and L-Tank obtained by the simulations for the change in the feed fraction into the D-Tank, δ, between 0.5 and 0.6. Note the units.

	0.5		0.55		0.6	
Tank	**D**	**L**	**D**	**L**	**D**	**L**
***U*-value [%]**	100.2	100.0	99.1	99.9	96.9	98.7
Y_L **[%]**	1.08	1.52	1.66	0.545	2.05	-0.651
Pr [$\times 10^{-4}$ g/(g min)]	1.17	1.65	1.80	0.592	2.23	-0.707
Y_S **[%]**	37.79	54.09	64.04	17.49	86.37	-18.56
Y **[%]**	51.35	51.85	52.09	50.79	52.70	49.53

Table 4.6 shows the obtained measures for the performance of the process. It is seen that an improvement is achieved for the separation of the D-AsnH_2O enantiomer from the D-Tank. This is indicated by the increase in the yields and the productivity. A slight decrease in the U-value is achieved showing an increase in the consumption of the preferred enantiomer due to crystal growth. Table 4.6 also shows that the increase of the fraction of feed entering the D-Tank has a negative effect on the performance of the process regarding the crystallization of the L-AsnH_2O enantiomer in the L-Tank. This is indicated by the negative values and the significant decrease in the yields and the productivity. This is likely to be because of the destabilization of the solid-liquid system. The U-value, however, indicates that more of the preferred enantiomer in the L-Tank is consumed, but is not consumed for crystal growth as the other measures indicate. The reason for the decrease in the U-value for the L-Tank is the fact that during the crystallization process the crystallizing suspension in the L-Tank is completely converted to a liquid solution with a higher concentration of the counter enantiomer D-Asn compared to the concentration of L-Asn, which becomes less than the concentration in the feed solution. Therefore, the concentration of L-Asn in the purge stream from the L-Tank becomes less than the concentration in the feed solution entering the L-Tank.

4.6.2.5 Mass of seeds and average size of seeds

Increasing the mass of seeds or decreasing the average size of the seeds supplied to each crystallizer should increase the production rate of solid product by crystal growth of the desired enantiomer due to larger surface area available for growth as indicated in equation (4.10). In this respect, the mass of the seeds supplied at the same average size is increased from 0.5 g (base case) to 5 g. Note that the mass of seeds for the base case are changed from the values given in Table 4.2 in order to obtain a clearer picture of the effect of change in the mass of seeds. Figure 4.8 shows the simulations of the concentration of enantiomers in the D- and L-Tank and Table 4.7 lists the obtained values of the measures of the performance of the process.

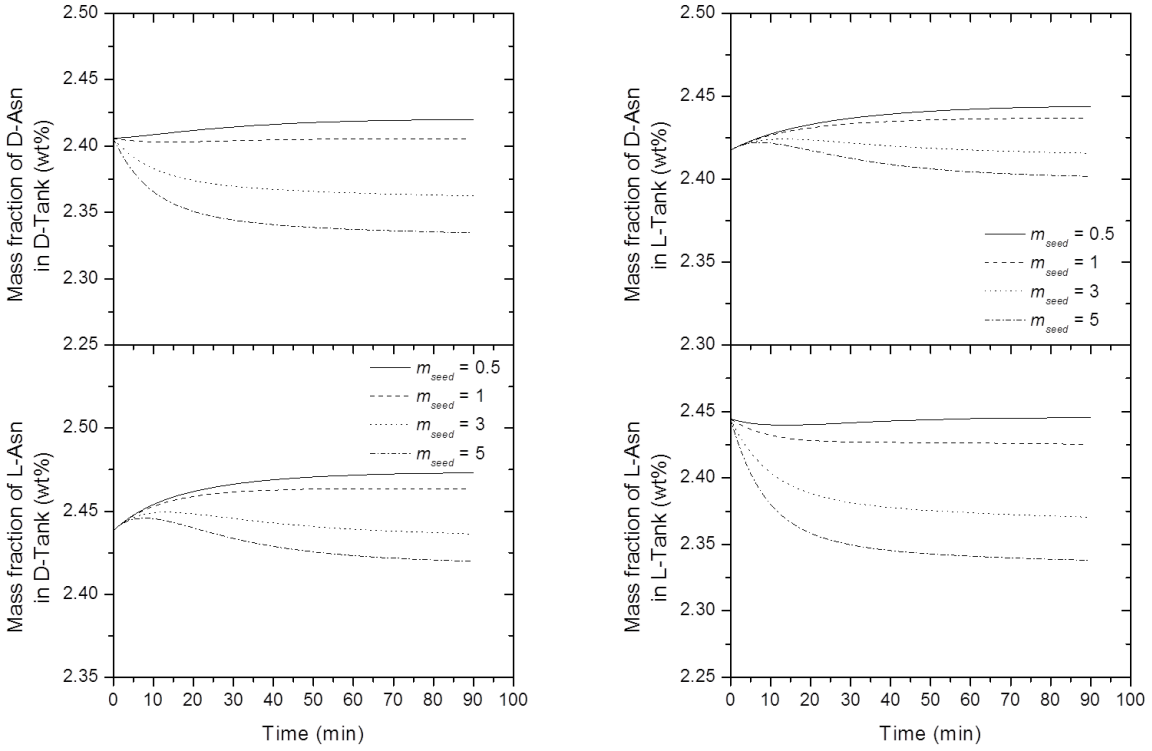

Figure 4.8: Model simulations of the concentration of enantiomers in the D-Tank (left) and the L-Tank (right) for the mass of seeds, m_{seed}, between 0.5 g (base case) and 5 g. The remaining process parameters are the same as given in Table 4.2. At time equals zero seeding is performed. Note the difference in the scale of the abscissa.

Figure 4.8 shows that increasing the mass of the enantiopure seed crystals supplied results in a decrease in the concentration of the preferred enantiomer in the crystallizing suspensions. This is due to the increased consumption for the deposition on the surface of the seed crystals due to the larger surface area available for crystal growth as expected. The decrease in the liquid phase concentration also decreases the crystallization driving force. Steady-state conditions for both the preferred and the

counter enantiomer in the liquid phase in each crystallizer are achieved after about 60 minutes corresponding to four residence times.

Table 4.7: Summary of the results of the U-value, yield based on feed solution, Y_L, productivity, Pr, the accumulated yield of solid products, Y_S, and the yield in crystal size, Y, from the D- and L-Tank obtained by the simulations for the change in the mass of seeds, m_{seed}, between 0.5 g and 5 g. Note the units.

	0.5 g		1 g		3 g		5 g	
Tank	**D**	**L**	**D**	**L**	**D**	**L**	**D**	**L**
N_2 **[m^2]**††	4.90	4.90	9.80	9.80	29.41	29.41	49.01	49.01
***U*-value [%]**	100.2	99.9	99.7	99.3	98.4	97.7	97.5	96.7
Y_L **[%]**	1.15	1.62	2.13	2.95	4.93	6.44	6.68	8.46
Pr [$\times 10^{-4}$ g/(g min)]	1.25	1.76	2.32	3.20	5.36	7.01	7.26	9.19
Y_S **[%]**	37.58	53.69	34.82	48.74	26.84	35.54	21.82	27.98
***Y* [%]**	51.34	51.84	51.27	51.73	51.06	51.39	50.90	51.16

As expected, the initial total surface area of the seed crystals supplied increases with increase in the mass of the seeds. As seen in Table 4.7, the performance of the process is improved with respect to the U-value, the yield based on the feed and the productivity. This indicates that the measures relating the production of solids relative to the amount of enantiomer in the feed solution are improved. Thus, the separation efficiency is improved. However, increasing the mass of seeds decreases the measures relating the production of solids due to crystal growth and the initially present seeds, i.e. yield of solid product based on the amount of seed supplied and the crystal size yield based on the initial size of the seed crystals. The reason for this decrease is the fact that crystal growth and thereby the production of solid is distributed on a larger number of seeds with the same average size.

Model simulations of the concentration of enantiomers in the D- and L-Tank for the different sieve fractions of the seeds, i.e. 250-355 μm (base case), 200-250 μm, and 150-200 μm, are depicted in Figure 4.9. The enantiopure seeds of both enantiomers are assumed uniform.

†† Total initial surface per m^3 suspension.

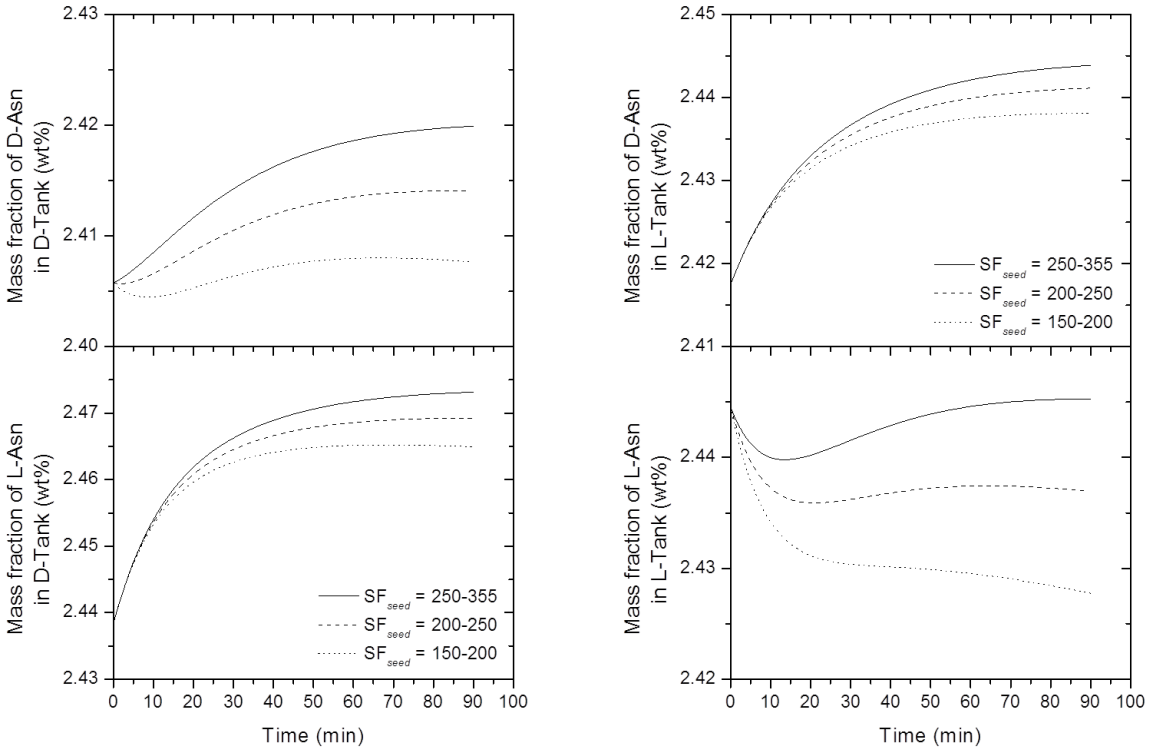

Figure 4.9: Model simulations of the concentration of enantiomers in the D-Tank (left) and the L-Tank (right) for the different sieve fractions of the seeds, SF_{seed}, of 250-355 μm (base case), 200-250 μm, and 150-200 μm. The remaining process parameters are the same as given in Table 4.2. At time equals zero seeding is performed. Note the difference in the scale of the abscissa.

As shown in Figure 4.9, the decrease in the average size of the enantiopure seed crystals supplied decreases the concentration of the preferred enantiomer in the liquid phase. This is due to the enhanced production of solid product due to crystal growth caused by the larger surface area available for crystal growth compared to the base case having larger size of seeds. Note that the initially larger decrease in the concentration ofL-Asn in the L-Tank compared to the concentration of D-Asn in the D-Tank may be caused by the higher growth rate of the seeds of L-AsnH_2O in the L-Tank. Note that steady-state concentration of the counter enantiomer in the liquid phase for the smaller size of seed crystals of the preferred enantiomer in each crystallizer is achieved earlier than when larger seed crystals are used.

Table 4.8: Summary of the results of the U-value, yield based on feed solution, Y_L, productivity, Pr, the accumulated yield of solid products, Y_S, and the yield in crystal size, Y, from the D- and L-Tank obtained by the simulations for the different sieve fractions of the seeds, SF_{seed}, of 250-355 μm (base case), 200-250 μm, and 150-200 μm. Note the units.

	250-355 μm		200-250 μm		150-200 μm	
Tank	**D**	**L**	**D**	**L**	**D**	**L**
N_2 **[m^2]**‡‡	4.90	4.90	6.59	6.59	7.87	7.86
***U*-value [%]**	100.2	99.9	100.0	99.7	99.8	99.4
Y_L **[%]**	1.15	1.62	1.56	2.20	2.01	2.84
Pr [$\times 10^{-4}$ g/(g min)]	1.25	1.76	1.69	2.39	2.18	3.09
Y_S **[%]**	37.58	53.69	50.79	72.77	65.50	93.93
***Y* [%]**	51.34	51.84	51.75	52.39	52.18	52.95

As seen in Table 4.8, the increase in the initial total surface area of the seed crystals supplied is not as significant as it is for the increase in the mass of seeds given in Table 4.7. Thus, the extent of the improvement of the performance of the CC-PC process is larger for the change in the mass of seeds supplied compared to the decrease in the average size of the seeds crystals. The decrease in the average size of the seed crystals provides a larger surface area for crystal growth thus increasing the production rate of the solid product. This is indicated by the increase in the yields and the productivity as shown in Table 4.8. In this respect, to obtain a smaller size of the seed crystals milling is necessary. This operation adds cost to the process and therefore should be compensated for by the increase in the productivity. A combination of the two parameters, i.e. the mass of the seeds and the size of the seeds, could be the optimal approach to improve the performance of the process significantly. Thus, to realize this approach the conversion of the CC-PC process to a fully continuous process is desirable.

4.6.2.6 Pre-exponential factor for growth rate

The change in the pre-exponential factor for the growth rate of the desired enantiomer affects the growth rate of the desired enantiomer significantly. The pre-exponential factor could count for the physical attributes of the seed crystals, i.e. morphology and surface structure of the seed crystals, and also counts for the growth rate of the different faces of the crystals. The following simulations are performed using two values for the pre-exponential factor, i.e. 25 m/s (base case) and 50 m/s. It should be emphasized that the base case value is the same for both crystallizing enantiomers.

‡‡ Total initial surface per m^3 suspension.

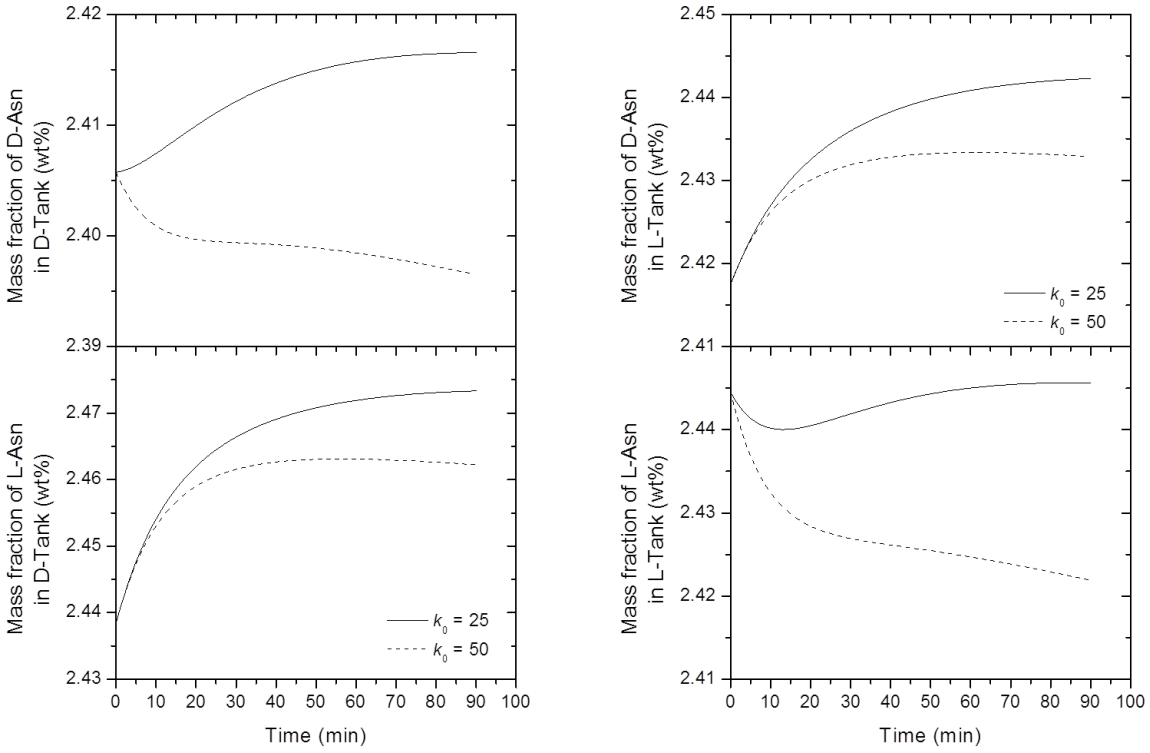

Figure 4.10: Model simulations of the concentration of enantiomers in the D-Tank (left) and the L-Tank (right) for the different values of the pre-exponential factor for the growth rate, k_0, i.e. 25 m/s (base case) and 50 m/s. The remaining process parameters are the same as given in Table 4.2. At time equals zero seeding is performed. Note the difference in the scale of the abscissa.

As shown in Figure 4.10, the increase in the pre-exponential factor decreases the concentration of the preferred enantiomer in the crystallizing suspensions. The reason is the enhanced rate of the overall crystal growth as expressed in equation (4.5) and (4.6) and thereby the increasing surface area of the growing seed crystals available for growth. Only the concentration of the counter enantiomer increases until steady-state in the liquid phase of this enantiomer is achieved.

Table 4.9: Summary of the results of the U-value, yield based on feed solution, Y_L, productivity, Pr, the accumulated yield of solid products, Y_S, and the yield in crystal size, Y, from the D- and L-Tank obtained by the simulations for the different values of the pre-exponential factor for the growth rate, k_0, of 25 m/s (base case) and 50 m/s. Note the units.

	25 m/s		50 m/s	
Tank	**D**	**L**	**D**	**L**
k_g **[$\times 10^{-8}$ m/s]**	4.16	4.16	8.33	8.33
***U*-value [%]**	100.1	100.0	99.4	99.2
Y_L **[%]**	1.39	1.60	2.80	3.26

(*continued*)

Table 4.9 – (*Continued*)

Tank	**D**	**L**	**D**	**L**
Pr [$\times 10^{-4}$ g/(g min)]	1.51	1.74	3.04	3.54
Y_S **[%]**	48.74	56.99	98.33	116.2
$\boldsymbol{Y}$ **[%]**	51.69	51.94	53.06	53.49

As shown in Table 4.9, the growth rate constant for the overall growth rate doubles when the pre-exponential factor doubles as expected. Due to the enhanced growth of the seed crystals, the performance of the process with respect to yields and the productivity is improved, except the U-value. The change in the pre-exponential factor could be achieved by a pretreatment of the seed crystals with a suitable solvent to allow for the change in the surface structure of the seed crystals and to activate the surfaces by providing a larger number of grow sites to obtain an acceleration of the surface integration of the preferred enantiomer into the surface of the seed crystals. The combination of such a pretreatment and the mass and size of seed crystals supplied would possibly provide the conditions of the supplied seed crystals necessary for enhanced crystal growth and process performance.

4.7 Validation of model assumptions

For model development, some simplifying assumptions were made. In this section, the most important ones are readdressed.

Primary homogeneous and heterogeneous nucleation of the preferred and the counter enantiomer in each crystallizer were neglected. This seems to be a reasonable assumption because the changes in the concentrations of the enantiomers in each crystallizer at the process conditions considered are small resulting in concentrations below the supersolubility limit. The reason is the low rate of crystal growth by surface integration as suggested by Petruševska-Seebach et al.[66].

Secondary nucleation of the seeded enantiomer was neglected. This is also reasonable under the process conditions considered, where the solid fraction in the crystallizing suspensions is below 5%, and is in accordance with the investigation carried out by Petruševska-Seebach et al.[66].

The presence of D-Asn in the liquid phase could result in crystal growth inhibition of the L-AsnH_2O in the L-Tank. This effect was neglected in the model development. This effect should be taken into account because it can have significant effect on the supersaturation, i.e. crystallization driving force, of the preferred enantiomer in the

liquid phase[66].

The overall growth rate of the seeded enantiomer in each crystallizer is assumed to be size-independent. This a reasonable assumption because the experimental investigation carried out by Petruševska-Seebach et al.[66] shows that no growth anomalies such as growth rate dispersion and/or size-dependent growth were observed in the case of asparagine monohydrate. During the present model validation against experimental data, however, the difference in the pre-exponential factor for crystal growth of the monohydrate enantiomers is obviously due to growth anomalies caused by the different surface structure of the seed crystals initially supplied according to the observations in the experimental investigation carried out by Chaaban et al.[11].

4.8 Conclusions

A mathematical model describing the CC-PC process for the continuous separation of enantiomers by preferential crystallization in a coupled crystallizer configuration under isothermal conditions was developed. Only the phenomenon of crystal growth of the preferred enantiomer in each crystallizer was included. Experimental data available were used for validation of the model and to estimate the important kinetic parameters relevant for crystal growth. Simulations for different process variables were performed to assess the predictability of the model, at least from a theoretical point of view, using the conglomerate forming system of asparagine monohydrate as model compound.

It was shown that the increase in the mean residence time of the liquid phase, the increase in the crystallization temperature, the increase in the mass of seeds, and the reduction of the size of the seed crystals all contribute positively to the overall process performance. The sensitivity of the model to theses parameters suggests that the conversion of the CC-PC process to a fully continuous process could be advantageous.

An important next step is to validate the predictability of the model by experimental data obtained for the change in the investigated process variables. Another equally important step is to extend the model to count for the nucleation, agglomeration, and crystal breakage phenomena, which could occur in the CC-PC process. The model developed in the present study could also be extended to cover the behavior of the CC-PC process using a racemic compound forming system. Finally, the model could be further modified to represent a fully continuous separation process including downstream processing units and continuous supply of seed crystals.

Chapter 5
Conclusions and suggestions for future work

In this chapter, summaries of the results of the work presented in the preceding chapters are provided. Suggestions for future continuation of the work will be presented.

5.1 Conclusions

Litterature survey – The strict regulatory requirements and the increasing public demand for the production of enantipure drugs have drawn great attention towards exisiting and new routes for the production of pure enantiomers to be utilized in the production of chiral active pharmaceutical ingredients (APIs). Crystallization is extensively used in the pharmaceutical industry for separation and purification purposes and for the control of solid product attributes, such as polymorphism, particle size, and particle size distribution (PSD). In this respect, Preferential Crystallization (PC), as a chiroselective separation technique, is an attractive approach for the separation of pure chiral APIs. However, the applicability is limited to conglomerate forming systems or racemic compound forming systems with sufficient enrichment of the desired enantiomer. Therefore, the selection of solvent, the crystallization mode to be employed, and the type and attributes of the solid product to be produced are of great importance and should be considered early in product and process development stages in conjunction with the prior synthesis steps and the subsequent downstream processing units.

Experimental realization of the Continuous Coupled PC (CC-PC) process – It is desirable for the pharmaceutical industry to convert from the conventional batch operation to the more attractive continuous operation. The potential of continuous operation for the preferential crystallization of enantiomers was investigated in the CC-PC process, in which only the liquid phase was operated continuously. The CC-PC process is considered a first step towards a fully continuous preferential crystallization process. The objectives of the study was to assess the achievement of the separate simultaneous crystal growth of enantiomers on existing enantiopure seed crystals in each

crystallizer, and the achievement of nearly racemic composition in the mother liquors. Experiments in triplicates were conducted to assess the robustness of the developed process. The chiral chemical compound used was asparagine monohydrate in water, which belongs to the conglomerate forming systems. An additional experiment was conducted to assess the performance of the process by changing the initial size of the seeds. It was found that the experiments were repeatable and the process was considered robust. Simultaneous separation of the enantiomers in each crystallizer was achieved and a nearly racemic composition of the mother liquors was maintained. Reasonable productivities, yields, and purities were achieved. However, the purity of L-asparagine monohydrate (L-$AsnH_2O$) decreased due to surface nucleation of the counter enantiomer D-asparagine monohydrate (D-$AsnH_2O$). The productivities, and yields increased slightly as a result of using smaller seed particles, and the purity for the L-$AsnH_2O$ increased due to the initially smoother surface morphology of the enantiopure seed crystals supplied. Moreover, from a steady-state mass balance the separation efficiency evaluated based on the quantity of unutilized enantiomer in the purge streams was found to be negligibly small indicating that almost no separation has occurred. This was ascribed to the very low growth rate caused by the slow surface integration on seed crystals and the possible growth inhibition by the presence of the counter enantiomer.

Modeling and simulations of the CC-PC process – As a tool to predict the performance of the newly developed CC-PC process, a one-dimensional model was developed. The model was developed based on the crystal population balance equation (PBE) for each population of crystals in each crystallizer, assuming that only crystal growth occurs, combined with a liquid phase mass balance for each component in each crystallizer. No source terms were included in the PBE. The PBE was transformed using the method of moments and combined with the mass balances to obtain a set of coupled ordinary differential equations (ODEs) for each component. Firstly, the model outputs were validated against the average experimental data obtained from the triplicate experiments previously conducted. It was found that the model outputs were in good agreement with the experimental data. Secondly, the predictability of the model was investigated through a sensitivity analysis to assess the most influential parameters on process performance. The analysis showed that the increase in the mean residence time of the liquid phase, the increase in crystallization temperature, the increase in mass of seeds, and the reduction of size of seeds initially supplied contribute positively to the overall process performance. However, the separation efficiency, indicated by the U-value, evaluated based on the quantity of unutilized enantiomer in the purge streams was found to be negligibly small, i.e. between zero and 3% at best, indicating that almost no separation has occurred. The reason is the

very low growth rate caused by the slow surface integration on seed crystals at the given operating conditions. It can thus be concluded that the conversion to a fully continuous process could be advantageous to improve the separation efficiency in case crystal growth kinetics can be improved by e.g. using another solvent. It could also turn out that the studied CC-PC process can only be industrially useful in case the nature of growth kinetics of the chemical system allows for sufficiently rapid surface integration or that the kinetics is controlled primarily by solute diffusion.

5.2 Suggestions for future work

Extension of the applicability of the CC-PC process – As previously mentioned, the applicability of the present CC-PC process is limited to the separation of enantiomers from a conglomerate forming system. It would be advantageous to address the flexibility of the CC-PC process in terms of the applicability for other conglomerate forming systems. Furthermore, a study on the polythermal operation instead of isothermal operation to increase the understanding of the performance of the CC-PC process is suggested. Additionally, studies on the applicability of the CC-PC process for the separation of enantiomers from a racemic compound forming system are desirable. In this respect, the study of the applicability of the CC-PC process for diastereomeric salt crystallization could give further insight into the potential of the process.

Conversion to a fully continuous process – The newly developed CC-PC process has the potential of further development into a fully continuous preferential crystallization process to improve the separation efficiency. The conversion to a fully continuous preferential crystallization process requires the integration of untis for the continuous supply of seed crystals or other means of generation of seed crystals, e.g. sonication. Additionally, solid product removal units have to be integrated as well in order to remove growing solids continuously thereby enabling the control of the supersaturation level and the PSD of solid product.

Modeling and model validation – The developed one-dimensional model was used for conducting a sensitivity analysis to achieve an understanding of the complexity of the CC-PC process. The drawback is though that the model does not include terms describing the secondary nucleation of the preferred enantiomer, primary nucleation of the counter enantiomer, inhibition of crystal growth of the preferred enantiomer by the presence of counter enantiomer, size-dependent growth rate, agglomeration and crystal breakage/attrition phenomena, the effect of morphology change during crystal growth on supersaturation level. Moreover, validation of the simulations conducted against experimental data for the variations in process parameters is suggested to

assess the predictability of the model. The model could also be extended to describe the preferential crystallization process for the separation of enantiomers from racemic compound forming systems. Finally, it is also suggested that the model is extended to describe the fully continuous process including downstream processing units and solid feed units, if any.

Abbreviations

Al-Cr	Aluminium-Chromium alloy
API	Active Pharmaceutical Ingredient
Asn	Asparagine
AsnH2O	Asparagine monohydrate
PC	Preferential Crystallization
CB-PC	Coupled Batch Preferential Crystallization
CC-PC	Coupled Continuous Preferential Crystallization
CEN	Center for Electron Nanoscopy
CHEC	Center for Harmful Emission Control
COGs	Cost Of Goods
CSTR	Continuously-Stirred Tank Reactor
DSC	Differential Scanning Calorimetry
DTU	Technical University of Denmark
EMA	European Medicine Agency
Exp	Experiment
FDA	Food and Drug Administration
PSD	Particle Size Distribution
XRPD	X-Ray Powder Diffraction
DSC	Differential Scanning Calorimetry
FBRM	Focused-Beam Reflectance Measurement
MATLAB	MAtrix LABoratory
MOM	Method Of Moments
MSMPR	Mixed Suspension-Mixed Product Removal
ODE	Ordinary Differential Equation
PAT	Process Analytical Technology
PBE	Crystal Population Balance Equation
PTFE	PolyTetraFluorEten (Teflon®)
Pt/Rh	Platinum/Rhodium alloy
R&D	Research and Development
SEM	Scanning Electron Microscopy
SMB	Simulated Moving-Bed

STA	Simultaneous Thermogravimetric Analysis
TGA	Thermogravimetric Analysis
UNIFAC	UNIversal quasichemical Functional-group Activity Coefficients
USA	United States of America
US$	US Dollar

Nomenclature

Variables

Symbol	Description	Unit
A	Total surface area	m^2
a	Order of nucleation process	–
A_0	Pre-exponential factor for homogeneous nucleation rate	No./(m^3 s)
B_0	Homogeneous nucleation rate	No./(m^3 s)
B_{sec}	Secondary nucleation rate	No./(m^3 s)
C	Concentration	kg/m^3
c	Counter enantiomer	–
E_a	Activation energy for crystal growth by surface integration	kJ/mol
G	Linear growth rate	m/s
K_0	Primary nucleation rate constant	No./(m^3 s)
k	Growth rate constant	m/s
k_0	Pre-exponential factor for growth rate constant	m/s
k_a	Area shape factor	–
k_B	Boltzmann's constant	kJ/K
k_{sec}	Empirical secondary nucleation constant	Empirical
k_v	Volume shape factor	–
L	Characteristic dimension of crystals	m
M	Slurry density	kg/m^3
m	Mass of species	kg
$\dot{m}$	Mass flow rate of species	kg/s
N	Moment of population balance	/(m^3 suspension)
n	Number density function	No./(m^3 suspension)
P	Stirring rate	rpm
p	Preferred enantiomer	–
Pr	Productivity	kg/(kg s)
R	Universal gas constant	kJ/(mol K)
S	Supersaturation ratio	–

s	Relative supersaturation	–
SF	Sieve fraction	μm
T	Temperature	K
t	Time	s
V	Volume in crystallizer	m^3
w	Mass fraction of species	–
x_{10}	Particle size at which the cumulative mass or volume is 10%	–
x_{50}	Particle size at which the cumulative mass or volume is 50%	–
x_{90}	Particle size at which the cumulative mass or volume is 90%	–
Y	Yield	–

Greek letters

Symbol	Description	Unit
α	Order of crystal growth	–
δ	Fraction of feed solution into one crystallizer	–
γ	Activity coefficient	–
μ	Chemical potential	kJ/mol
ν	Molecular volume	m^3/mol
ϕ	Surface tension	kJ/m^2
ρ	Density	kg/m^3
σ	Supersaturation	–
τ	Mean residence time of liquid phase	s

Subscripts

Symbol	Description
$cryst$	Crystallization
E	Effluent of liquid phase from crystallizer
eq	Equilibrium
F	Feed
f	Final
g	Growth
i	Crystallizer 1 or 2 (D- or L-Tank)
j	Crystallizer 1 or 2 (D- or L-Tank)
L	Liquid phase

P	Purge
S	Solid
x	Index for moments of population balance

Superscripts

Symbol	Description
b	Empirical exponent for supersaturation (Secondary nucleation)
c	Counter enantiomer
k	Counter enantiomer or preferred enantiomer
l	Empirical exponent for stirring rate (Secondary nucleation)
p	Preferred enantiomer
r	Empirical exponent for slurry density (Secondary nucleation)

Bibliography

1 S. Aitipamula, R. Banerjee, A. K. Bansal, K. Biradha, M. L. Cheney, A. R. Choudhury, G. R. Desiraju, A. G. Dikundwar, R. Dubey, N. Duggirala, P. P. Ghogale, S. Ghosh, P. K. Goswami, N. R. Goud, R. R. K. R. Jetti, P. Karpinski, P. Kaushik, D. Kumar, V. Kumar, B. Moulton, A. Mukherjee, G. Mukherjee, A. S. Myerson, V. Puri, A. Ramanan, T. Rajamannar, C. M. Reddy, N. Rodriguez-Hornedo, R. D. Rogers, T. N. G. Row, P. Sanphui, N. Shan, G. Shete, A. Singh, C. C. Sun, J. A. Swift, R. Thaimattam, T. S. Thakur, R. Kumar Thaper, S. P. Thomas, S. Tothadi, V. R. Vangala, N. Variankaval, P. Vishweshwar, D. R. Weyna, and M. J. Zaworotko. Polymorphs, salts, and cocrystals: What's in a name? *Crystal Growth and Design*, **12**(5):2147–2152, 2012.

2 T. Allen. *Particle Size Measurement*. Chapman and Hall, UK, 1996.

3 D. J. Am Ende. *Chemical Engineering in The Pharmaceutical Industry: R & D to Manufacturing*. John Wiley and Sons, USA, **2011**.

4 Y. Andemichael, J. Chen, J. S. Clawson, W. Dai, A. Diederich, S. V. Downing, A. J. Freyer, P. Liu, L. M. Oh, D. B. Patience, S. Sharpe, J. Sisko, J. Tsui, F. G. Vogt, J. Wang, L. Wernersbach, E. C. Webb, J. Wertman, and L. Zhou. Process development for a novel pleuromutilin-derived antibiotic. *Organic Process Research and Development*, **13**(4):729–738, 2009.

5 M. Balawejder, D. Kiwala, H. Lorenz, A. Seidel-Morgenstern, W. Piatkowski, and D. Antos. Resolution of a diasteromeric salt of citalopram by multistage crystallization. *Crystal Growth and Design*, **12**(5):2557–2566, 2012.

6 R. T. Berendt, R. Samy, A. S. Carlin, A. Pendse, P. Schwartz, M. A. Khan, and P. J. Faustino. Spontaneous carbonate formation in an amorphous, amine-rich, polymeric drug substance: Sevelamer hcl product quality. *Journal of Pharmaceutical Sciences*, **101**(8):2681–2685, 2012.

7 A. J. Blacker, S. Brown, B. Clique, B. Gourlay, C. E. Headley, S. Ingham, D. Rit-

son, T. Screen, M. J. Stirling, D. Taylor, and G. Thompson. A low-waste process to sertraline by diastereomeric crystal resolution and waste isomer racemisation. *Organic Process Research and Development*, **13**(6):1370–1378, 2009.

8 N. Blagden, M. de Matas, P. T. Gavan, and P. York. Crystal engineering of active pharmaceutical ingredients to improve solubility and dissolution rates. *Advanced Drug Delivery Reviews*, **59**(7):617–630, 2007.

9 G. Blaschke, H. P. Kraft, K. Fickentscher, and F. Köhler. Chromatographic separation of racemic thalidomide and teratogenic activity of its enantiomers. *Arzneimittel–forschung*, **29**(10):164–1642, 1979.

10 S. Byrn, R. Pfeiffer, M. Ganey, C. Hoiberg, and G. Poochikian. Pharmaceutical solids: A strategic approach to regulatory considerations. *Pharmaceutical Research*, **12**(7):945–954, 1995.

11 J. H. Chaaban, K. Dam-Johansen, T. Skovby, and S. Kiil. Separation of enantiomers by continuous preferential crystallization: Experimental realization using coupled crystallizer configuration. *Organic Process Research and Development*, page Submitted for publication, 2013.

12 K. M. Christensen, M. J. Pedersen, K. Dam-Johansen, T. L. Holm, T. Skovby, and S. Kiil. Design and operation of a filter reactor for continuous production of a selected pharmaceutical intermediate. *Chemical Engineering Science*, **71**:111–117, 2012.

13 A. N. Collins, G. N. Sheldrake, and J. Crosby. *Chirality in Industry II: Developments in the Commercial Manufacture and Applications of Optically Active Compounds*. John Wiley and Sons, USA, 1997.

14 G. Coquerel. *Novel Optical Resolution Technologies–Topics in Current Chemistry*. Springer–Verlag, Germany, 2007.

15 R. Davey and J. Garside. *From Molecules to Crystallizers: An Introduction to Crystallization*. Oxford University Press, USA, 2006.

16 P. L. Edward, T. Hsien-Hsin, and M. Midler. Organic crystallization processes. *Powder Technology*, **150**(2):133–143, 2005.

17 E. L. Eliel and S. H. Wilen. *The Stereochemistry of Organic Compounds*. John

Wiley and Sons, USA, **1994**.

18 M. P. Elsner, M. F. Menéndez, E. A. Muslera, and A. Seidel-Morgenstern. Experimental study and simplified mathematical description of preferential crystallization. *Chirality*, **17**(S1):S183–S195, 2005.

19 M. P. Elsner, G. Ziomek, and A. Seidel-Morgenstern. Simultaneous preferential crystallization in a coupled, batch operation mode–part i: Theoretical analysis and optimization. *Chemical Engineering Science*, **62**(17):4760–4769, 2007.

20 M. P. Elsner, G. Ziomek, and A. Seidel-Morgenstern. Efficient separation of enantiomers by preferential crystallization in two coupled vessels. *Journal of American Institute of Chemical Engineers*, **55**(3):640–649, 2009.

21 M. P. Elsner, G. Ziomek, and A. Seidel-Morgenstern. Simultaneous preferential crystallization in a coupled batch operation mode. part ii: Experimental study and model refinement. *Chemical Engineering Science*, **66**(6):1269–1284, 2011.

22 E. Fogassy, M. Nógrádi, D. Kozma, G. Egri, E. Pálovics, and V. Kiss. Optical resolution methods. *Organic Biomolecular Chemistry*, **4**(16):3011–3030, 2006.

23 H. S. Fogler. *Elements of Chemical Reaction Engineering*. Pearson Education, USA, **2006**.

24 Food and Drug Administration (FDA). Announcement: Fda's policy statement for the development of new stereoisomeric drugs. *Chirality*, **4**(5):338–340, 1992.

25 Food and Drug Administration (FDA). Approved drug product list: Appendix a - product name index, **2012**.

26 E. Francotte. Enantioselective chromatography as a powerful alternative for the preparation of drug enantiomers. *Journal of Chromatography A*, **906**(1–2):379–397, 2001.

27 E. Francotte. Enantioselective chromatography: From its emergence to its successful implementation in the pharmaceutical environment. *CHIMIA*, **63**(12):867–871, 2009.

28 E. J. J. Gabrowski. Enantiopure drug synthesis: From methyldopa to imipenem to efavirenz. *Chirality*, **17**(S1):S249–S259, 2005.

29 S. Garnier, S. Petit, F. Mallet, M.-N. Petit, D. Lemarchand, S. Coste, J. Lefebvre, and G. Coquerel. Influence of ageing, grinding and preheating on the thermal behavior of α-lactose monohydrate. *International Journal of Pharmaceutics*, **361**(1–2):131–140, 2008.

30 M. Gibson. *Pharmaceutical Preformulation and Formulation.* CRC Press/Interpharm, USA, 2004.

31 G. G. T. Guarini and L. Dei. Kinetics and mechanism of the thermal dehydration of l. asparagine monohydrate microcrystals and single crystals: Role of ageing. *Thermochimica Acta*, **311**(1–2):129–140, 1998.

32 P. Hadik, L. P. Szabó, E. Nagy, and Z. Farkas. Enantioseparation of D,L-lactic acid by membrane techniques. *Journal of Membrane Science*, **251**(1–2):223–232, 2005.

33 S. Han, F. Rabie, E. Marand, and S. M. Martin. Enantioselective separations using chiral supported liquid crystalline membranes. *Chirality*, **24**(7):519–525, 2012.

34 W. Hauck, P. Adam, C. Bobier, and N. Landmesser. Use of large-scale chromatography in the preparation of armodafinil. *Chirality*, **20**(8):896–899, 2008.

35 W. M. Haynes. *CRC Handbook of Chemistry and Physics.* CRC Press, USA, 2013.

36 Q. He, S. Rohani, J. Zhu, and H. Gomaa. Resolution of sertraline with (*R*)-mandelic acid: Chiral discrimination mechanism study. *Chirality*, **24**(2):119–128, 2012.

37 Q. He, Rohani S., J. Zhu, and H. Gomaa. Crystallization of the racemic compound and conglomerate of (*RS*)-2-chloromandelic acid. *Crystal Growth and Design*, **10**(12):5136–5145, 2010.

38 M. W. Hermanto, P. S. Chow, and R. B. H. Tan. Operating strategy to produce consistent csd in combined antisolvent-cooling crystallization using fbrm. *Industrial and Engineering Chemistry Research*, **51**(42):13773–13783, 2012.

39 L. C. Hsu, H. Kim, X. Yang, and D. Ross. Large scale chiral chromatography for the separation of an enantiomer to accelerate drug development. *Chirality*,

23:361–366, 2011.

40 D. Hudecz. Continuous crystallization of an active pharmaceutical ingredient–focus on crystal size and crystal size distribution. M.Sc. thesis, 2011.

41 J. Jacques and A. Collet. *Enantiomers, Racemates and Resolutions*. John Wiley and Sons, USA, 1981.

42 M. Jiang, M. H. Wong, Z. Zhu, J. Zhang, L. Zhou, K. Wang, A. N. F. Versypt, T. Si, L. M. Hasenberg, Y.-E. Li, and R. D. Braatz. Towards achieving a flattop crystal size distribution by continuous seeding and controlled growth. *Chemical Engineering Science*, **77**:2–9, 2012.

43 M. Jim and K.-J. Kim. Effect of supersaturation on polymorphs of clopidogrel hydrogen sulfate in drowning-out crystallization. *Chemical Engineering and Technology*, **35**(6):995–1002, 2012.

44 C. Jiménez-González, P. Poechlauer, Q. B. Broxterman, B.-S. Yang, D. am Ende, J. Baird, C. Bertsch, R. E. Hannah, P. Dell'Orco, H. Noorman, S. Yee, R. Reintjens, A. Wells, V. Massonneau, and J. Manley. Key green engineering research areas for sustainable manufacturing: A perspective from pharmaceutical and fine chemicals manufacturers. *Organic Process Research and Development*, **15**(4):900–911, 2011.

45 A. G. Jones. *Crystallization Process Systems*. Butterworth-Heinemann, UK, 2002.

46 S. Kim, B. Lotz, M. Lindrud, K. Girard, T. Moore, K. Nagarajan, M. Alvarez, T. Lee, F. Nikfar, M. Davidovich, S. Srivastava, and S. Kiang. Control of the particle properties of a drug substance by crystallization engineering and the effect on drug product formulation. *Organic Process Research and Development*, **9**(6):894–901, 2005.

47 H. J. M. Kramer, S. K. Bermingham, and G. M. van Rosmalen. Design of industrial crystallizers for a given product quality. *Journal of Crystal Growth*, **198–199**(1):729–737, 1999.

48 S. Lee. *Encyclopedia of Chemical Processing*. Taylor and Francis, USA, **2006**.

49 C. Leuner and J. Dressman. Improving drug solubility for oral delivery using

solid dispersions. *European Journal of Pharmaceutics and Biopharmaceutics*, **50**(1):47–60, 2000.

50 Y. Li, J. Han, and G. Zhang. In situ dehydration of carbamazepine dihydrate: A novel technique to prepare amorphous anhydrous carbamazepine. *Pharmaceutical Development and Technology*, **5**(2):257–266, 2000.

51 G. Q. Lin, Y. M. Li, and A. S. C. Chan. *Principles and Applications of Asymmetric Synthesis*. John Wiley and Sons, USA, 2001.

52 R. Liu. *Water-Insoluble Drug Formulation*. Interpharm Press, USA, 2000.

53 E. Lo, E. Mattas, C. Wei, D. Kacsur, and C.-K. Chen. Simultaneous api particle size reduction and polymorph transformation using high shear. *Organic Process Research and Development*, **16**(1):102–108, 2012.

54 H. Lorenz, A. Perlberg, D. Sapoundjiev, M. P. Elsner, and A. Seidel-Morgenstern. Crystallization of enantiomers. *Chemical Engineering and Processing*, **45**:863–873, 2006.

55 Y. Lu, X. Wang, and C. B. Ching. Application of preferential crystallization for different types of racemic compounds. *Industrial Engineering and Chemical Research*, **48**(15):7266–7275, 2009.

56 Y. H. Lu and C. B. Ching. Physicochemical properties, binary and ternary phase diagrams of ketoprofen. *Chirality*, **16**(8):541–548, 2004.

57 E. A. Manoel, K. C. Pais, A. G. Cunha, A. B. C. Simas, M. A. Z. Coelho, and D. M. G. Freire. Kinetic resolution of 1,3,6-tri-*O*-benzyl-*myo*-inositol by novozym 435: Optimization and enzyme reuse. *Organic Research and Development*, **16**(8):1378–1384, 2012.

58 J. McMurry. *Organic Chemistry*. Thomson Learning, C. A., **2008**.

59 IMS Health MIDAS. Top 20 global products, 2011, total audited markets. http://www.imshealth.com/. [Online; accessed 10-February-2013].

60 S. Milmo. Special report: Continuous technology update. *Pharmaceutical Technology Europe*, **24**(1):35, 2012.

61 J. W. Mullin. *Crystallization*. Butterworth-Heinemann, UK, 2001.

62 A. S. Myerson. *Handbook of Industrial Crystallization*. Butterworth-Heinemann, USA, 2002.

63 Z. G. Nagy, M. Fujiwara, and R. D. Braatz. Modelling and control of combined cooling and antisolvent crystallization processes. *Journal of Process Control*, **18**(9):856–864, 2008.

64 NASA. Chirality in amino acids. http://www.nai.arc.nasa.gov/. [Online; accessed 09-February-2013].

65 F. Pavlou. Continuous processing: Is the pharma industry finally coming round to the idea?–a roundtable of experts. *Pharmaceutical Technology Europe*, **22**(9):44–50, 2010.

66 K. Petruševska-Seebach, A. Seidel-Morgenstern, and M. P. Elsner. Preferential crystallization of L-asparagine in water. *Crystal Growth and Design*, **11**(6):2149–2163, 2011.

67 D. Polenske, H. Lorenz, and A. Seidel-Morgenstern. Potential of different techniques of preferential crystallization for enantioseparation of racemic compound forming systems. *Chirality*, **21**(8):728–737, 2009.

68 V. M. Profir, E. Furusjö, L.-G. Danielsson, and Å. C. Rasmuson. Study of the crystallization of mandelic acid in water using in situ atr-ir spectroscopy. *Crystal Growth and Design*, **2**(4):273–279, 2002.

69 V. M. Profir and M. Matsuoka. Processes and phenomena of purity decrease during the optical resolution of DL-threonine by preferential crystallization. *Colloids and Surfaces A: Physicochemical and Engineering Aspects*, **164**(2–3):315–324, 2000.

70 A. D. Randolph and M. A. Larson. *Theory of Particulate Processes: Analysis and Techniques of Continuous Crystallization*. Academic Press, USA, 1971.

71 J. E. Rekoske. Chiral separations. *AIChE Journal*, **47**(1):2–5, 2001.

72 J. F. Richardson and J. H. Harker. *Particle Technology and Separation Processes*. Butterworth-Heinemann, UK, 2002.

73 A. M. Rouhi. The right stuff. *Chemical and Engineering News*, **81**(8):32–35, 2003.

74 A. Santomaso, P. Lazzaro, and P. Canu. Powder flowability and density ratios: the impact of granules packing. *Chemical Engineering Science*, **58**(13):2857–2874, 2003.

75 B. Schuur. Focus on chiral technologies–continuous enantioseparation by liquid-liquid extraction. *Chemistry Today*, **27**(6):9–12, 2009.

76 B. Schuur. Enantioselective liquid-liquid extraction of (*R,S*)-phenylglycinol using a bisnaphthyl phosphoric acid derivative as chiral extractant. *Tetrahedron*, **67**(2):462–470, 2011.

77 J. D. Seader and E. J. Henley. *Separation Process Principles*. John Wiley and Sons, USA, 2006.

78 R. A. Sheldon. Chirotechnology: Designing economic chiral syntheses. *Journal of Chemical Technology and Biotechnology*, **67**(1):1–14, 1996.

79 R. A. Sheldon. *Chirotechnology: Industrial Synthesis of Optically Active Compounds*. Taylor and Francis, USA, **1993**.

80 S. C. Stinson. Chiral drugs. *Chemical and Engineering News*, **73**(41):44–74, 1995.

81 S. C. Stinson. Chiral pharmaceuticals. *Chemical Engineering News*, **79**(40):79–97, 2001.

82 G. Subramanian. *Chiral Separation Techniques–A Practical Approach*. Wiley–VCH Verlag, Germany, **2007**.

83 A. Svang-Ariyaskul, W. J. Koros, and R. W. Rousseau. Chiral separation using a novel combination of cooling crystallization and a membrane barrier: Resolution of DL-glutamic acid. *Chemical Engineering Science*, **64**(9):1980–1984, 2009.

84 H. Takiyama. Supersaturation operation for quality control of crystalline particles in solution crystallization. *Advanced Powder Technology*, **23**(3):273–278, 2012.

85 K. Tang, L. Song, Y. Liu, Y. Pan, and X. Jiang. Separation of flurbiprofen enantiomers by biphasic recognition chiral extraction. *Chemical Engineering Journal*, **158**(3):411–417, 2010.

86 W. Thiemann. Disproportionation of enantiomers by precipitation. *Journal of Molecular Evolution*, **4**(1):85–97, 1974.

87 H.-H. Tung, E. L. Paul, M. Midler, and J. A. McCauley. *Crystallization of Organic Compounds–An Industrial Perspective*. John Wiley and Sons, USA, **2009**.

88 N. Variankaval and A. S. Cote. From form to function: Crystallization of active pharmaceutical ingredients. *Journal of American Institute of Chemical Engineers*, **54**(7):1682–1688, 2008.

89 G. P. Vitorino, N. R. Sperandeo, M. R. Caira, and M. R. Mazzieri. A supramolecular assembly formed by heteroassociation of ciprofloxacin and norfloxacin in the solid state: Co-crystal synthesis and characterization. *Crystal Growth and Design*, **13**(3):1050–1058, 2013.

90 F. G. Vogt, J. Brum, L. M. Katrincic, A. Flach, J. M. Socha, R. M. Goodman, and R. C. Haltiwanger. Physical, crystallographic, and spectroscopic characterization of a crystalline pharmaceutical hydrate: Understanding the role of water. *Crystal Growth and Design*, **6**(10):2333–2354, 2006.

91 S. Wacharine-Antar, G. Levilain, V. Dupray, and G. Coquerel. Resolution of (±)–imeglimin–2,4–dichlorophenylacetate methanol solvate by preferential crystallization. *Organic Research and Development*, **14**(6):1358–1363, 2010.

92 X. J. Wang, H. Wiehler, and C. B. Ching. Study of the characterization and crystallization of 4-hydroxy-2-pyrrolidone. *Chirality*, **16**(4):220–227, 2004.

93 Y. Wang and A. M. Chen. Enantioenrichment by crystallization. *Organic Process Research and Development*, **12**(2):282–290, 2008.

94 K. W*ü*rges, U. Mackfeld, M. Pohl, S. L*ü*tz, S. Wilhelm, W. Wiechert, and T. Kubitzki. An efficient route to both enantiomers of *allo*-threonine by simultaneous amino acid racemase-catalyzed isomerization of threonine and crystallization. *Advanced Synthesis and Catalysis*, **353**(13):2431–2438, 2011.

95 K. W*ü*rges, K. Petruševska-Seebach, M. P. Elsner, and S. L*ü*tz. Enzyme-assisted physicochemical enantioseparation processes–part iii: Overcoming yield limitations by dynamic kinetic resolution of asparagine via preferential crystallization and enzymatic racemization. *Biotechnology and Bioengineering*, **104**(6):1235–

1239, 2009.

96 N. Wermester, E. Aubin, M. Pauchet, S. Coste, and G. Coquerel. Preferential crystallization in an unusual case of conglomerate with partial solid solutions. *Asymmetry*, **18**(7):821–831, 2007.

97 N. Wermester, O. Lambert, and G. Coquerel. Preferential crystallization (as3pc mode) of modafinic acid: an example of productivity enhancement by addition of a non-chiral base. *Crystal Engineering Communication*, **10**(6):724–733, 2008.

98 A. W. White. A patent lawyer's perspective. *Biochemical Society Transactions*, **19**(2):469–472, 1991.

99 D. D. Wirth and G. A. Stephenson. Purification of dirithromycin: Impurity reduction and polymorph manipulation. *Organic Process Research and Development*, **1**(1):55–60, 1997.

100 R. Xie, L. Y. Chu, and J. G. Deng. Membranes and membrane process for chiral resolution. *Chemical Society Reviews*, **37**(6):1243–1263, 2008.

101 J. M. Yi, S. J. Huang, Y. R. Jiang, and K. W. Tang. Enantioselective extraction of fenvaleric acid enantiomers by two-phase (w/o) recognition chiral extraction. *Journal of Inclusion Phenomena and Macrocyclic Chemistry*, **68**(3–4):271–275, 2010.

102 H. Zhang, J. Quon, A. J. Alvarez, J. Evans, A. S. Myerson, and B. Trout. Development of continuous anti-solvent/cooling crystallization process using cascaded mixed suspension, mixed product removal crystallizers. *Organic Process Research and Development*, **16**(5):915–924s, 2012.

Appendix A

Process Development: Stages and Decisions

A.1 Process system selection

The Ph.D. project was initially concerning the design and development of a continuous crystallization process for the separation of enantiomers of APIs from a racemic compound forming system provided by H. Lundbeck A/S. The objective was to replace the expensive countercurrent SMB chromatography and/or the diastereomeric salt crystallization process thereby ultimately improving process economy.

After numerous discussions, it turned out that it is thermodynamically impossible to separate the enantiomers by the frequently used seeded cooling preferential crystallization unless a thermodynamically unstable conglomerate is formed in the desired range of operating conditions. The search for solvent(s) and temperature(s) at which such a conglomerate can be formed and stabilized for the provided racemic compound forming system was considered time-consuming and out of the scope of the present Ph.D. project.

It was then decided to consider other alternatives to the racemic compound forming system and a conglomerate forming system was provided by H. Lundbeck A/S. On the basis of that the focus of the further work in the Ph.D. project was directed to the design, establish, and experimentally investigate a new preferential crystallization process. The next step was to generate different design alternatives and to decide which to select for further investigation based on the following considerations:

- Flexibility and versatility
- Cheap in operation and maintenance
- Easy to implement, operate, and upscale
- Minimum use of mechanical parts
- Implementation of PAT tools for PSD control

A number of designs was generated, but due to limited time, it was decided to modify the already studied coupled-batch preferential crystallization (CB-PC) process developed by Elsner et al.[20]. The modification should consist of the conversion to a fully continuous PC process. Different considerations for the implementation of solid feeding units and systems for continuous filtration at lab-scale were presented and discussed. Even though the designs could possibly be implemented in commercial scale, it was difficult to find alternatives for downstream processing units such as continuous filtration at lab-scale. All in all, it was found to be a complex process network to handle in a single Ph.D. project due to time limitation. Therefore, it was decided to systematically study the conversion from the batch PC to the continuous PC.

The systematic study of the conversion consisted of building a PC process in which the liquid phase was operated continuously and the solid phase remained in batch. Some of the solid phase harvested could be used as heel seeds for a subsequent repeat of the PC process. The result was the newly developed coupled continuous PC (CC-PC) process. The CC-PC process was experimentally realized and investigated as a proof-of-concept. The investigation should answer two main questions:

1. Does simultaneous crystal growth of enantiopure seed crystals of the the preferred enantiomer in each crystallizer occur?
2. Is it possible to achieve a nearly racemic composition, i.e. nearly 50:50 composition, of the mother liquor in each crystallizer and maintain a constant driving force throughout the process duration?

To answer these questions and to assess the robustness of the CC-PC process, experiment in triplicates were conducted. The results of this work were considered potential scientific material for publication and it was decided that a manuscript should be produced for publication. However, the CC-PC process was only proven using a conglomerate forming system. Future work should focus on the flexibility of the process.

A theoretical investigation through model establishment and solution and sensitivity analysis was desirable to improve process understanding of the complex CC-PC process for the separation of enantiomers of conglomerate forming systems. Furthermore, suggestions for process improvements were also highlighted. This work was also successfully conducted and the outcome was considered valuable scientific material for publication. A second manuscript was therefore produced.

A.1.1 Fluidized bed vs. Stirred vessel

Continuous fluidized bed technology is to a limited extent commercially used for the production of pure enantiomers. Merck & Co. has already a continuous fluidized bed process for the separation of an API salt intermediate implemented at commercial scale. However, the predominant system in the pharmaceutical industry is the stirred vessel, either batch ore semi batch. The versatility of the fluidized-bed technique is limited to particular purposes because of specific requirements to mixing properties and flexibility. Some of the important features of fluidized bed crystallizers and stirred vessel crystallizers are listed in Table A.1.

Table A.1: Features of fluidized bed crystallizers and stirred vessel crystallizers[87].

Function	**Fluidized bed**	**Stirred vessel**
Continuous and/or batch	Continuous	Both
Cooling	Excellent	Good
Evaporative	NA	Good
Antisolvent	NA	Good
Reactive	NA	Good
Type of mixer	Fluidization	Variety of impellers
Macromixing	Excellent	Poor to Good
Mesomixing	NA	Poor to Good
Micromixing	NA	Poor to Good
Supersaturation range	Low	Wide
Control of supersaturation	Excellent at low supersaturation	Achievable
Nucleation	Minimum	Wide range
Crystal growth	Maximum	Wide range
Seeding	Massive	Wide range
Scale up	Good with good seed	Can be difficult

In general and as shown in Table A.1, stirred vessels are more versatile and flexible regarding the different crystallization modes applicable. Furthermore, specific requirements to mixing behavior and seeds should be met in order to operate a successful fluidized bed crystallization process. Particularly, the availability of the required seed amount and quality are of importance to the applicability of fluidized bed crystallizations in the pharmaceutical industry. This is due to the effects on product quality attributes and process performance. Additionally, the operating window regarding

the supersaturation range is also of great importance in order to allow for a controlled crystallization process and to meet the metastability window, i.e. metastable zone width, for the particular solute-solvent system.

A.2 Chemical system selection

The chemical system was selected based on the following criteria:

- Since the CC-PC process is a modification of the CB-PC process, which has limited applicability to conglomerate forming systems, the solute-solvent system should belong to the conglomerate forming systems, e.g. asparagine monohydrate or threonine.
- To avoid complicated ATEX approval of the CC-PC process for the given solvent volumes used and due to impractical implementation of reflux systems for the CC-PC process, aqueous solutions are desirable.
- Solubility of pure enantiomer is lower than that of conglomerate to enable the separation of pure enantiomers from a racemic mixture.
- Solubility should increase with increasing temperature to facilitate cooling crystallization.
- Width of the metastable region should be sufficiently wide to allow for seeding and thereby crystal growth.
- Data for crystallization kinetics and solubility data are available in literature due to time limitation to generate the required data.
- Cheap and safe for ease of handling, i.e. safety approval not necessary.

The chemical system selected based on the given criteria was the conglomerate forming system of the amino acid asparagine monohydrate in water (solvent). The necessary solubility data and data for crystallization kinetics are available in Thiemann[86] and Petruševska-Seebach et al.[66].

A.3 Equipment and auxiliary selection

A.3.1 Pump selection

The selection of the pumps to be used in the establishment of the CC-PC process was based on the following criteria:

- Cheap, flexible, and multipurpose.

- Fluid not in contact with mechanical parts of the pump. The reason is to avoid excessive evaporation of solvent and thereby undesired nucleation. Furthermore, crystal breakage/attrition during slurry transport should be avoided.
- Suitable for slurry transport.
- Ease of maintenance, setup, and operation.
- Operation at a wide range of flow rates/pressures.

In this respect, it was decided to select a positive displacement pump which is suitable for slurry transport in case the further development of the CC-PC process to fully continuous process is conducted. Therefore, and based on the given criteria above, peristaltic pumps with both dispensing and flow options were selected. All six pumps were identical and of the type Longer Pump LP-BT-100-1F with YZ1515x (single tube with three rollers, flow rate uncertainty ±2%) pump head from the manufacturer Baoding Longer Precision Pump Co. Ltd., Hebei, China. Three rollers were sufficient for continuous flow without excessive pulsation. The pump head is easy to setup and handle. All the pumps were calibrated before use to ensure the desired flow rate.

A.3.2 Tubings and fittings

The selection of the tubings for the setup of the CC-PC process was mainly based on the following criteria:

- Dimensions for the required flow rate. Note that it is recommended that the desired flow rate is within 20-80% of the maximum flow rate for the tubing.
- Chemical and heat resistance.
- Hardness and lifetime.
- Smoothness of inner surface to avoid excessive friction resistance and deposition of solids.

The tubes selected based on the given criteria above were Silicone peroxide tubes from VWR. The dimensions were 1.6 mm in inner diameter and a wall thickness of 1.6 mm. The tubes were inserted in other silicone tubes with large inner diameter (9 mm) in order to make the tubings more rigid to handle and to decrease cooling of the fluid transferred in the smaller tubings if operation of the CC-PC system at higher temperatures is desired. Some fittings ordered from Mikrolab A/S were used for tube connections and thermocouple installations. The dimensions and chemical resistance of the fittings were taken into account.

A.3.3 Impeller selection for mixing

The selection of the impeller type for mixing purpose was made based on the following criteria:

- Provide axial mixing pattern to facilitate both improved micromixing but also suspendability (macromixing) of the crystals.
- Avoidance of crystal breakage/attrition. Reduced tip speed (shear) to avoid secondary nucleation and to allow the control of PSD of the final product.
- Chemical resistance (stainless steel or PTFE).
- Dimensions fitted to crystallizer dimensions.

The impeller selected was a 45 mm stainless steel (both impeller and shaft) propeller type impeller with guided ring to reduce the shear of crystals. The stirrer (shaft and impeller) was purchased from Heidolph Instruments, Schwabach, Germany.

Appendix B

Manual for the CC-PC Process

Technical University of Denmark

Department of Chemical and Biochemical Engineering

Manual for the Coupled Continuous Preferential Crystallization Process:

Preferential Crystallization of Asparagine Monohydrate Enantiomers

Instruction Manual

Author:

Joussef Hussein Chaaban,

Ph.D. student

April 1, 2013

B.1 Introduction

Crystallization is a frequently applied method in many industries to produce pure solids from a solution. On a very large scale, inorganic salts, e.g. NaCl, are crystallized from a supersaturated solution, but also simple and complex organic compounds, e.g. sugar and ketoprofen, respectively, and complex proteins, e.g. insulin, are crystallized during manufacturing.

In the pharmaceutical industry, crystallization is used for two objectives: 1) Separation and purification, and 2) control of critical attributes of the product. In this respect, crystallization is used for the separation of chiral compounds from a racemic mixture. For this purpose, crystallization can be performed by seeding to allow for the production of highly pure crystals of the wanted chiral compound. This process is commonly known as *preferential crystallization* (PC). Seeding is often also used to control the final particle size, particle size distribution (PSD), and morphology of the final product.

Separation of chiral compounds from a racemic mixture is commonly conducted in batch mode. To increase process yield and improve control of product attributes, continuous operation is desirable. To investigate the performance of a continuous PC process, a process in which only the liquid phase is continuously operated and the solid phase is in batch. The process is called *coupled continuous PC* (CC-PC) process. This is regarded as a first step towards fully continuous PC process. This manual provides an step-by-step guide for the operation of the CC-PC process with an example using the chiral asparagine monohydrate in water as the racemic mixture.

B.2 Objective(s)

The purpose of the experiment is to investigate the separation of enantiomers of asparagine monohydrate ($AsnH_2O$) from an aqueous racemic mixture by seeded cooling crystallization in the CC-PC process. The achievement of a nearly racemic composition of the mother liquor and the achievement of crystal growth of the seed crystals with the desired enantiomers are studied. Quantitative analyses are performed to evaluate the performance of the separation process and product quality in terms of optical purity.

B.3 Equipment and setup

The setup is a lab-scale setup designed and built in lab 103 at the Center for Harmful Emission Control (CHEC) at Department of Chemical and Biochemical Engineering

(KT) at the Technical University of Denmark (DTU). The main components are the feed tank, feed pumps, crystallizers (D- and L-Tank), mother liquor exchange pumps, and purge pumps. The CC-PC process is shown in a photograph in Figure B.1. Note the small insert which shows the main instrumentation parts in each crystallizer.

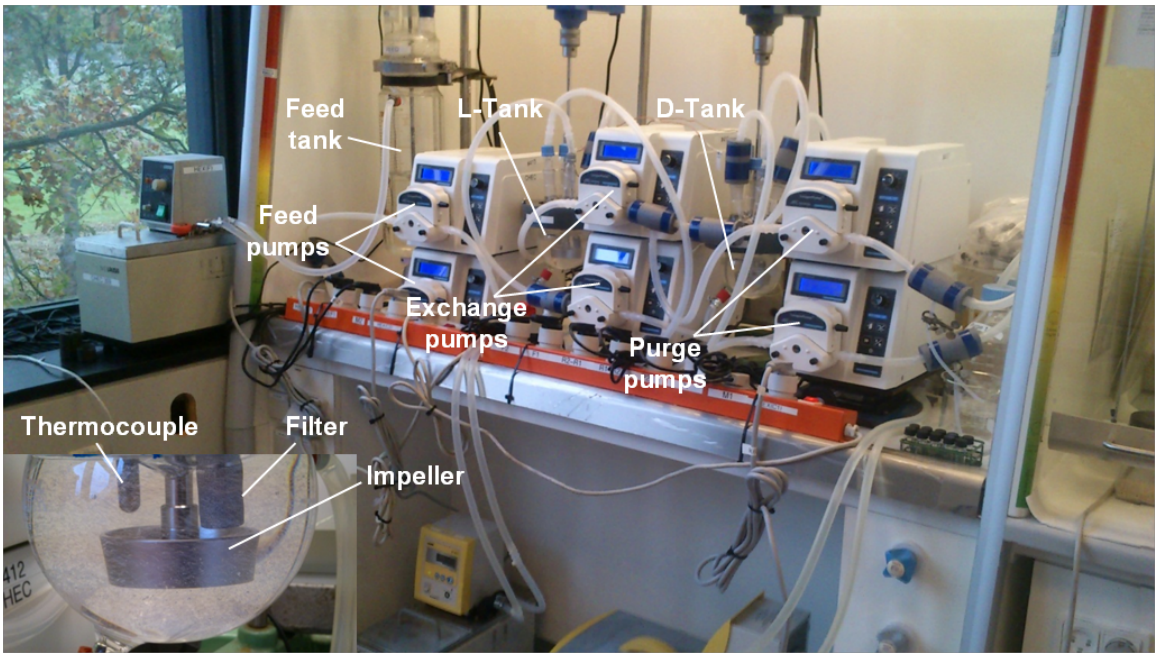

Figure B.1: Photograph of experimental setup for the preferential crystallization experiments. The small insert (lower left corner) shows the instrumentation in the crystallization vessels. Six individual pumps are necessary to run the setup in a continuous mode.

The process is also depicted in a schematic diagram in Figure B.2. The crystallizers, C1 and C2, consist of two rounded-bottom glass vessels of a total volume of 250 mL each with heating/cooling jacket and they comprise the central part of the setup. In the crystallizers, the separation of enantiomers by crystal growth of the pure seed crystals supplied takes place. The effective volume is 220 mL of solution.

B.3.1 Crystallization units

The crystallizers are mounted on a ring holder by assembling the bottom part, which is the crystallizer itself, and the top part, which is a 75 mm lid with five necks/openings (Figure B.3).

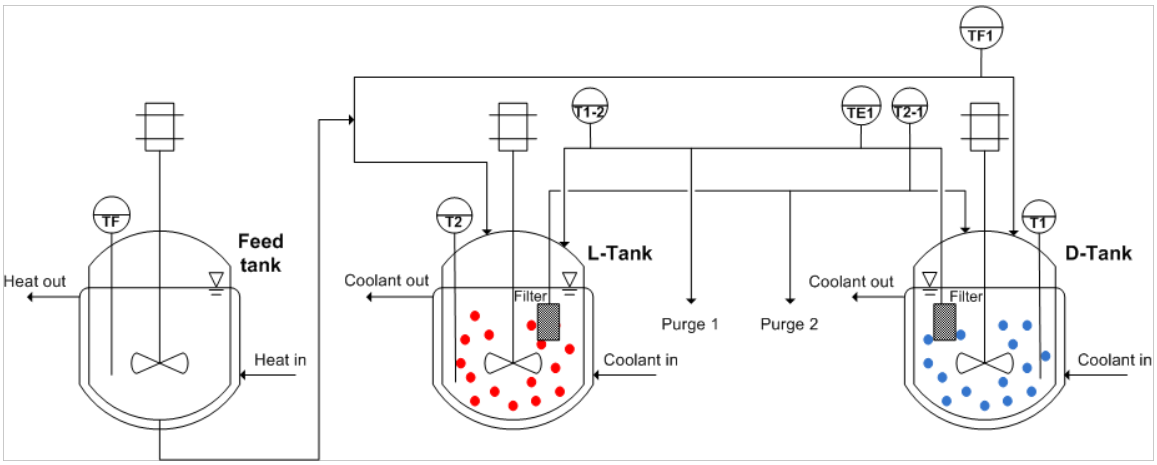

Figure B.2: Schematic diagram of the CC-PC process for the preferential crystallization experiments. TF symbolizes the temperature in the feed tank, TF1 is the temperature of feed entering the D-Tank, T1 is the temperature in the D-Tank (C1), T2 is the temperature in the L-Tank (C2), TE1 is the temperature of mother liquor effluent from the D-Tank, T1-2 is the temperature of exchange stream from the D-Tank to the L-Tank and T2-1 is the temperature of exchange stream from the L-Tank to the D-Tank. Blue and red filled circles symbolize growing enantiopure seeds of D-AsnH_2O and L-AsnH_2O in the D- and L-Tank, respectively. The grey boxes in the D- and L-Tank represent filters for mother liquor exchange.

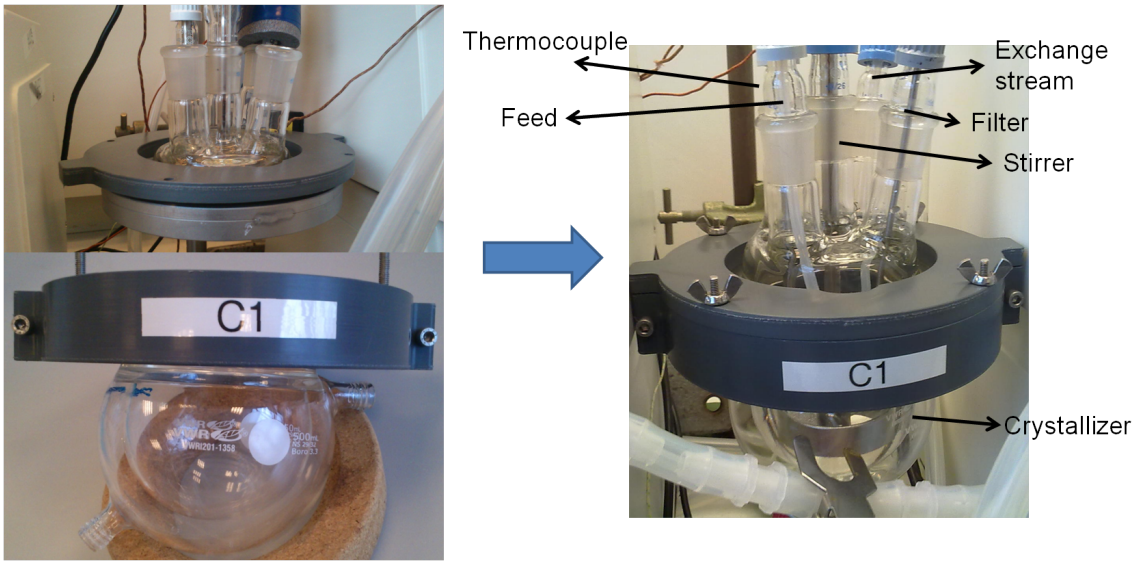

Figure B.3: Assembling the parts of the crystallization units.

The screws, four for each unit, are fastened and the stirrer is lowered so the impeller is about 1/3 apart from the bottom of the crystallizer. Make sure that the stirrer does not touch the sides of the neck and the bottom of crystallizer. Insert the different connections, i.e. thermocouples Temp1 and Temp2 (each inside steel tubes), tubes etc., into each opening on the lid as shown in Figure B.3. Make sure that the thermocouple does not touch the impeller and the inside wall of the crystallizer and is placed just above the impeller. Also make sure that the tubes are not in contact

with the wall of crystallizer and impeller.

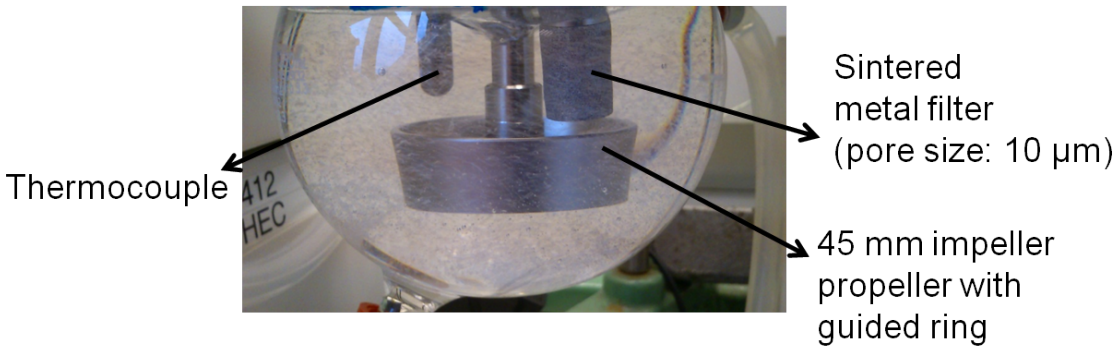

Figure B.4: Components in the crystallization units.

Inside each crystallizer, three components are implemented: 1) Stirrer with 45 mm propeller impeller with guided ring, 2) thermocouple inserted into a steel tube containing liquid silicone to improve heat transfer, and 3) a stainless steel sintered metal filter with pore size of 10 μm (IDEX Health and Science, Wertheim-Mondfeld, Germany). The propeller impeller with guided ring is more gentle on crystals due to reduced tip speed. The stirrer speed can be adjusted by turning the knob on the motor (M1 and M2). The filter is used to retain solids in the crystallizing suspensions.

The crystal-free mother liquor is exchanged between the crystallizers by two pumps (C1-C2 and C2-C1) (Longer Pump LP-BT-100-1F, YZ1515x, Baoding Longer Precision Pump Co. Ltd., Hebei, China) with an uncertainty in flow rate of ±2%. The temperature of the transferred mother liquor is recorded at three positions: 1) At the suction side of the pump C1-C2 (TEX-1) using the software of Texas Instruments thermosensor (grey box analog to digital converter), 2) at the inlet to crystallizer C1 (Temp4), and 3) at the inlet to crystallizer C2 (Temp6). Moreover, the temperature of the feed into crystallizer C1 (Temp3) is also monitored. Temperatures Temp1-6 are all connected to the Logger Lite 1.6.1 software interface.

B.3.2 Cooling system

The cooling is performed by using demineralized water as coolant with a constant cooling rate of 14 K/h. Alternatively, other coolants such as ethylene glycol can be used. Each crystallizer has a cooling unit (HEX(C1) and HEX(C2)) connected to it by Silicone tubes with appropriate length and an inner diameter of 19 mm. The tubes are connected from the discharge of the cooling unit marked 'OUT' and to the bottom opening of the crystallizer. The tube connected to the inlet of the cooling unit marked 'IN' is connected to the top opening of the crystallizer (Figure B.5).

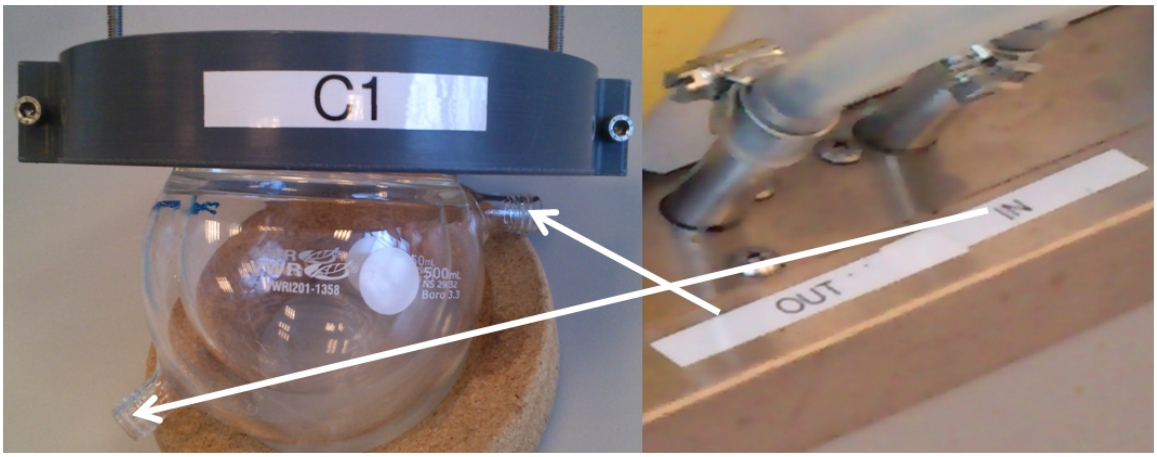

Figure B.5: Cooling unit and the connected tubes.

The cooling unit is turned on and off by the 'ON/OFF' button on the control board on the top of the cooling unit (Figure B.6).

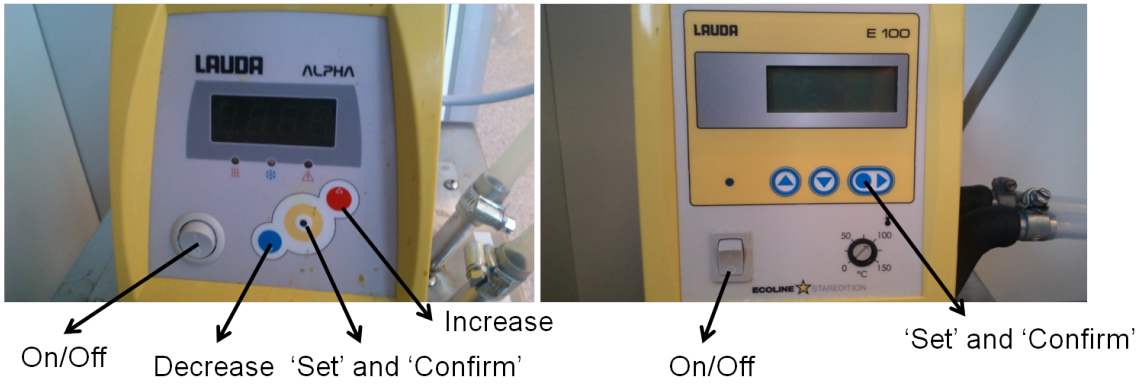

Figure B.6: Control board on cooling unit.

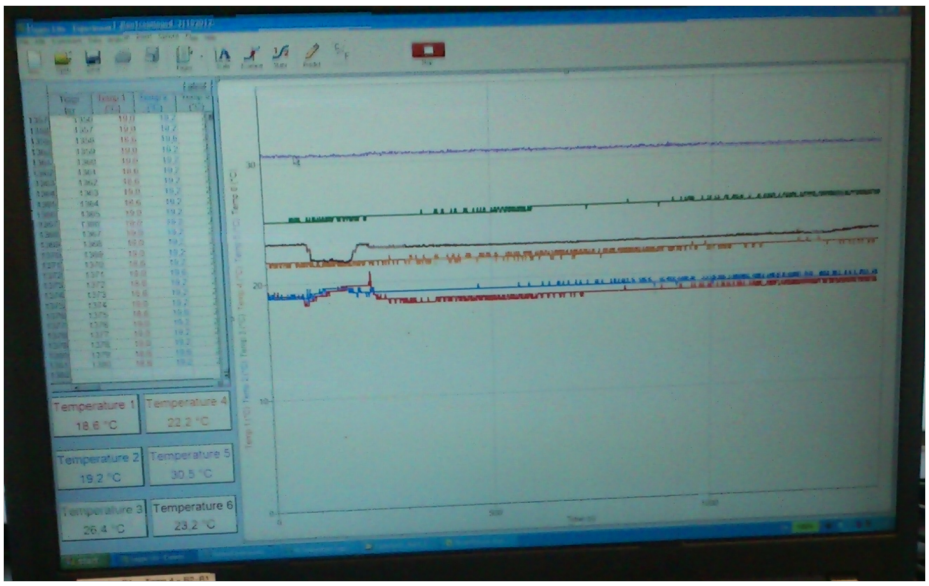

Figure B.7: Computer screen showing the interface of Logger Lite 1.6.1 software for temperature logging through the GO!Link thermocouple connection sensor.

Note that the two cooling units are different in coolant capacity and control modes. To decrease or increase the coolant temperature use the respective buttons on the control board on each cooling unit. Note that there is no automatic control of temperature in crystallizer. The control of temperature is performed manually by observing the temperature (Temp1 and Temp2) on the computer screen through the Vernier Software package Logger Lite 1.6.1 using the thermocouple sensor connected to Go! Link interface (Vernier Software and Technology LLC, Beaverton, OR, USA) (Figure B.7). The temperature is logged automatically.

B.3.3 Feed system

The feed system is shown in Figure B.8.

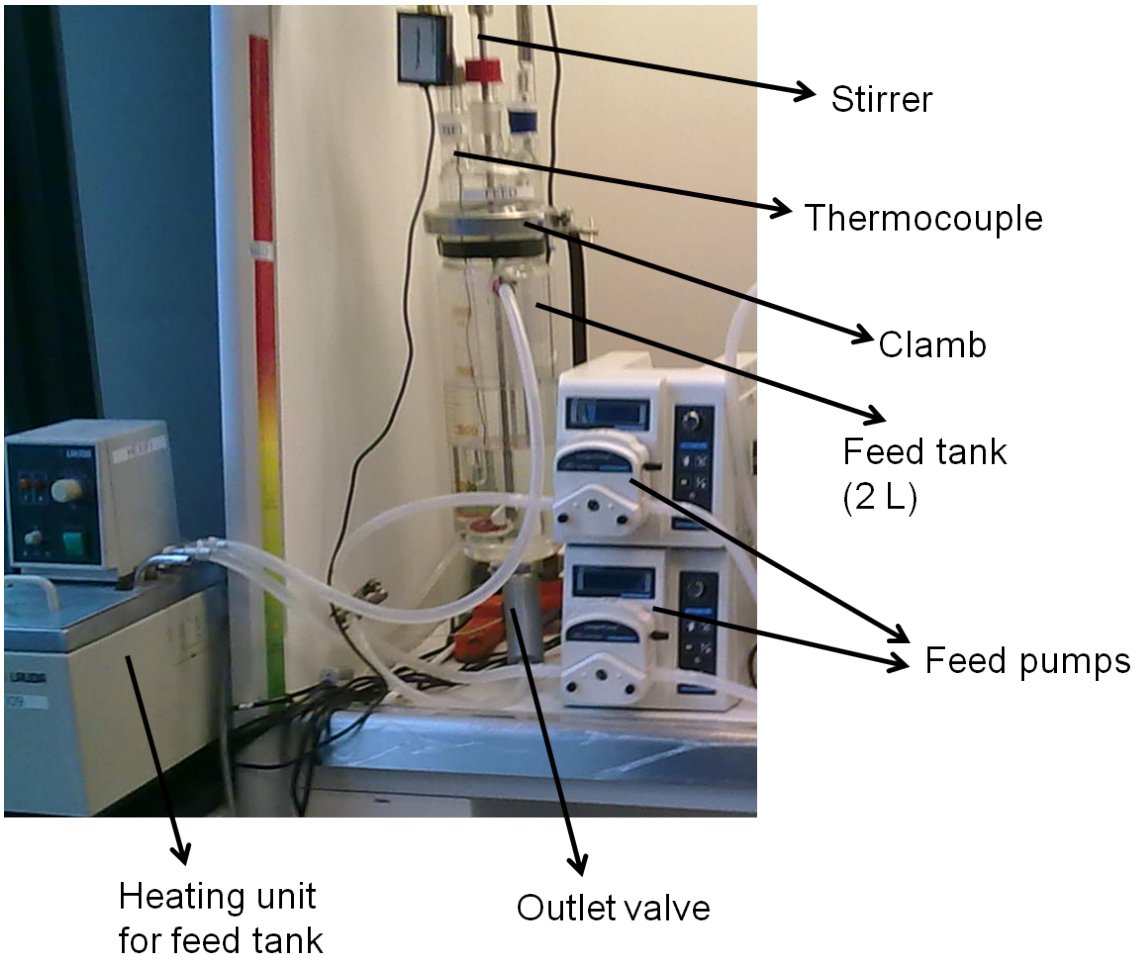

Figure B.8: Feed system.

The feed tank (FEED) is a cylindrical glass vessel of a maximum volume of about 2.5 L. It has a 75 mm flange and a lid with three necks/openings is connected to it by a fastening clamb. In the openings, a thermocouple marked Temp5 (inside a glass tube) and the stirrer are inserted. An in-house made stirrer shaft fitted with

a half-moon impeller of PTFE mounted on a motor (MF) (IKA Eurostar Power Control-Visc, Staufen, Germany) is placed in the center of the feed vessel. The last opening is kept closed by a plastic/glass plug to avoid impurities to enter the feed solution and to avoid faster cooling of the solution. The heating is conducted by

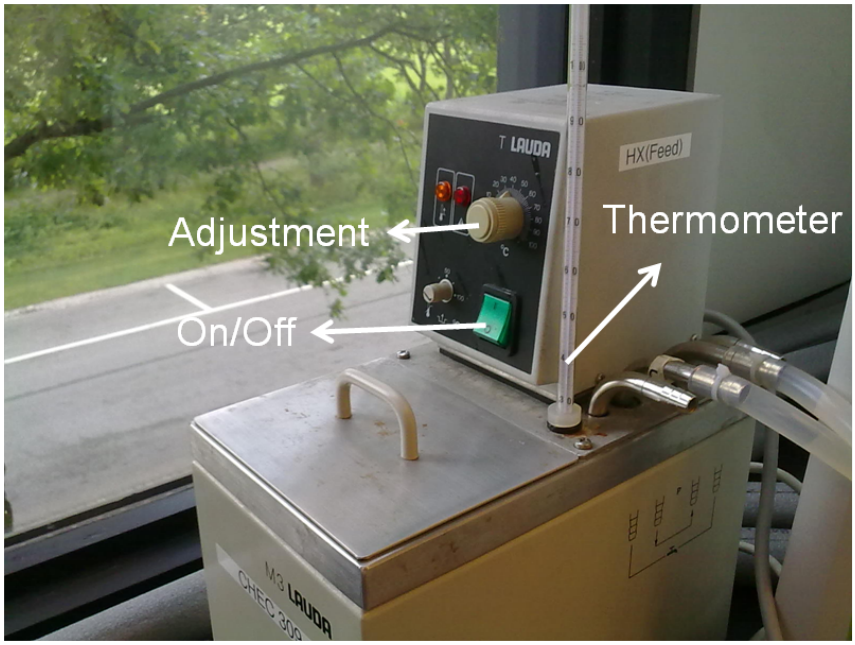

Figure B.9: Heating unit for feed system.

the connected heating unit (HEX(F)) (LAUDA M3, Lauda-Königshofen, Germany) and the temperature is controlled manually by observing the solution temperature on the connected computer screen (Temp5). The temperature is adjusted through the control board of the heating unit. The temperature is monitored via the Vernier Software package Logger Lite 1.6.1 using the thermocouple sensor connected to Go! Link interface (Vernier Software and Technology LLC, Beaverton, OR, USA). Note that the unit is only used for heating, so it has no cooling unit installed. The feed solution is transferred to the crystallizers through the pumps F1 and F2 (Longer Pump LP-BT-100-1F, YZ1515x, Baoding Longer Precision Pump Co. Ltd., Hebei, China) with an uncertainty in flow rate of ±2%.

B.3.4 Purge system

The purge system for the CC-PC process is shown in Figure B.10. The purge system consists of two pumps (P1 and P2) (Longer Pump LP-BT-100-1F, YZ1515x, Baoding Longer Precision Pump Co. Ltd., Hebei, China) with an uncertainty in flow rate of ±2%, two purge collection tanks of 1 L each (Purge 1 and Purge 2), and two sample valves. The purpose of the purge system is to withdraw mother liquor from the crystallizers to maintain a nearly constant volume of the crystallizing suspensions.

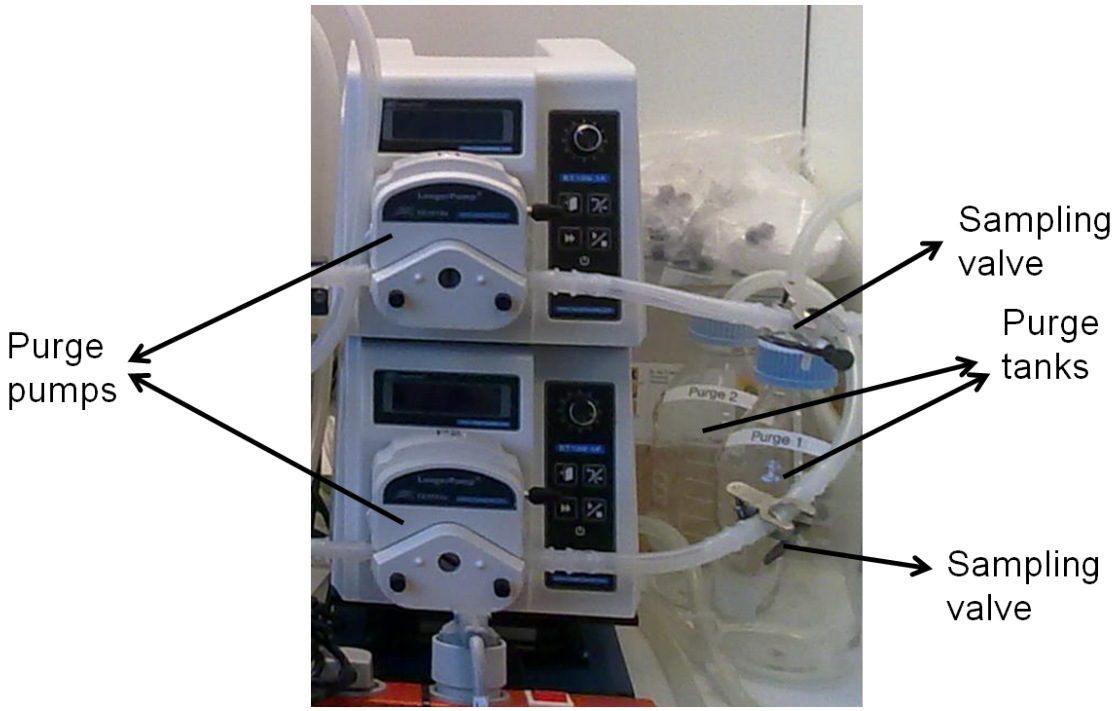

Figure B.10: Purge system.

The solutions collected in the purge collection tanks can, if needed, be reused as feed for additional experiments together with fresh feed solution.

B.3.5 Analysis equipment

B.3.5.1 Liquid phase analysis: Polarimetry

To determine the concentration of the enantiomers in the mother liquor, a polarimeter is used to determine the observed optical rotation in the solution. The polarimeter (PerkinElmer 341 Polarimeter, PerkinElmer Life and Analytical Sciences, Shelton, CT, USA) can be accessed in the Department of Chemistry at DTU (building 201, Organic synthesis). The polarimeter used is shown in Figure B.11.

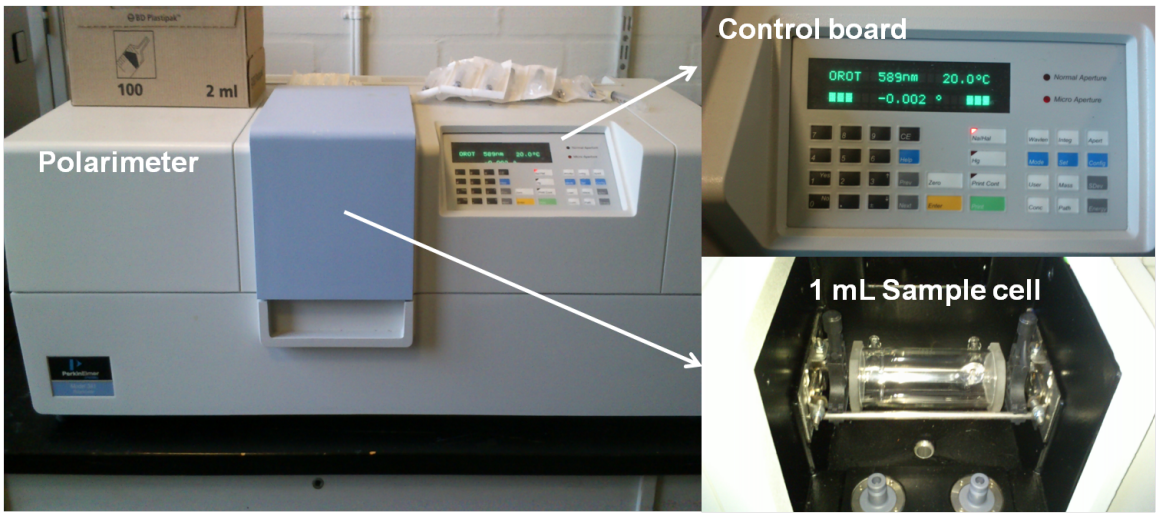

Figure B.11: The polarimeter and the accompanied 1 mL cell used.

The polarimeter is turned on by the 'ON/OFF' button at the top. The polarimeter is left for about 10 minutes to heat up the Na-lamp to full strength. The used spectrum line is the Sodium D-line of a wavelength of 589 nm. The measurement temperature of the polarimeter is set by default to 20 °C and the measurement reproducibility is ±0.002°.

B.3.5.2 Liquid phase analysis: Densitometry

The density measurement is conducted to determine the total concentration of the solution. The liquid density is measured using a Density Meter DMA 35 (Anton Paar GmbH, Graz, Austria) shown in Figure B.12 with a reproducibility of ±0.0005 g/mL.

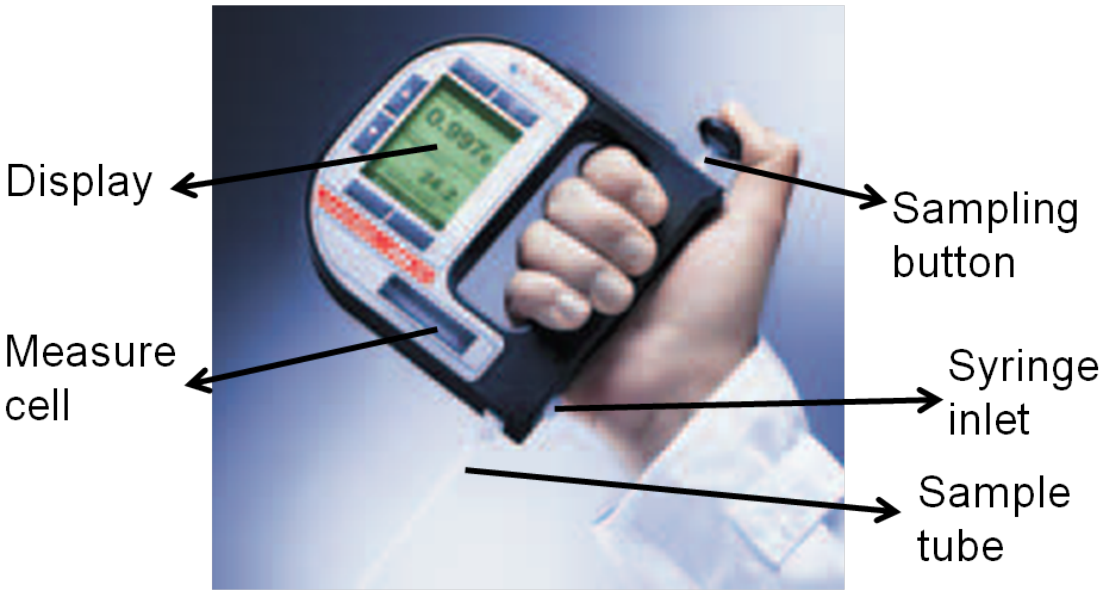

Figure B.12: The densitometer with 1 mL sampling cell.

The sample solution is pumped through the sample tube by pressing the sampling button and slowly releasing it. The sample then enters the 1 mL sample cell and the measurements is conducted. Note that no air bubbles are allowed to enter the sample cell while measuring. The presence will cause error in measurement. The sample temperature is also measured. Alternatively, if small volume of sample is required, a syringe filled with more than 1 mL sample is pumped into the syringe inlet and the density and sample temperature are recorded.

B.3.5.3 Solid phase imaging: Scanning Electron Microscopy (SEM)

The equipment used for SEM imaging of the dry seed crystals and the produced crystals is a Quanta 200 ESEM FEG scanning electron microscope. The equipment is located at the Center for Nanoscopy at DTU. Booking with the responsible technician for an introduction to the equipment is necessary prior to the use of the equipment. The SEM equipment is shown in Figure B.13.

The samples to be analyzed are first of all placed on the respective sample holders. These consist of circular stainless steel holders of about 2 cm in diameter and are covered with double-gluing carbon sheets. After adding a small amount of sample, the samples are coated with gold particles in a specialized coating apparatus. This is to allow for clear imaging and to avoid heating of the sample which destroys it.

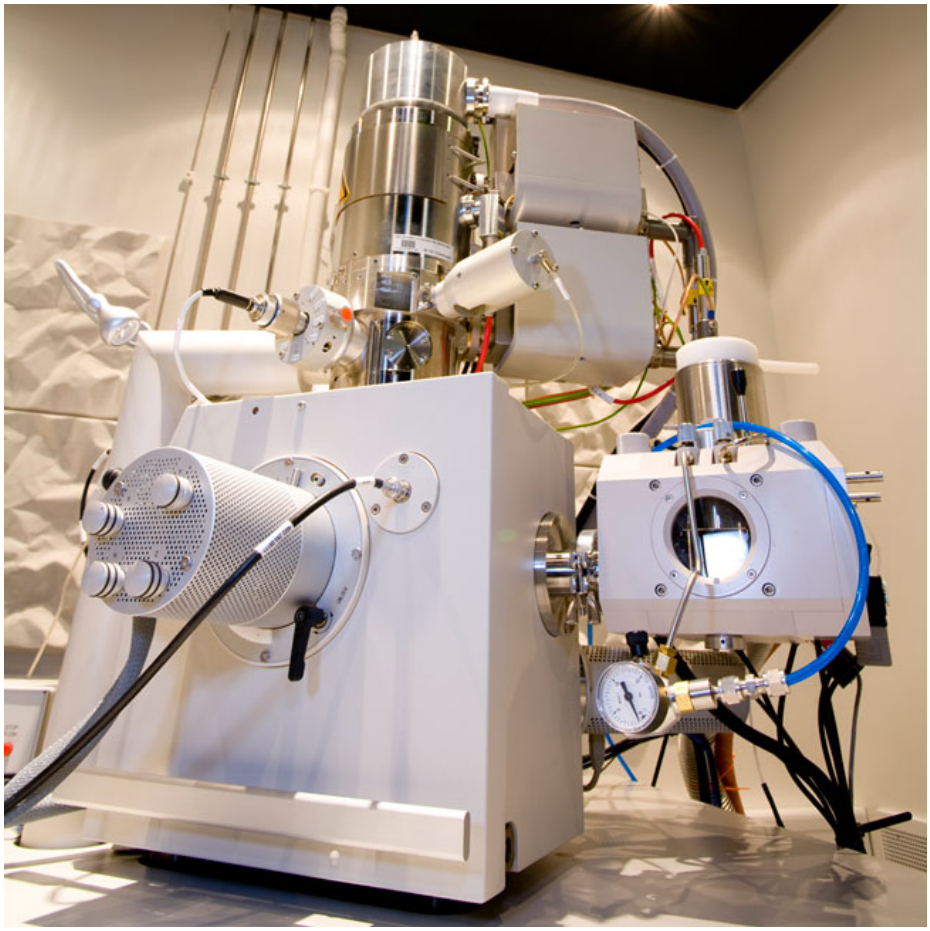

Figure B.13: The SEM microscope at CEN, DTU.

B.4 Experimental procedure

Before starting any practical work spend some time to inspect the equipment and identify the main components and utilities. Use the flow diagram in Figure 3.1 for assistance. Also get yourself familiar with the control board of the cooling and heating units and how to navigate around in the computer interface. Fill out the safety data sheet (APV) for DL-, D-, and L-asparagine monohydrate.

B.4.1 Precautions

There are some precautions to count for before starting the experiments:

- The temperature in the vessels is not automatically controlled. Manual control by adjustment of temperature of cooling/heating units is necessary.
- The pumps used are peristaltic (positive displacement) pumps with an uncertainty in flow rate of ±2%. Before turning on the feed pumps F1 and F2 make sure that the outlet valve in the bottom of the feed tank is released.

- The pumps can operate with bidirectional flow. Make sure that the pump is set to pump the desired direction according to pump instruction manual.
- The tubes in the pump heads should rest on the rollers and should not be elongated.
- Make also sure that the tubes are not bend so that transport of solution is hindered.
- Make sure that air bubbles present in the tubes are removed.
- The impellers should turn unhindered and should not touch the walls of the vessels.
- Tubes should not fold around the impeller and should not touch the walls of the crystallizers.
- Thermocouples should not touch the impeller and should be placed about 1/3 of the solution height from the bottom of the vessel.
- Thermocouple sensors should be placed away from any heating source. Heating can influence the voltage measured in the sensor.
- Sampling valves are closed and are only opened when sampling is conducted.

B.4.2 Materials

The chiral compounds to use as enantiopure seeds are D-(+)-Asparagine monohydrate (D-AsnH_2O) ($\geq$99%) and L-(-)-Asparagine monohydrate (L-AsnH_2O) ($\geq$99%) can be purchased from Sigma-Aldrich (Copenhagen, Denmark). DL-($\pm$)-Asparagine monohydrate (DL-AsnH_2O) ($\geq$99%)) can also obtained from Sigma-Aldrich (Copenhagen, Denmark). Demineralized water is used as solvent.

B.4.3 Seed preparation: Sieve analysis and Particle size distribution (PSD)

B.4.3.1 Sieve analysis

To prepare the enantiopure seeds of D- and L-AsnH_2O, a sieve analysis was conducted on each compound. The sieve size used are 106 μm, 125 μm, 150 μm, 250 μm, 355 μm, and 500μm. Prior to use, each sieve is cleaned according to the following procedure:

1. Treat each sieve with ultrasound in clean demineralized for about 10 minutes to remove deposits from previous use.

2. Remove additional deposits by scrapping them off the sieve.
3. Wash the sieve with demineralized water.
4. Spray the sieve with 96% EtOH and dry by flushing with air.
5. Place the sieves for complete drying.

When the sieves are dried completely, they are weighed and the weight is recorded. Then the sieves are placed in descending order from top to bottom in the Vibratory Sieve Shaker AS 300 control (located in the oven lab, CHEC, DTU). Before adding the lid, the mass of solid AsnH_2O to be sieved is poured on the top sieve. The lid is then mounted. The sieve shaker is turned on and is set according to the following settings:

- Amplitude = 150 mm/'g'
- Sieving time = 10 min

Subsequently, the sieves with solids are weighed and the weight is recorded. The sieved solids from each sieve are then transferred to small glass flasks marked with the sieve number. Note if any agglomerates appear and transfer them separately.

B.4.3.2 PSD measurement

The mass of seeds is collected from a certain sieve fraction and analyzed offline for the PSD with laser diffraction particle size analyzer (Malvern Mastersizer 2000, Malvern Instruments Ltd.). The eluent used is EtOH and the amount of sample size is about 1 g (a full 0.5 mL Eppendorf tube). Before sample measurement, a specification sheet should be filled and handed in to the responsible technician.

B.4.4 Preparation of undersaturated racemic feed solution

The racemic feed solution is prepared according to the following procedure:

1. Add 1.90 kg of demineralized water in the feed tank (FEED).
2. Turn on the stirrer motor (MF) and set to 270 rpm.
3. Heat the water to about 31 °C through HEX(F) (setpoint: 30 °C).
4. Remove the plug from the opening and put the paper funnel (made by user). Make sure that all the solids are supplied.
5. Add 100 g (one flask) of solid DL-AsnH_2O into the heated water.

6. Maintain the temperature of the slurry at 31 °C for about one hour for complete dissolution. The temperature of feed solution is maintained at that temperature throughout the duration of the experiment.

After complete dissolution, a single sample of the feed solution of ca. 4 mL (in vial with lid) is withdrawn by releasing the outlet valve of the feed tank and turning on pump F1. After sampling, the pump F1 is turned off and the outlet valve is closed.

B.4.5 Preferential crystallization experiments

The preferential crystallization experiments using the CC-PC process are conducted according to the following experimental procedure:

1. Start the computer and start the Logger Lite 1.6.1 interface and the Texas Instrument software.
2. Adjust the time for data logging and the increment for temperature recording. Save the files. Note that only the temperature TEX-1 is recorded by the Texas Instrument software.
3. Turn on the cooling units HEX(C1) and HEX(C2) connected to the crystallizers C1 and C2.
4. Set the setpoint of the cooling units to 22.3 °C. The crystallizers are thereby heated to about 22 °C.
5. Transfer 220 mL feed solution to C1 and C2 by the dispensing function of the pumps F1 and F2, respectively, according to the pump instruction manual.
6. Weigh about 0.4648 g of enantiopure seed crystals of each enantiomer of the desired sieve fraction. Collect in 0.5 mL Eppendorf tubes.
7. Add 50 mL 96% EtOH in each cap bottle and bring to cool in refrigerator.
8. When the solution is transferred turn on the stirrers M1 and M2 at a speed of 250 rpm.
9. Return to flow rate mode on the pump according to the pump instruction manual.
10. Adjust the flow rate to 7.3333 mL/min on pump F1 and F2. The flow rate corresponds to a predefined residence time of the liquid phase of 15 min in each crystallizer.

11. Start data logging. Note the time.
12. Set the setpoint of the cooling units to a temperature so that the crystallizers are cooled to about 19 °C.
13. Start the pumps according to the sequence: C1-C2, C2-C1, F1, F2, P1, and P2. Note the time.
14. Adjust the cooling units to obtain a temperature in the crystallizers of about 19 °C.
15. When a temperature of about 19 °C is reached, observe if crystallization occurs or not.
16. Withdraw one liquid sample of about 4 mL (in vial with lid) from each crystallizer.
17. Supply the predefined mass of enantiopure seeds into each crystallizer. This is done be removing the thermocouples and inserting paper funnels into the openings of the crystallizers and emptying the Eppendorf tubes into the crystallizers. Note the time for seeding.
18. Immediately withdraw a liquid sample from each crystallizer simultaneously through the purge streams and mark the sample vial. Remember to close the sampling valves after each sampling.
19. Observe for volume change in the crystallizers and maintain the crystallization temperature in the crystallizers. Also maintain the feed temperature.
20. At every residence time (15 min) withdraw a liquid sample simultaneously from each crystallizers. Remember to close the sampling valves after each sampling.
21. Prepare for solid harvest by filtration using ashless cellulose filter paper with 7.0 cm in diameter and pore size of 3 μm placed on a Büchner funnel with vacuum suction. Note the mass of the dry filter and the filter holder.

After a process duration of about 90 minutes, the termination of the experiment is conducted through the following procedure:

1. Adjust the temperature of the cooling units to 19 °C.
2. Stop the data logging and note the time.
3. Stop the feed pumps F1 and F2.
4. Stop the purge pumps P1 and P2.

5. Stop the exchange pumps C1-C2 and C2-C1.
6. Stop the cooling unit for crystallizer C1 and dismantle the tubings connected to the crystallizer from the cooling unit. Remember to dismantle the top tube first.
7. Dismantle the crystallizer glass vessel from the ring holder by screwing off the screws around the crystallizer.
8. Start the vacuum pump and add the slurry on the filter, which is wetted by 96% EtOH.
9. Wash the harvested solids with 50 mL ice cold 96% EtOH.
10. Stop the vacuum pump and put the solids to dry under ventilation overnight (about 24 hours).
11. Repeat points 6–10 for the second crystallizer, C2.

After the solids are dried, the mass of solid produced is estimated by a simple mass analysis. The results are used for further evaluation of the performance of the separation process in terms of the U-value, solid product yield, productivity, and optical purity.

B.5 Process metrics

B.5.1 Liquid phase concentration of enantiomers

The concentration, in mass fraction, of each enantiomer in the liquid phase (mother liquor) is estimated using a combination of the measurements of optical rotation of the liquid solution and liquid phase density. The expressions used are:

$$w_i^{\mathrm{D}}(t) = \frac{1}{2}\left(\frac{\rho_L(t) - \rho_W}{k^d} + \frac{\alpha_{obs,L}}{k^P}\right) \tag{B.1}$$

$$w_i^{\mathrm{L}}(t) = \frac{1}{2}\left(\frac{\rho_L(t) - \rho_W}{k^d} - \frac{\alpha_{obs,L}}{k^P}\right) \tag{B.2}$$

For explanation of the symbols used please see the Nomenclature. The necessary calibration data and curves are given in Appendix C.

B.5.2 Separation efficiency: *U*-value

To assess the efficiency of the CC-PC process, the ratio between the total concentration of the preferred enantiomer in the purge streams and the total concentration

of the preferred enantiomer in the feed solution entering the crystallizers, calculated by a steady-state mass balance, is considered at final time. The ratio is denoted the U-value and is expressed as:

$$U - \text{value} = \frac{w_i^{(p)} + w_j^{(p)}}{w_{F,i}^{(p)} + w_{F,j}^{(p)}} \times 100\%, \quad i \in \{1,2\} \neq j \in \{1,2\} \tag{B.3}$$

where 1 refers to crystallizer C1 and 2 refers to crystallizer C2.

B.5.2.1 Productivity and yield based on seeds

The productivity from the simulations of the preferred enantiomer in each crystallizer at the end of the process duration is estimated as the ratio between the accumulated mass of the solid product produced and the product of the total mass of enantiomer fed into the crystallizer and the duration of the process, t_f:

$$\text{Pr}_i^{(p)} = \frac{m_{produced,i}^{(p)}}{m_{F,i}^{(p)} t_f} \tag{B.4}$$

Similarly, the yield of the solid product of the preferred enantiomer produced in each crystallizer at the end of the duration of the process, t_f, is defined as the ratio between the accumulated mass of solid product produced and the mass of the enantiopure seeds initially supplied to the crystallizer:

$$Y_{S,i}^{(p)} = \frac{m_{produced,i}^{(p)}}{m_{seeds,i}^{(p)}} \times 100\% \tag{B.5}$$

B.5.2.2 Optical purity of solid product

The optical purity of the solid product is determined quantitatively by polarimetry using the observed optical rotation of a pure reference of the preferred enantiomer in solution with the same concentration as the solid product from each crystallizer in solution. The optical purity is thus calculated by the following expression:

$$\text{Pu}_{S,i}^{(p)} = \frac{\alpha_{obs,i}^{(p)}}{\alpha_{ref,i}^{(p)}} \times 100\% \tag{B.6}$$

B.5.3 Final remarks

At the end of each experiment, remember to flush the tubes with demineralized water and wash the crystallizers and the feed tank from any residual solution or solids. Use always demineralized water. Do not leave the setup while running and make sure that the fume hood is closed during operation. All the pumps should be calibrated before use. The thermocouples were calibrated according to the thermocouple for TEX-1 calibrated at Risøe, Termometri section. All the thermocouples were inserted in demineralized water and left overnight for equilibration. Afterwards the temperatures of the thermocouples, besides the one for TEX-1 measurement, are set according to the thermocouple calibrated at Risøe. Documentation for the calibration is enclosed with this manual.

Nomenclature

Variables

Symbol	Description	Unit
c	Counter enantiomer	–
k^d	Calibration constant for liquid phase density	kg/m^3
k^P	Calibration constant for optical rotation	$^\circ$
m	Mass of species	kg
Pr	Productivity	kg/(kg s)
Pu	Optical purity	–
t	Time	s
w	Mass fraction of species	–
Y	Yield of solid product	–

Greek letters

Symbol	Description	Unit
ρ	Density	kg/m^3

Subscripts

Symbol	Description
F	Feed
f	Final
i	Crystallizer 1 or 2
j	Crystallizer 1 or 2
L	Liquid phase
obs	Observed
produced	Produced solids
ref	Reference
S	Solid
seeds	Seeds
W	Water

Superscripts

Symbol	Description
D	D-isomer
L	L-isomer
p	Preferred enantiomer

Appendix C
Calibration Curves

C.1 Calibration procedure for estimation of concentration difference by polarimetry

For the observed optical rotation dependence on the difference in the mass fractions of D-Asn and L-Asn in aqueous solutions, the observed optical rotation of several aqueous solutions of mixtures of D-Asn and L-Asn ($w^{\text{D-Asn}}$ = 0, 0.24, 0.49, 0.97, 1.46, 1.73, 2.00 wt% with $w^{\text{L-Asn}}$ = 2.00, 1.76, 1.51, 1.02, 0.53, 0.27, 0 wt%) was measured by offline polarimetry at 20 °C and 589 nm (sodium D-line) in 1 mL glass cell (PerkinElmer 341 Polarimeter, PerkinElmer Life and Analytical Sciences, Shelton, CT, USA). The polarimeter was zeroed by demineralized water. 1 mL from each solution was transferred to the glass cell by a 2.5 mL syringe with needle. After each measurement, the glass cell was washed three times with demineralized water. The obtained data are depicted in Figure C.1.

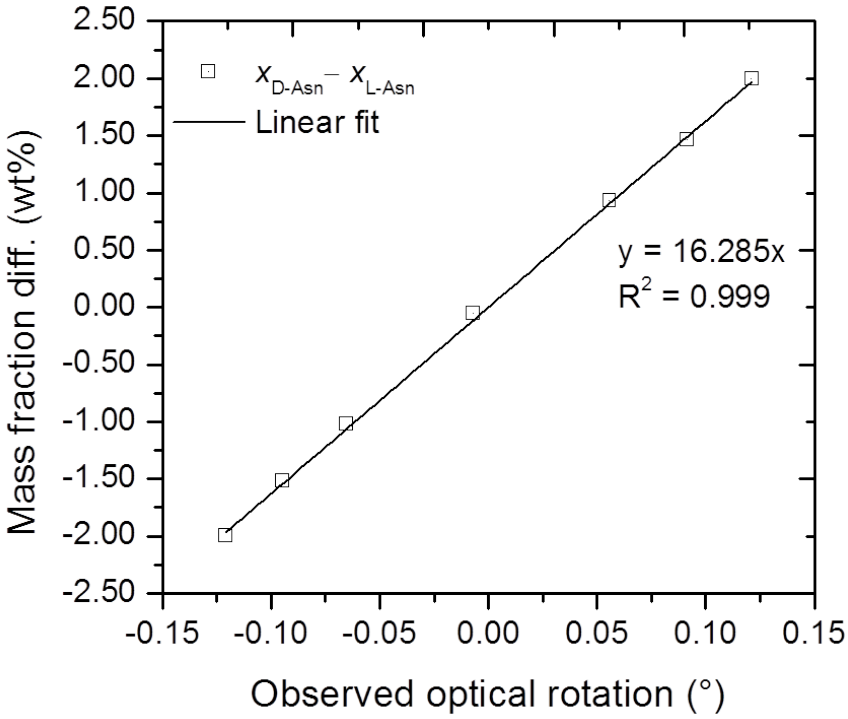

Figure C.1: Calibration curve and linear fit for the mass fraction difference between D-Asn and L-Asn in aqueous solution as function of the observed optical rotation.

C.2 Calibration procedure for estimation of total concentration by densitometry

For the liquid density dependence on the total concentration of D-Asn and L-Asn in aqueous solutions, the liquid density of several aqueous solutions of mixtures with varying total concentration of D-Asn and L-Asn ($w^{\text{D-Asn}} = w^{\text{L-Asn}} = 2.16$, 2.20, 2.24, 2.29, 2.35 wt%) was measured by offline densitometry at about 23 °C (±0.1 °C) using Density Meter DMA 35 (Anton Paar GmbH, Graz, Austria). First of all, a sample of demineralized water was measured using a 2.5 mL syringe without needle to transfer the liquid sample to the densitometer. The temperature and density of sample were recorded. Similarly, liquid solution samples with the above mentioned concentrations were analyzed. After each measurement, the densitometer was washed three times with demineralized water. The data obtained are depicted in Figure C.2.

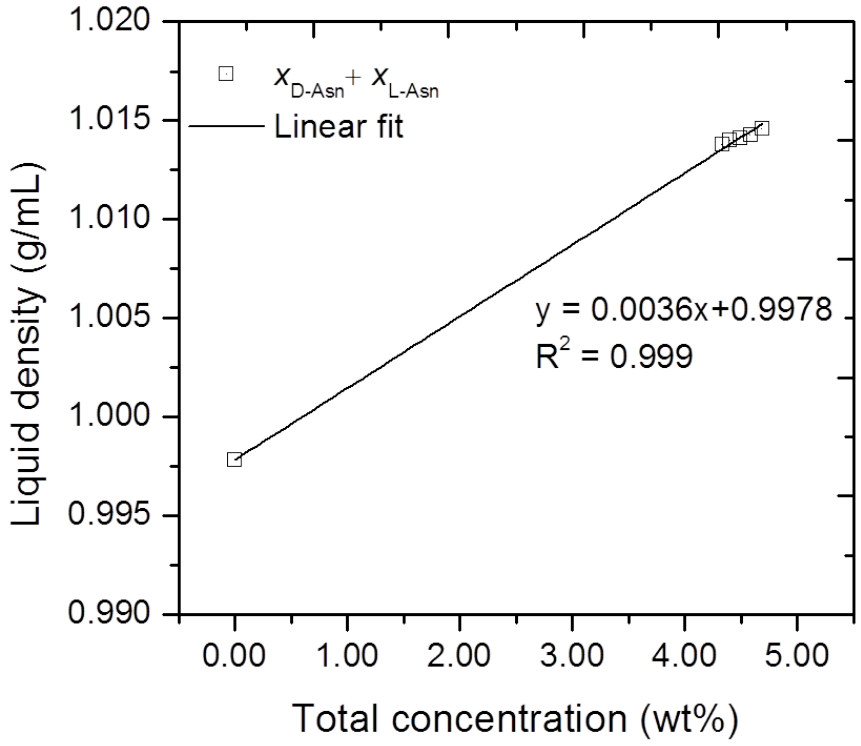

Figure C.2: Calibration curve and linear fit for the liquid density as function of the total concentration of enantiomers in aqueous solutions.

C.3 Calibration procedure for optical purity estimation by polarimetry

For the observed optical rotation dependence on the mass fraction of pure L-Asn in aqueous solutions, the observed optical rotation of several aqueous solutions of L-Asn ($w^{\text{L-Asn}} = 0$, 0.27, 0.53, 1.02, 1.51, 1.76, 2.00 wt%) was measured by offline polarimetry at 20 °C and 589 nm (sodium D-line) in 1 mL glass cell (PerkinElmer 341 Polarimeter, PerkinElmer Life and Analytical Sciences, Shelton, CT, USA). The polarimeter was zeroed by demineralized water. 1 mL from each solution was transferred to the glass cell by a 2.5 mL syringe with needle. After each measurement, the glass cell was washed three times with demineralized water. The obtained data are depicted in Figure C.3.

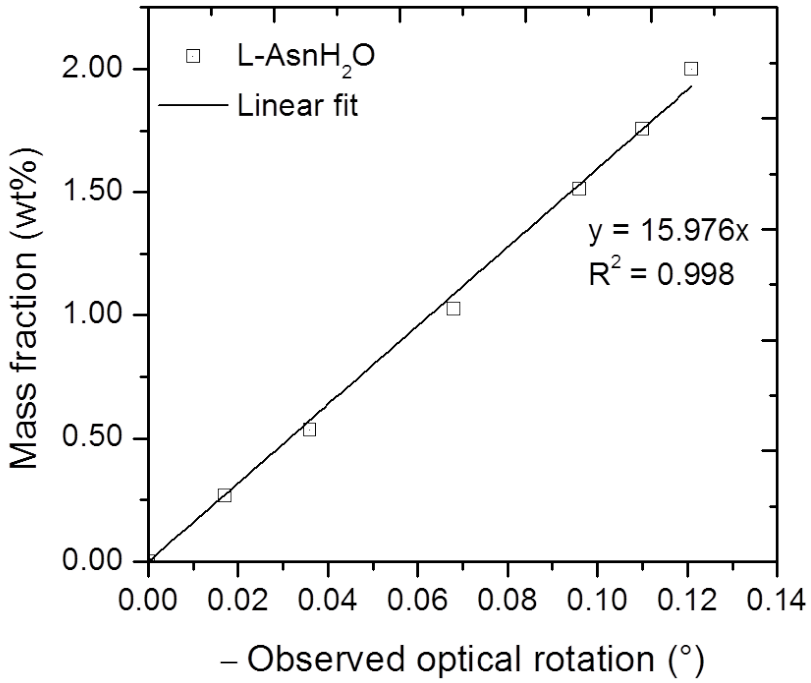

Figure C.3: Calibration curve and linear fit for the mass fraction of L-AsnH_2O in aqueous solution as function of the observed optical rotation.

Appendix D

STA Measurements

D.1 Purity assessment by STA measurements

DSC and TGA thermograms for purity assessment of the purity of the solid products produced from the D-Tank in Exp 1 after washing with ice cold 96% EtOH and subsequent drying for 24 hours in fume hood are shown in Figure D.1 (a) and (b). Similarly, the thermograms for the solid products from the L-Tank in Exp 1 are shown in Figure D.2 (c) and (d).

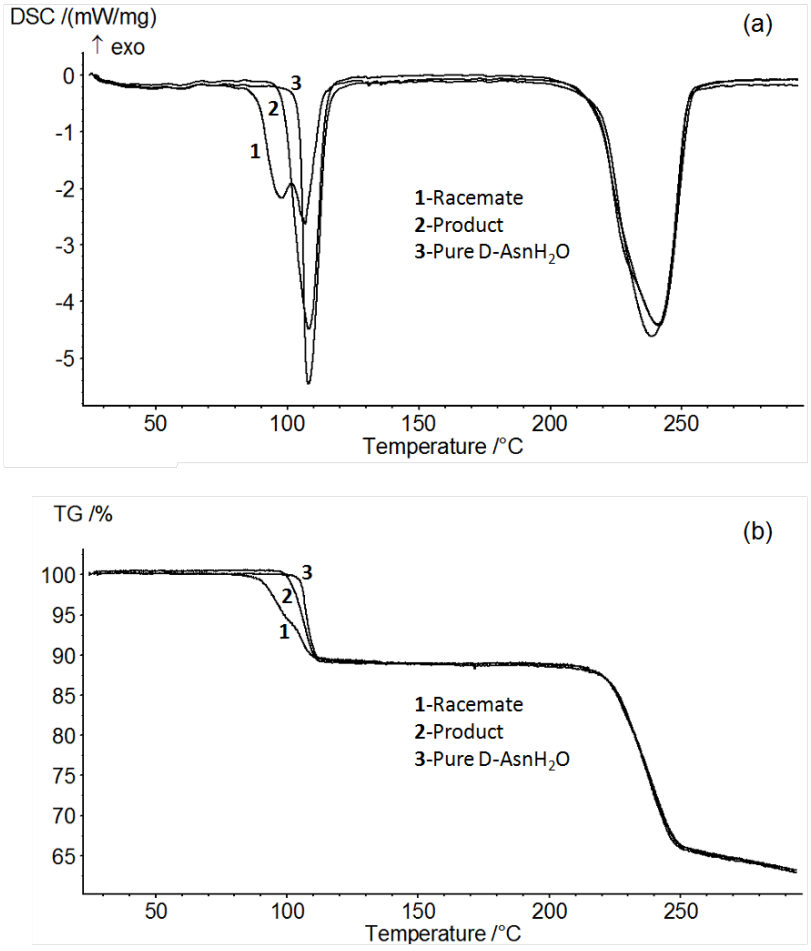

Figure D.1: DSC and TGA thermograms for the solid product from the D-Tank in Exp 1 ((a) and (b), respectively).

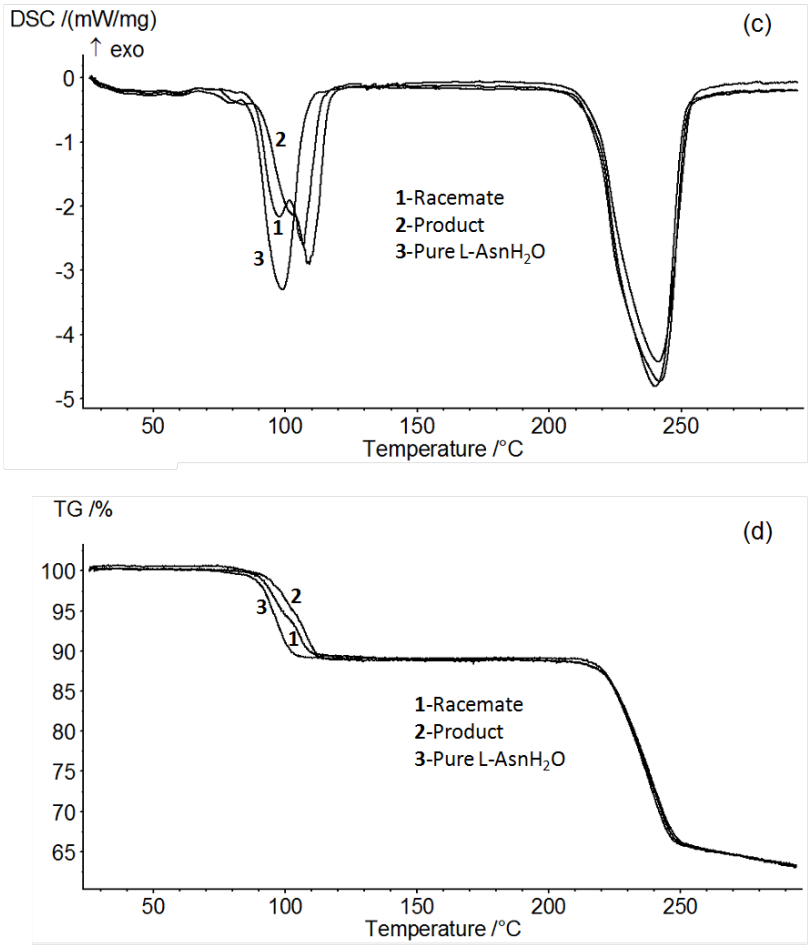

Figure D.2: DSC and TGA thermograms for the solid product from the L-Tank in Exp 1 ((b) and (d), respectively).

Appendix E

PBE Transformation by MOM

E.1 Transformation of the Population Balance Equation (PBE) by the Method Of Moments (MOM)

The PBE, assuming the growth rate of the preferred enantiomer, p, in crystallizer i, $G_i^{(p)}$, is size-independent, is given as:

$$\frac{\partial n_i^{(p)}(t,L)}{\partial t} = -G_i^{(p)}(t)\frac{\partial}{\partial L}n_i^{(p)}(t,L), \quad i \in \{1,2\} \tag{E.1}$$

Multiplying by L^x on both sides of the PBE and rearranging gives:

$$L^x\frac{\partial n_i^{(p)}(t,L)}{\partial t} + G_i^{(p)}(t)\,L^x\frac{\partial}{\partial L}n_i^{(p)}(t,L) = 0 \tag{E.2}$$

Integrating on both sides:

$$\int_{L=0}^{\infty} L^x\frac{\partial n_i^{(p)}(t,L)}{\partial t}\mathrm{d}L + G_i^{(p)}(t)\int_{L=0}^{\infty} L^x\frac{\partial}{\partial L}n_i^{(p)}(t,L)\,\mathrm{d}L = 0 \tag{E.3}$$

Rewriting:

$$\frac{\partial}{\partial t}\int_{L=0}^{\infty} L^x n_i^{(p)}(t,L)\,\mathrm{d}L + G_i^{(p)}(t)\int_{L=0}^{\infty} L^x\frac{\partial}{\partial L}n_i^{(p)}(t,L)\,\mathrm{d}L = 0 \tag{E.4}$$

In general the moments, N_x, where x = 0,1,2,3, of the number distribution functions are defined as follows:

$$N_{x,i}^{(p)}(t) = \int_{L=0}^{\infty} L^x n_i^{(p)}(t,L)\,\mathrm{d}L \tag{E.5}$$

Inserting equation (E.5) into equation (E.4) and conducting integration by parts gives:

$$\frac{\mathrm{d}N_{x,i}^{(p)}(t)}{\mathrm{d}t} + G_i^{(p)}(t)\left(\left[L^x n_i^{(p)}(t,L)\right]_0^{\infty} - \int_0^{\infty} xL^{x-1}n_i^{(p)}(t,L)\,\mathrm{d}L\right) = 0 \tag{E.6}$$

Integrating the integral (the third term on the right hand side) gives:

$$\frac{\mathrm{d}N_{x,i}^{(p)}(t)}{\mathrm{d}t} + G_i^{(p)}(t)\left(\left[L^x n_i^{(p)}(t,L)\right]_0^{\infty} - xN_{x-1,i}^{(p)}(t)\right) = 0 \tag{E.7}$$

Inserting the limits in the second term on the right hand side gives:

$$\frac{\mathrm{d}N_{x,i}^{(p)}(t)}{\mathrm{d}t} + G_i^{(p)}(t)\left(\left[\infty^x n_i^{(p)}(t,\infty) - 0^x n_i^{(p)}(t,0)\right] - xN_{x-1,i}^{(p)}(t)\right) = 0 \tag{E.8}$$

Since it is assumed that $n_i^{(p)}(t, L=\infty) = 0$ and $n_i^{(p)}(t, L=0) = 0$, the change of the moments of the number distribution function with time are given by rearranging equation (4.8) to obtain the following general expression:

$$\frac{\mathrm{d}N_{x,i}^{(p)}(t)}{\mathrm{d}t} = xN_{x-1,i}^{(p)}(t)\,G_i^{(p)}(t) \tag{E.9}$$

Appendix F

MATLAB Codes